A computerized model of the Cori cycle in patients with critical illness

Eric Kassebaum

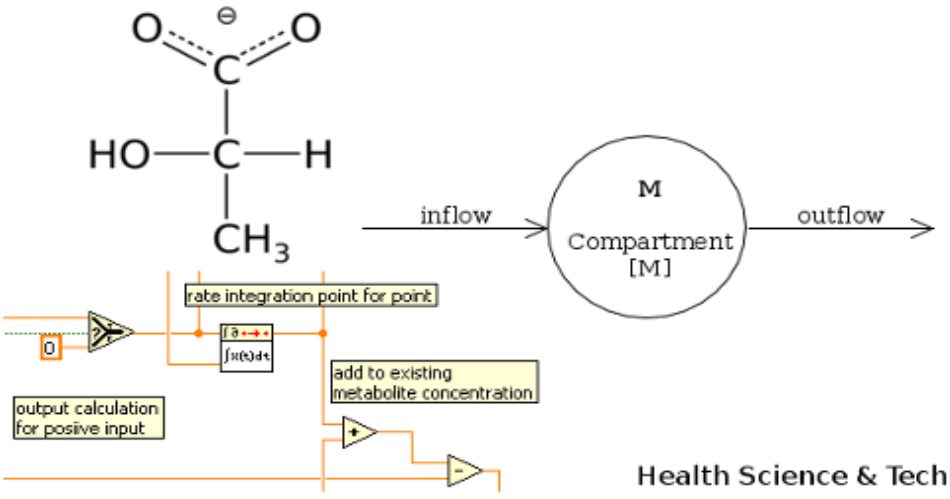

Health Science & Technology Aalborg University
June 3. 2015

AALBORG UNIVERSITY
STUDENT REPORT

Department of Health Science and Technology
Fredrik Bajers Vej 7D
9200 Aalborg
http://st.hst.aau.dk

Title: A computerized model of the Cori cycle in patients with critical illness

Theme:
Modeling Physiological Processes

Project period:
3rd and 4th semester Master
September 2. 2014 till June 3. 2015

Project group:
980

Members:
Eric Kassebaum

Supervisor:
Ulrike Pielmeier

No. of copies: 1

No. of pages: 152

Concluded: June 3, 2015

Synopsis:

Critically ill patients suffer from loss of lean body mass caused an increased metabolism, which can become life threatening in it self and independently of the underlying cause of critical illness. Supplying the body with external nutrition in the right amount, time, and composition might reduce the effect of an increasing catabolism over time and reduce mortality. Supporting that assumption, the Cori cycle describes the underlying metabolic pathways that exchange glucose, lactate, and alanine between liver, muscle, and other organs. In this project the Cori cycle was modeled mathematically using Michaelis-Menten kinetics for differential equations that describe the cellular carbohydrate metabolism. This was used as the basis to build a compartment model that describes the accumulation and transfer of the metabolites main metabolites between the producing and consuming organs, respectively. The combined model was subsequently adapted into a computer program that uses LabVIEW for the simulation of the Cori cycle over time.

This report was written using Texmaker 3.2 on a PC running an Ubuntu 12.04 LTS 64-bit OS. Figures were created and edited using GChemPaint 0.12.10, GIMP 2.6.12, Shutter 0.88.1, SOLIDWORKS 2007, and UMLet 11.3. The bibliography was created using JabRef 2.7b. Programming and simulation of the model were performed using LabVIEW 2011 on a Windows XP 32-bit OS run inside VirtualBox 4.3.20.

Preface

This report contains the project work performed by Eric Kassebaum in 3rd and 4th semester Master studies in Biomedical Engineering and Informatics at Aalborg University, over the time period 2nd of September 2014 till 3rd of June 2015. The overarching theme of the two semesters was "Modeling Physiological Processes" and the title of the project is "A computerized model of the Cori cycle in patients with critical illness".

The target group of the project include students, supervisors, researchers, and others with an interest in biomedical engineering.

Reading Guide

Source references in the report will be listed according to the Harvard method, with given [Surname of author, Publication year] in the text. All references are collected in the bibliography at the end of the project and listed alphabetically.

If no reference is given for a figure or table, these have been created by Eric Kassebaum. Tables and figures are numbered according to the chapter in question, e.g. first figure in chapter 2 has the referencing number 2.1. the next one of 2.2, etc. Therefore, there is a possibility of table 2.1 and figure 2.1 in same section. Used abbreviations are defined with first usage and placed in brackets. An abbreviations list is enclosed in the beginning of the document.

Eric Kassebaum

Abbreviations

ACA	acetyl coenzyme A
ADP	adenosine diphosphate
ALA	alanine
ALDase	aldolase
AMP	adenosine monophosphate
ATP	adenosine triphosphate
ATPase	adenosine triphosphatase
BGL	blood glucose level
BLL	blood lactate level
CNS	central nervous system
e.g.	for (the sake of) example
ENOase	enolase
F6P	fructose-6-phosphate
FADH	flavin adenine dinucleotide (FAD)
FBP	fructose-1,6-biphosphate
FBPase	fructose-1,6-biphosphatase
G6P	glucose-6-phosphate
G6Pase	glucose-6-phosphatase
GAP	glyceraldyde-3-phosphate
GDHase	glyceraldehyde dehydrogenase
GDP	guanosine diphosphate
GKase	glucokinase
GLG	glycogen
GLU	glucose
GLUT	glucose transporter
GPIase	glucose-6-phosphate isomerase
GTP	guanosine triphosphate
HKase	hexokinase
ICU	intensive care unit
ICUAW	intensive care unit acquired weakness
LAC	lactate
LDHase	lactate dehydrogenase
LED	light-emitting diode
MCT	monocarboxylate transporter
NAD^+	oxidized nicotinamide adenine dinucleotide

NADH	nicotinamide adenine dinucleotide (NAD)
NADPH	nicotinamide adenine dinucleotide phosphate (NADP)
$NADH + H^+$	reduced nicotinamide adenine dinucleotide
$NADPH + H^+$	reduced nicotinamide adenine dinucleotide phosphate
ODE	ordinary differential equation
PCase	pyruvate carboxylase
PDCase	pyruvate dehydrogenase complex
PEP-CKase	phosphoenolpyruvate carboxykinase
PFKase	phosphofructokinase
PGKase	phosphoglycerate kinase
PGMase	phosphoglycerate mutase
P_i	inorganic phosphate
PKase	pyruvate kinase
SIRS	systemic inflammatory response syndrome
TPIase	triosephosphate isomerase

Contents

Chapter 1

Introduction

This chapter describes the breakdown of muscle proteins in critically ill patients as a side effect of an intensive care unit (ICU) stay. Aspects of epidemiology, etiology, prevalence and prognosis of the resulting acquired weakness are presented and linked to the lactate metabolism.

1.1 Intensive Care Unit Acquired Weakness

The body response to injury is mobilizing reserves (e.g. glycogen, proteins and fat), to provide substrates for the metabolism [Saxena and Hodgson, 2012]. Especially the breakdown of skeletal muscle proteins allows for a quick reaction to altering physiological requirements [Wischmeyer, 2013], [Lecker et al., 1999]. This increased catabolism is associated with muscle degradation and loss of lean body mass, which is leading to intensive care unit acquired weakness (ICUAW) [Saxena and Hodgson, 2012], [Mansoor et al., 1996]. This loss amounts to 2% in muscle proteins and $3-4\%$ in the muscle fibers daily [Griffiths and Hall, 2010]. Consequently, 20% of all body proteins are being lost over the first three weeks, especially within the first 10 days after injury [Mansoor et al., 2007].
ICUAW is characterized by an acute severe illness, associated with prolonged immobilization and required organ support, resulting in diminished reflexes, symmetrical motor weakness that do not result from an underlying neurological condition [Saxena and Hodgson, 2012]. Patients generally tend to survive their stay in an ICU but suffer from the results of acquire weakness later [Wischmeyer, 2013], [Appleton and Kinsella, 2012]. ICUAW leads to increased costs, due to prolonged ICU and hospital stay, as well as extended mechanical ventilation [Wischmeyer, 2013], [Saxena and Hodgson, 2012], [de Jonghe et al., 2009]. Further consequences include physical disability, increasing the recovering time from weeks to months with the probability of persistent long term symptoms, as well as a higher mortality rate of affected patients [Saxena and Hodgson, 2012]. $25-60\%$ of patients surviving the acute phase of critical illness and being mechanically ventilated for more than a week, suffer from ICUAW [Griffiths and Hall, 2010], [de Jonghe et al., 2009]. 45% of those die during their hospital stay, with another 20% dying over the first year

after their discharge from the ICU. Moreover, approximately 68% of the patients who survive, regain full functional capacity, while around 28% suffer from persistent disability [Appleton and Kinsella, 2012].
This prevalence makes it necessary to pinpoint risk factors and take preventive action, as well as not exclusively focusing ICU treatment on patient survival, but also emphasize the improved patient outcome in the long term [Wischmeyer, 2013], [de Jonghe et al., 2009]. Risk factors such as hyperglycemia, muscle immobilization, multi organ failure and the use of neuromuscular blockers or corticosteroids have been isolated [Griffiths and Hall, 2010], [de Jonghe et al., 2009]. However, it remains debatable on whether the medical consequences of ICUAW are the result of ICUAW and not the underlying medical condition and on whether they could be improved by different treatment [Saxena and Hodgson, 2012], [Griffiths and Hall, 2010], [de Jonghe et al., 2009].

1.2 Critical Illness

Critical illness and injury is considered to be a process, where the body is subjected to certain phases of response to the underlying condition, as depicted in figure 1.1 [Wischmeyer, 2013].

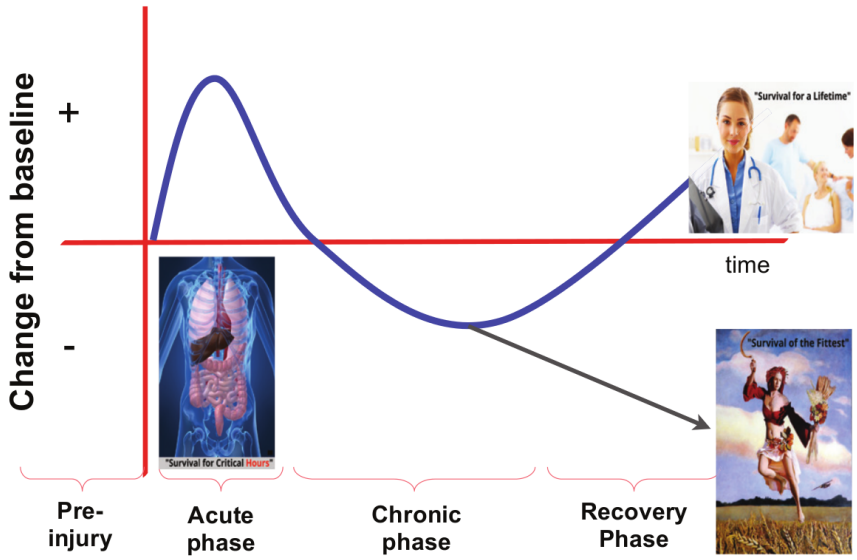

Figure 1.1: The graph shows the initial phases of the metabolic body reaction to injury and critical illness [Wischmeyer, 2013].

The graph describes the increased metabolism as a reaction to injury in the acute phase, which is fueled by the physiological reserves the body can naturally provide for a limited period of time. When entering the chronic phase those reserves are depleted and the organism begins to break down body structures, e.g. muscles for substrates. Over time this drain can cause irreversible damage to the organism causing death. However, when dealt with the injury before that critical point, a patient can recover, repair the damage, and rebuild reserves to complete health [Wischmeyer, 2013].
The acute phase lasts $12 - 24$ hours post-injury and is characterized by sepsis and shock, which frequently leads to resuscitation, mechanical ventilation and requires a

suitable drug therapy [Wischmeyer, 2013], [Van Cromphaut, 2009]. During the following chronic phase, the patient is exposed to an increased risk for recurring infections and various complications, potentially leading to a relapse into the acute phase [Wischmeyer, 2013].This phase is associated with protein catabolism, hyperglycemia, insulin resistance, increased energy requirements and cardiovascular activity such as tachypnea, tachycardia, and vasodilatation. Moreover, signs of infection such as hyper- or hypothermia and leukocytosis are present. Depending on the illness severity this phase peaks at approximately $3-5$ days after the initial injury and declines over the next $7-10$ days [Mizock, 2001]. However, if the patient is stabilized and survived this far, he enters a recovery phase over the next couple of weeks, which is characterized by the prospect to regain a sufficient health level that prevents a relapse to either of the two previous phases and general anabolism [Wischmeyer, 2013], [Mizock, 2001]. The patient is then usually discharged from the ICU to a normal hospital ward or rehabilitation facility [Wischmeyer, 2013].
Surviving the acute phase of acute injury primarily requires hemostasis and suppressing inflammation, especially with systemic inflammatory response syndrome (SIRS) and sepsis [Wischmeyer, 2013]. This is achieved by an accelerated metabolism, where critically ill patients show a protein catabolism resulting from stress hormone and cytokine release [Elke et al., 2014], [Wischmeyer, 2013]. The protein catabolism is fueled by amino acids (e.g. glutamine), especially drawn from the muscles (70%) and used for energy supply and immune response [Wischmeyer, 2013], [Mansoor et al., 2007], [Lecker et al., 1999]. How long the organism can drain its resources apparently depends on the individual pre-injury muscle mass and nutritional state before the injury, as e.g. glutamine reserves in the blood plasma can be exhausted within two days post-injury. According to this, increased protein intake during the acute and chronic phase of critical illness, should provide the metabolism with enough substrate, to retain reserves and body mass for recovery [Wischmeyer, 2013].

1.3 Nutrition in Critical Care

A quite common problem in hospitals is the malnutrition of patients, occurring in $30-50\%$ and being higher in critically ill patients (more than 50% worldwide). To reduce the protein catabolism in these times of diminished caloric gain, it is suggested to support the critically ill metabolism with proteins from an external source during the chronic and acute phase [Wischmeyer, 2013]. It remains debatable on how exactly ICU patients benefit from feeding, as e.g. low enteral nutrition is recommended for sepsis patients by the Surviving Sepsis Campaign, but it recently has been shown, that full enteral nutrition improves the outcome (reduced mechanical ventilation and mortality) for those patients [Elke et al., 2014].

1.4 Sepsis

Sepsis is among the 10 most frequent causes of death in the United States of America and a serious health problem worldwide, especially in the critically ill [Garcia-Alvarez et al., 2014a], [Wischmeyer, 2013]. It often results in the death of $\geq 25\%$ of the affected, with increasing incidence of e.g. $8.7-13\%$ in the United States of America over the last 30 years [Marik, 2014], [Dellinger et al., 2013], [Wilhelms et al., 2010]. In Europe the incidence of sepsis and severe sepsis is 37% and 30%,respectively [Marik, 2014]. Sepsis is diagnosed by clinical and laboratory assessment, where an increased blood lactate level (BLL) and its development over time can suggest the severity of a disease [Garcia-Alvarez et al., 2014a], [Handy, 2006]. Moreover, lactate is considered to be a major factor in restoring wounds and the healing process as a whole, as it e.g. nearly doubles collagen synthesis [Hunt et al., 2007], [Gladden, 2004], [Trabold et al., 2003].

1.5 Motivation

An important but not necessarily reliable indicator for sepsis severity and mortality rate is the amount of lactate in the blood. Larger quantities of lactate is produced in an accelerated, more catabolic metabolism. However, the specific lactate balance in both, normal metabolism and accelerated catabolism is not known [Garcia-Alvarez et al., 2014a]. Therefore it might be beneficial to simulate the development of e.g. sepsis in a model based on the lactate metabolism and use the gained knowledge and probably derived therapy to potentially reduce mortality from sepsis.

Part I

Problem Analysis

Chapter 2

Lactate Metabolism

This chapter introduces general agreements in nomenclature and considerations for future reference. Moreover it provides a basic overview on biochemical background information such as glycolysis and general lactate metabolism.

2.1 Introduction and Definitions

2.1.1 Lactate and Lactic Acid

The human organism can derive two molecules of lactic acid from one molecule of glucose by glycolysis and subsequent pyruvate conversion, which is presented in more detail in section 2.2.1 [Baynes and Dominiczak, 2014]. Glycolysis takes place in aqueous solutions, which means strong acids exist predominantly in their dissociated form - that is, cations and anions [Lane et al., 2009], [Horn, 2009],[Gladden, 2008], [Handy, 2006], [Robergs et al., 2004]. In the case of lactic acid that would be a hydrogen ion H^+ and a lactate ion, respectively. However, it is commonly not precisely distinguished between acid, ion, and salt, as lactate is used for all of them interchangingly. Consequently, this is not necessarily representing reality and leading to confusion in the understanding of the related metabolic reactions [Handy, 2006]. Moreover, since only L-lactate is produced naturally in the human metabolism, it is usually simply referred to as lactate [Lenzen, 2012], [Deutsch, 2003]. In the following lactate will therefore refer to the L-lactate anion, as depicted in figure 2.1.

2.1.2 Inorganic Phosphate

The anions of phosphoric acid ($H_xPO_4^{3-x-}$) are usually named inorganic phosphate (P_i) without distinguishing dihydrogen phosphate ($H_2PO_4^-$) from hydrogen phosphate (HPO_4^{2-}). Both exist physiologically in a pH-value depending equilibrium, which is described by the Henderson–Hasselbalch equation [Handy, 2006], [Robergs et al., 2004], [Mortimer and Schilling, 1980].

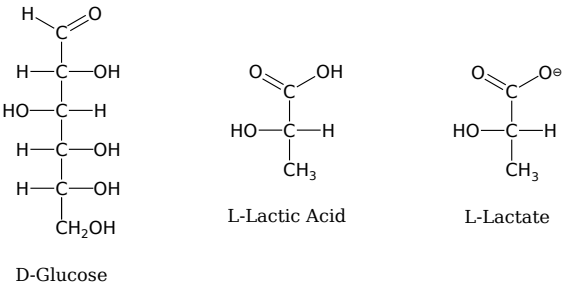

Figure 2.1: The figure shows the Fischer projections of glucose, lactic acid and lactate.

$$\mathrm{pH} = pK_a + log\frac{[\mathrm{H}^+][\mathrm{A}^-]}{[\mathrm{HA}]} \tag{2.1}$$

Rearranging this equation and inserting the values of physiological pH-value (pH = 7.4) and acid ionization degree ($pK_a = 7.2$) leads to [Löffler et al., 2007], [Handy, 2006], [Mortimer and Schilling, 1980]:

$$10^{(7.4-7.2)} = \frac{[\mathrm{H}^+][\mathrm{HPO}_4^{2-}]}{[\mathrm{H_2PO}_4^-]}. \tag{2.2}$$

Accordingly, hydrogen phosphate exists predominantly ($\approx 60\%$) and is further referred to as $\mathrm{P_i}$. However, the relation shifts towards dihydrogen phosphate with dropping pH-value [Weiler and Nover, 2008], [Robergs et al., 2004]. $\mathrm{P_i}$ is depicted in figure 2.2 as part of the ATPase reaction [Robergs et al., 2004].

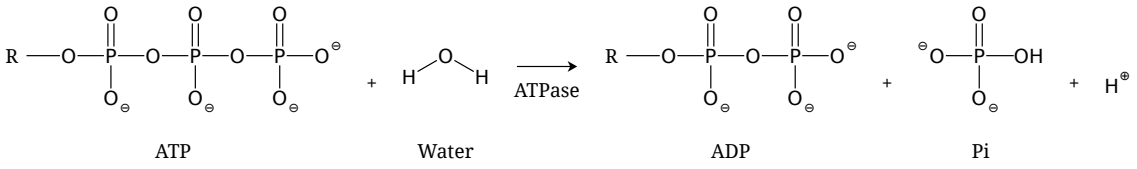

Figure 2.2: The figure shows the ATP hydrolysis generating ADP, $\mathrm{P_i}$ and a H^+. R denotes the adenosin and ribose backbone of the compound, which does not participate in the conversion.

2.1.3 Redox Coenzymes

The abbreviations of nicotinamide adenine dinucleotide (NADH), flavin adenine dinucleotide (FADH), and nicotinamide adenine dinucleotide phosphate (NADPH) are generally used for the redox coenzymes of the human body without distinguishing their oxidized from the reduced forms. Thus e.g. NADH comprises the oxidized form (NAD^+) as well as its reduced form ($\mathrm{NADH} + \mathrm{H}^+$) of NADH [Horn, 2009].
Redox coenzymes are coenzymes of oxydoreductases, they take part in the electron shift of redox reactions (electrons and protons are shifted simultaneously e.g. during glycolysis) [Horn, 2009; Berg et al., 2002]. Enzymes can only work with one type of coenzyme, which

enables a simultaneous catabolism (e.g. glycolysis, using NAD^+) and anabolism (e.g. fatty acid synthesis, using $NADPH + H^+$) [Horn, 2009].

2.2 Biochemistry and Physiology

2.2.1 Glycolysis

Glycolysis is the first step of glucose metabolism and can be found in the cytosol of any body cell. The second step is the breakdown of pyruvate into CO_2 and H_2O in the respiratory chain of the mitochondria (endoxidation) yielding $\geq$ 30 ATP [Baynes and Dominiczak, 2014], [Horn, 2009], [Handy, 2006].
Glycolysis describes the breakdown of glucose into pyruvate, during which energy is yielded in a two-phase process, as depicted in figure 2.3. The investment phase consumes two molecules of ATP, creating a gradient along the reaction chain and synthesizing fructose-1,6-biphosphate. Fructose-1,6-biphosphate is subsequently split in two molecules of glyceraldehyde-3-phosphate per glucose molecule, causing the following reactions to run twice, as depicted in figure 2.3.
In the beginning of the yield phase glyceraldehyde-3-phosphate is oxidized to 1,3-biphosphoglycerate using P_i and reducing NAD^+ to $NADH + H^+$. The reaction temporarily stores energy in the anhydride bond of carboxylic and phosphoric acid, to transfer the prior attached phosphate to ADP in the subsequent phosphoglycerate kinase reaction. This substrate-level phosphorylation regains the ATP molecules invested in the first phase of glycolysis. After an intramolecular redistribution phosphoenol pyruvate is generated by dehydration and subsequently converted into pyruvate to generate a total of two more ATP molecules, as seen in figure 2.3 [Horn, 2009]. The rate at which ATP is generated by glycolysis is more than twice the rate of ATP synthesis in the endoxidation [Juel, 1997]. The conversion of glucose-6-phosphate to lactate takes about $20 - 100$ms [Cerretelli and Samaja, 2003]. Moreover, it can be adjusted within a few seconds, allowing for quick reactions to a changing energy demand [Juel, 1997].

Glucose-Lactate Balance

During glycolysis two molecules of pyruvate are formed from one molecule of glucose, synthesizing two molecules of H_2O, ATP and $NADH + H^+$. However, the conversion of pyruvate into lactate reoxidizes the prior produced $NADH + H^+$ to NAD^+, as depicted in figure 2.4 [Horn, 2009], [Handy, 2006], [Berg et al., 2002]. Thus the net balance of the conversion from glucose into lactate can be found as [Bakker et al., 2013], [Lane et al., 2009], [Horn, 2009], [Rehm and Hammar, 2005], [Robergs et al., 2004]:

$$C_6H_{12}O_6 + 2ATP + 2HPO_4^{2-} \longrightarrow 2C_3H_5O_3^- + 2H^+ + 2ADP + 2H_2O. \tag{2.3}$$

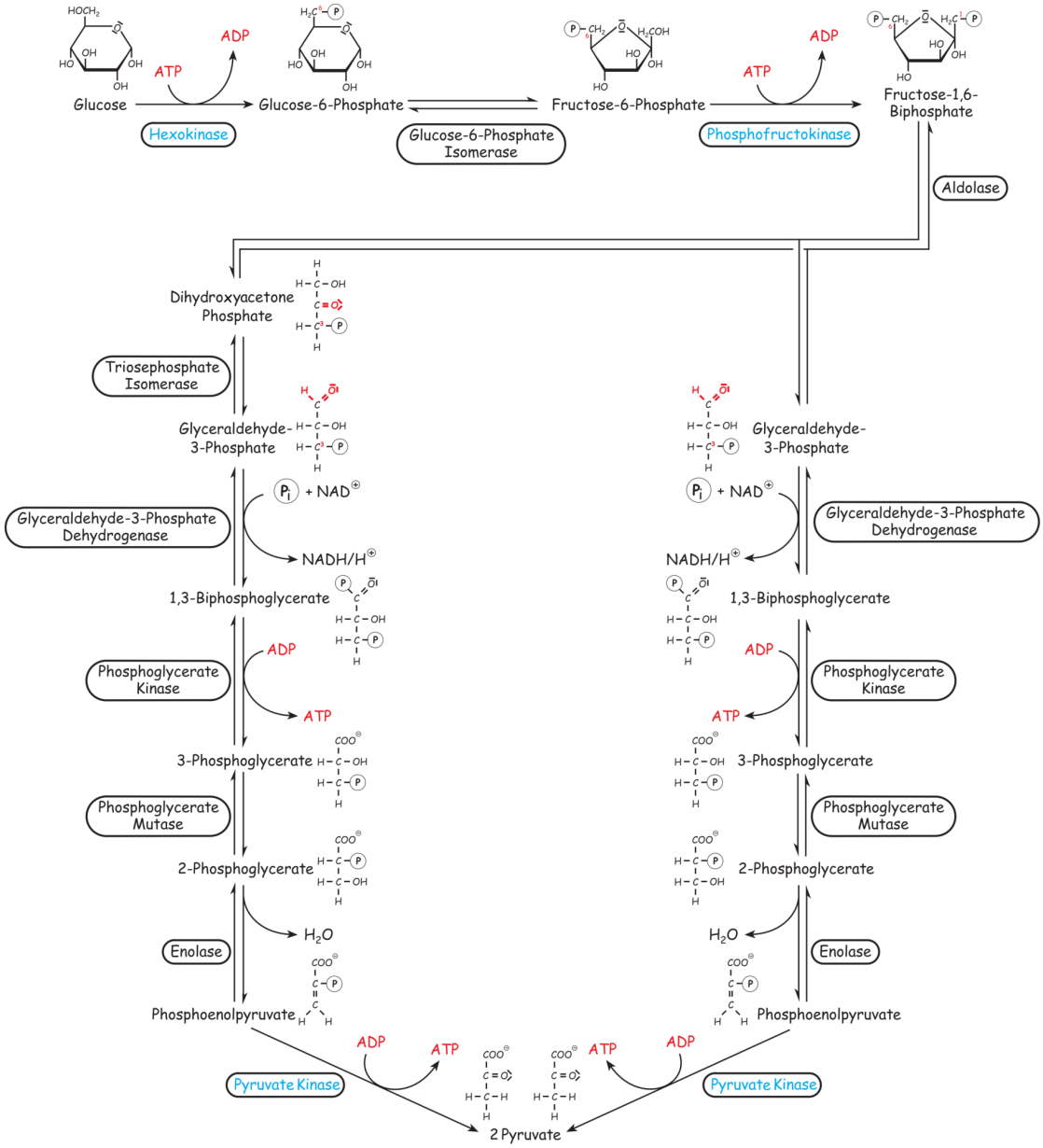

Figure 2.3: The figure shows a systematic overview of glycolysis. Key enzymes and thus the irreversible steps of glycolysis are marked blue. Edited from [Horn, 2009].

2.2.2 Lactate Metabolism

The reduction of pyruvate into lactate (outside of the mitochondria), as depicted in figure 2.4, gains NAD^+ for the glycolysis in case a NAD^+ shortage is built up in the cytosol [Horn, 2009], [Bolton, 2007], [Handy, 2006]. The conversion from pyruvate into lactate can occur for several reasons [Horn, 2009], [Handy, 2006].

- Reduced oxygen availability leading to increasing pyruvate concentration
- Pyruvate build up due to increased metabolism e.g. muscle activity

- Glycolysis exceeding mitochondria capacity caused by drugs e.g. catecholamines
- Metabolism of erythrocytes (no mitochondria)

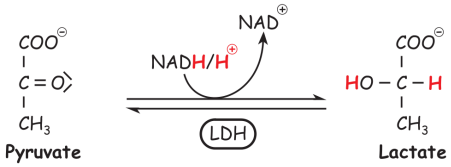

Figure 2.4: The figure shows the conversion of pyruvate into lactate, catalyzed by LDHase. Edited from [Horn, 2009].

Lactate then enters the bloodstream (along with its H^+) and is transported to well oxygenated areas of the body, e.g. liver and heart, to be oxidized into pyruvate, which is needed for many cellular reactions Horn [2009], [Bolton, 2007], [Handy, 2006], [Juel, 2004], [Juel, 1997], [Vincent, 1995]. During a stress situation (e.g. exercise or critical illness) the lactate production increases, exceeding the liver metabolism and leading to an accumulation of lactate in the blood [Garcia-Alvarez et al., 2014b], [Horn, 2009], [Bolton, 2007]. Lactate producing tissues include erythrocytes (20%), skeletal muscles (25%), brain (20%), adipose tissue (25%) and gut (10%), while lactate metabolizing tissues are heart, liver and kidneys. The resulting Cori cycle is depicted in figure 2.5 [Garcia-Alvarez et al., 2014b], [Handy, 2006], [Levy, 2006], [Cori, 1981].

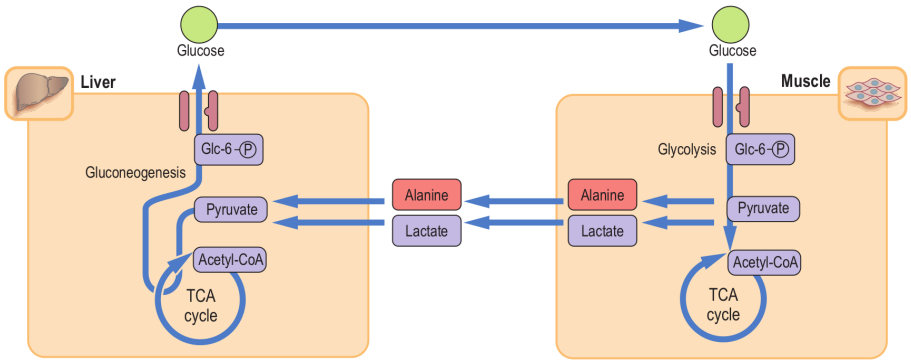

Figure 2.5: The figure shows the basic concept of constant lactate recycling in the Cori cycle. Following the glycolysis in one tissue (e.g. muscle) lactate is synthesized and released into the blood. Another tissue (e.g. liver) includes the lactate to gluconeogenesis synthesizing glucose, which is released into the blood. Other tissues can subsequently absorb glucose from the blood as required [Baynes and Dominiczak, 2014]. A more refined schematic of the Cori cycle is presented in figure 8.7 for the developed model.

Lactate Dehydrogenase

The puruvate lactate conversion is catalyzed by lactate dehydrogenase, which maintains an intracellular lactate-pyruvate ratio of 10 : 1 (20 : 1 or more during metabolic stress like sepsis) and is found as five isoenzymes in different organs of the human body [Garcia-Alvarez et al., 2014b], [Horn, 2009], [Handy, 2007], [Levy, 2006], [Levy et al., 2005], [Fall and Szerlip, 2005], [Levy et al., 1997], [Vincent, 1995]. A complete LDHase enzyme is formed by four subunits of the categories M or H [Horn, 2009].

- The heart isoenzyme LDH1 (H_4) oxidizes lactate to pyruvate
- The muscle isoenzyme LDH5 (M_4) reduces pyruvate to lactate.

However, the LDHase-5 predominantly found in the liver usually catalyzes the oxidation from lactate to pyruvate. Although being an intracellular enzyme, LDHase can be found in the bloodstream at a normal concentration of $40-230\text{IU/l}$ resulting from tissue breakdown [Horn, 2009], [Nathwani et al., 2005], [Vassella et al., 1967].

2.2.3 Gluconeogenesis

Gluconeogenesis describes the synthesis of glucose from lactate (from erythocytes and skeletal muscles), amino acids (e.g. alanine from the skeletal muscles), and glycerol (from the adipose tissue). Several organs are capable of gluconeogenesis [Baynes and Dominiczak, 2014], [Horn, 2009], [Gerich et al., 2001].

- Liver, which supplies the remaining organism with glucose.
- Kidneys, which also contributes to the blood glucose level (BGL) regulation as well as pH-value stabilization.
- Gut, to facilitate homeostasis during digestion.

The lactate dehydrogenase in cells of these organs and heart cells oxidize lactate to pyruvate, which can subsequently be used as input for either respiratory chain or gluconeogenesis. In gluconeogenesis the key reactions of glycolysis have to be circumvented using alternative reactions and different enzymes, as depicted in figure 2.6. Pyruvate is the precursor of gluconeogenesis, so alanine is also converted into pyruvate by alanine transaminase in the cytosol. Pyruvate is transported into a mitochondrion and carboxylated to oxaloacetate, consuming one molecule of HCO^- to form the coenzyme biotin-CO_2 and reducing one molecule of ATP to ADP in the process. Oxaloacetate has to be converted into malate in order to leave the mitochondrion before it is subsequently decarboxylated into phosphoenolpyruvate. At high-level lactate availability and thus sufficient $NADH + H^+$ (e.g. caused by high muscle activity) oxaloacetate can be directly converted into phosphoenolpyruvate by phosphoenolpyruvate carboxylase to avoid producing additional $NADH + H^+$ in the cytosol. The following conversions have to run twice to synthesize fructose-1,6-biphosphate and are the exact reversal of the glycolysis reactions, depicted in figure 2.3. Fructose-1,6-biphosphate is subsequently hydrolyzed to fructose-6-phosphate, which is converted into glucose-6-phosphate and finally hydrolyzed to glucose in the endoplasmic reticulum. Glucose is then released into the blood, as depicted in figure 2.6 [Horn, 2009].

The synthesis of one molecule glucose requires an equivalent of six ATP [Horn, 2009], [Levy, 2006]. However, two ATP are yielded from the glucose conversion during glycolysis, leading to a net loss of four ATP in gluconeogenesis [Horn, 2009]. Lactate is a permanently

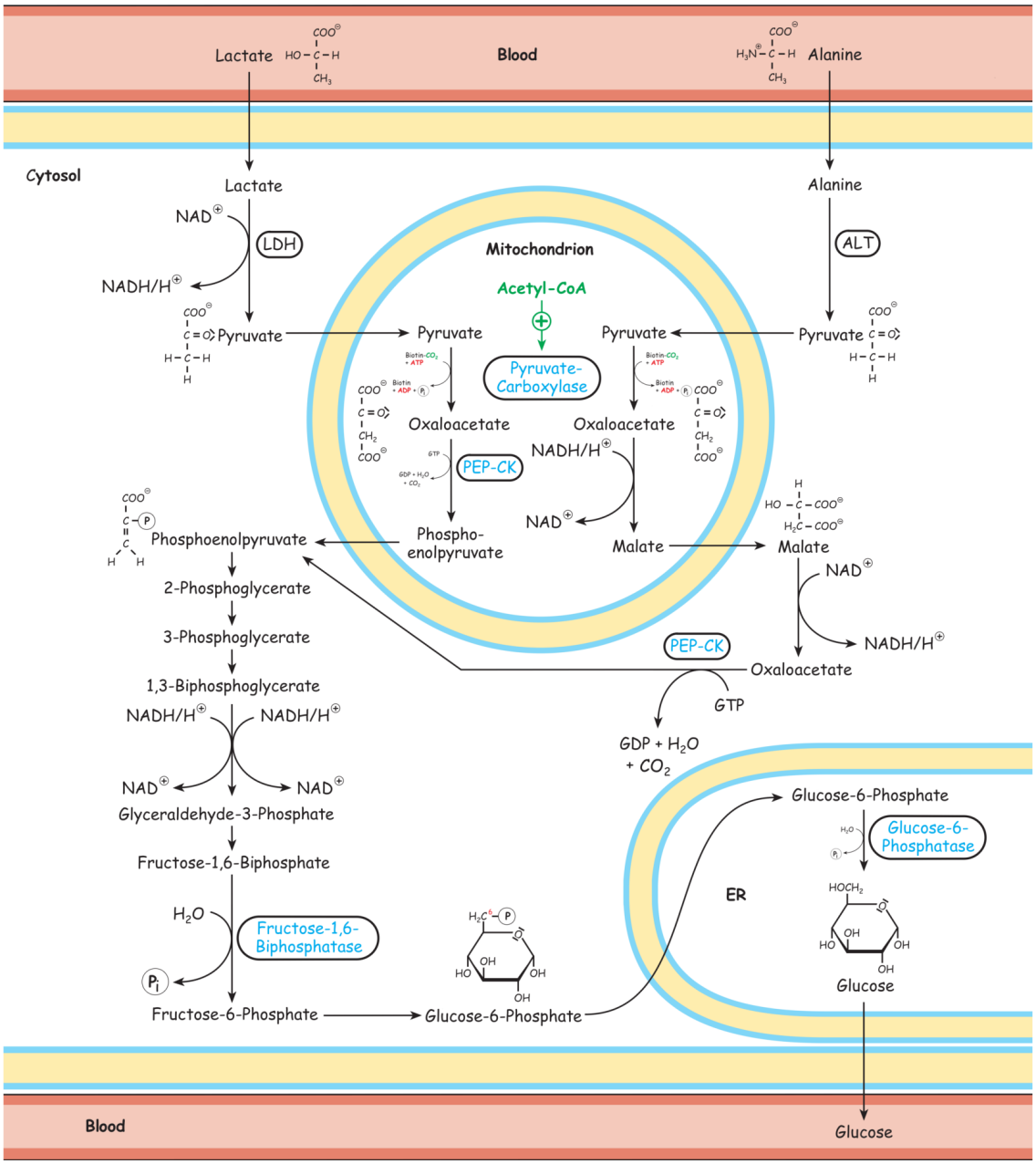

Figure 2.6: The figure shows a systematic overview of gluconeogenesis. Key enzymes and thus the irreversible steps of gluconeogenesis are marked blue, emphasizing the alternative pathways in comparison with glycolysis. Edited from [Horn, 2009]. LDH: lactate dehydrogenase, PDH: pyruvate dehydrogenase, PEP-CK: phosphoenolpyruvate carboxylase, ER: endoplasmic reticulum

available and the quantitatively most important substrate for gluconeogenesis, which is supplemented by alanine (liver) and glutamine (kidney) in times of need [Garcia-Alvarez et al., 2014a], [Horn, 2009], [Gerich et al., 2001]. The fatty acid decomposition delivers the energy required for this process, as well as glycerol, which can also be used as a substrate. Glycerol can enter gluconeogenesis after it has been converted into dihydroxyacetone phosphate, to form fructose-1,6-biphosphate. Other glucogenic amino acids ($3-4$ C-atoms) can enter gluconeogenesis when converted into pyruvate or via the the citric acid cycle into oxalocatate, respectively [Horn, 2009]. All free amino acids in blood and tissue combined amount to $70-100g$ in a 70kg adult [Löffler et al., 2007].

Glycogen

Glycogen is the storage polysaccharide of glucose in animal tissues, being stored in skeletal muscles (1g/100g tissue) and liver (10g/100g tissue) for own usage in energy metabolism and to supply the remaining organism with glucose, respectively. However, those reserves only last about 12 hours [Baynes and Dominiczak, 2014], [Horn, 2009], [Löffler et al., 2007]. Moreover, the breakdown of muscle glycogen results in the release of lactate into the blood, while hepatic glycogen breakdown releases glucose [Gerich et al., 2001]. The intersecting pathways of the underlying glucose metabolism are depicted in figure 2.8.

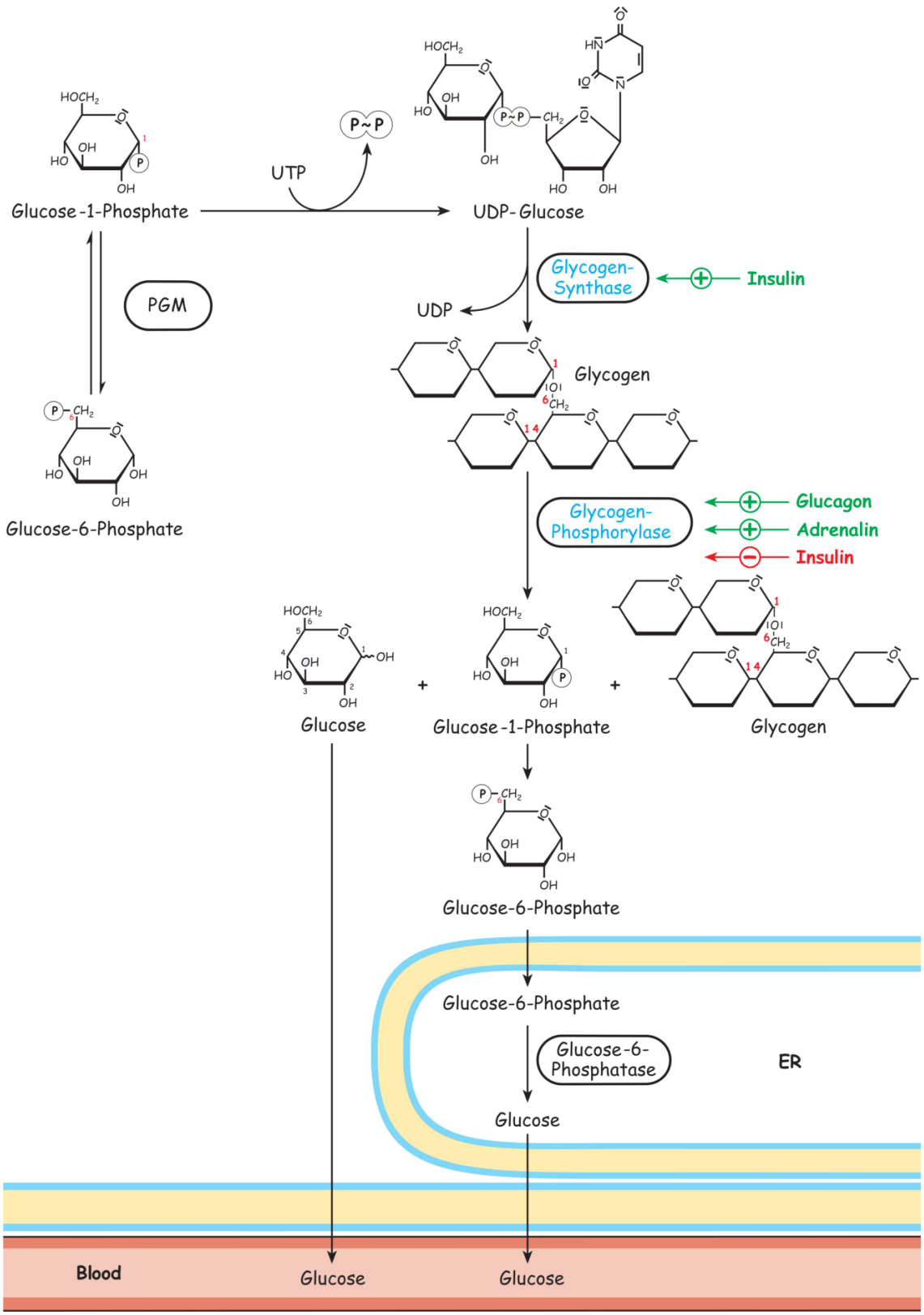

Figure 2.7: The figure shows a systematic overview of glycogen synthesis and glycogenolysis. Edited from [Horn, 2009]. PGM: phosphoglucomutase, ER: endoplasmic reticulum

2.3 General Metabolic Model

Based on the reaction chains of glycolysis, gluconeogenesis, and the glycogen metabolism of figures 2.3, 2.6,and 2.8, a diagram of the interacting main metabolites involved in the Cori cycle can be derived, as depicted in figure 2.8.

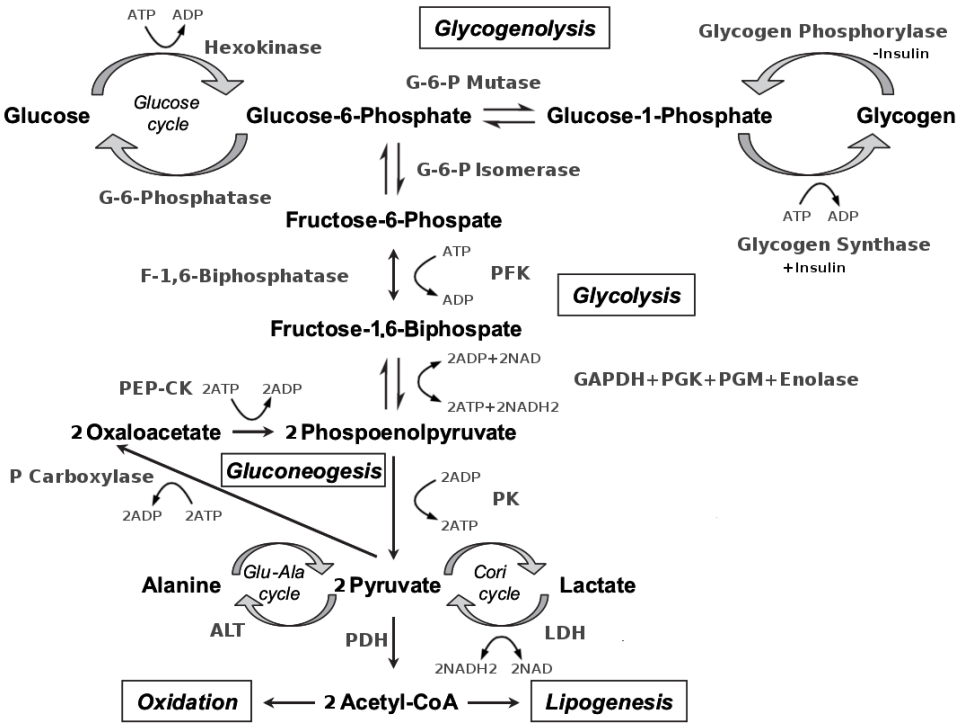

Figure 2.8: The figure shows a schematic overview of the intersecting pathways of glucose metabolism close to how they were modeled. Edited from [Van Cromphaut, 2009]. G-6-: glucose-6-, G-6-P: glucose-6-phosphate, F-1,6-: fructose-1,6-, PFK: phosphofructokinase, GAPDH: glyceraldehyde-3-phosphate dehydrogenase, PGK: phosphoglycerate kinase, PGM: phosphoglycerate mutase, PK: pyruvate kinase, ALT: alanine transaminase, PDH: pyruvate dehydrogenase, LDH: lactate dehydrogenase

Figure 2.8 forms the structural basis of the developed model. The reactions are adopted for the different organs and modified where necessary. The details are discussed in chapter 8 The $\rightleftharpoons$ arrows indicate that the reaction is catalyzed by the same enzyme in the forward and reverse reaction and also includes the alanine transferase and lactate dehydrogenase reactions. The $\longleftrightarrow$ indicates that the forward reaction is catalyzed by a different reaction then the reverse reaction and also applies to the glucose cycle and glycogen metabolism. All reactions, except the pyruvate dehydrogenase reaction, are essentially depicted reversible. The irreversible reactions (indicated by $\longrightarrow$) of gluconeogenesis were lumped in the model to make them reversible in one reaction, excluding oxaloacetate as relevant metabolites in the process. Combining several reactions the glycogen metabolism for the model also eliminated glucose-1-phosphate as a contributor to that process, as seen in chapter 7.3. The inhibiting and promoting effect of insulin in the glycogen metabolism is shown but not the inhibition or activation of any other enzyme that were incorporated in the model, as presented in chapter 7.3. The reaction of the pyruvate dehydrogenase complex to form acetyl-CoA is kept irreversible, as acetyl-CoA can not be reintroduced to the carbohydrate metabolism, which is indicated by its oxidation and contribution to

lipogenesis [Horn, 2009]. The redox coenzyme conversion by lactate dehydrogenase was divided between lactate and alanine in the model, as presented in their respective equations in chapter 7.3. Moreover, no H_2O, P_i or other contributing metabolites to specific reactions are shown, to focus on the model environment. As not all of the depicted reactions take place in the same cell at the same time, they have to be distributed to their respective organs, which are then individually considered for their contribution to the Cori-cycle.

Chapter 3

Clinical Relevance of Lactate

This chapter introduces the two major conceptions on why the blood lactate concentration is a valuable laboratory parameter to be considered in critically ill patients. Moreover, the parallels of hyperlactatemia and hyperglycemia are briefly mentioned.

3.1 Hyperlactatemia

Hyperlactatemia describes an elevated BLL ($> 2mmol/l$) at normal pH-value and has to be distinguished from lactic acidosis [Lee et al., 2008], [Bolton, 2007], [Vincent, 1995]. The development of a patients BLL and pH-value over time is used as solid predictor of mortality and illness severity and provides a basis for risk assessment in patients suffering from e.g. sepsis, shock, and trauma Garcia-Alvarez et al. [2014a], [Lee et al., 2008], [Bakker and Jansen, 2007], [Bolton, 2007], [Levy, 2006]. However, details in this mechanism remain unclear and it is debated on whether hyperlactatemia is a protective, maladaptive or physiological stress response of the human organism [Garcia-Alvarez et al., 2014b]. However, the causes of hyperlactatemia are various and it can be increased by hepatic dysfunction [Vincent, 1995].

- acute circulartory failure (e.g. by sepsis or obstructive shock)
- maloxygenation (e.g. by hypoperfusion or anemia)
- malnutrition

There are two major concepts for the origin of hyperlactatemia and they can be illustrated by equation 3.1, which is derived from the pyruvate-lactate conversion at equilibrium as seen in figure 2.4 [Levy, 2006], [Vincent, 1995], [Oliva, 1970], [Williamson et al., 1967], [Huckabee, 1958].

$$\frac{\text{Lactate}}{\text{Pyruvate}} = K\frac{[\text{NADH} + \text{H}^+]}{[\text{NAD}^+]} = \frac{10}{1} \tag{3.1}$$

Rewritten this equation indicates two possibilities for hyperlactatemia [Handy, 2007], [Levy, 2006], [Vincent, 1995], [Kruse et al., 1990], [Oliva, 1970], [Huckabee, 1958].

$$\text{Lactate} = \text{Pyruvate} \cdot K\frac{[\text{NADH} + \text{H}^+]}{[\text{NAD}^+]} \tag{3.2}$$

Type A Reoxidation of NADH + H^+ to NAD^+ in the mitochondria is suspended by hypoxia (hypoxia-associated hyperlactatemia)

Type B Lactate increase caused by increased substrate consumption in glycolysis leading to a pyruvate accumulation and subsequently more lactate (hyperlactatemia associated with increased glycolysis but not stress from hypoxia)

There is no general agreement on which of the factors or to what extent they contribute to the clinical observation hyperlactatemia. However, more recently type A and B are considered as equally valid to explain hyperlactatemia in different situations [Handy, 2007], [Levy, 2006], [Vincent, 1995], [Kruse et al., 1990], [Oliva, 1970], [Huckabee, 1958].

3.1.1 Sepsis-Associated Hyperlactatemia

Patients suffering from sepsis can exhibit an elevated BLL of up to 15mmol/l. However, the exact pathomechanism is debated and unclear [Garcia-Alvarez et al., 2014a]. Sepsis-associated hyperlactatemia is generally assumed to indicate hypoxia as a result of hypoperfusion, leading to organ failure. This relative lack of oxygen is said to suspend the endoxidation in mitochondria of the affected tissue, forcing the tissue to convert pyruvate from the glycolysis into lactate to restore the redox potential and enable further glycolysis [Garcia-Alvarez et al., 2014a], [Levy, 2006]. Thus the oxygen deficient metabolism is characterized by an increased lactate-pyruvate ratio, glucose usage, and BLL as well as a decreased energy production [Levy, 2006]. Hyperlactatemia resulting from hypoperfusion is especially likely in shock situations resulting from reduced cardiac output e.g. septic shock with catecholamine-resistent cardiocirculatory collapse [Levy, 2006]. More recently it is assumed that lactate is an important metabolite in the physiological stress response of the human organism that indicates inflammation or metabolic stress rather then hypoperfusion [Garcia-Alvarez et al., 2014a], [Bolton, 2007], [Gladden, 2004]. Accordingly, inflammation and catecholamines (e.g. adrenalin) triggered an increased glycolysis and muscle lactate production that rise above the oxidative capacities of the mitochondria. The resulting elevated BLL is attributed to pyruvate, which is produced by this accelerated glycolysis and transamination and subsequently converted into lactate, since the concentration of pyruvate and lactate is continuously balanced by LDHase [Garcia-Alvarez et al., 2014a], [Garcia-Alvarez et al., 2014b], [Bakker et al., 2013], [Levy,

2006]. Moreover, lactate clearance appears to be reduced in septic patients, which slightly contributes to the accumulation of lactate in the blood [Bolton, 2007], [Levraut et al., 1998].

3.1.2 Exercise-Associated Hyperlactatemia

The BLL increases not only as a result of pathophysiological stress e.g. sepsis, but also physiologically during exercise [Garcia-Alvarez et al., 2014b]. This exercise-associated hyperlactatemia is often considered to result from insufficient oxygenation (hypoxia), which caused muscle fatigue and led to tissue damage by acidosis. This does not necessarily have to be true, as acidosis and muscle fatigue both can be attributed to various other factors (e.g. increased H^+ concentration) and increased BLL being only one of them, implying a grater complexity. Moreover, lactate and glucose apparently compete with each other over being a substrate for oxidation in skeletal muscles. With lactate being the preferred one, more glucose is left to be consumed by other body tissues. During this process the gluconeogenesis remained constant, indicating the significance of lactate as a valuable precursor in gluconeogenesis [Gladden, 2004]. However, the issue has not been resolved with clear results yet [Garcia-Alvarez et al., 2014b], [Gladden, 2004].

3.2 Lactic Acidosis

Acid-base imbalances in ICU patients are seen frequently and with various implications for the outcome. However, it is often unknown where they originate from [Gunnerson et al., 2006]. A metabolic acidosis is associated with a negative balance of nitrogen moieties and body protein loss by increased protein breakdown in the skeletal muscles [Mitch et al., 1994]. Lactic acidosis is defined as a metabolic acidosis (pH-value of < 7.35) accompanied by an arterial BLL of $\geq 5 mmol/l$ [Lee et al., 2008], [Fall and Szerlip, 2005], [Hardern and Quinn, 2003], [Stacpoole et al., 1994]. Among hospitalized and non-surgical patients the prevalence of lactic acidosis is approximately 1% Fall and Szerlip [2005]. Acidosis refers to the elevated H^+ concentration, as a decreasing pH-value from e.g. 7.4 to 7.2 leads to a 60% increase in H^+ concentration, rising from 40 to $63 nmol/l$ [Boyd and Walley, 2008]. However, lactate or an increased BLL does not in itself contribute to that [Robergs et al., 2004], [Vincent, 1995]. And neither does the conversion from pyruvate to lactate [Lane et al., 2009]. The balance equation for glucose-lactate conversion 3.3 does not accurately represent the causality H^+ generation [Lane et al., 2009], [Robergs et al., 2004].

$$C_6H_{12}O_6 + 2ATP + 2H_xPO_4^{3-x-} \longrightarrow 2C_3H_5O_3^- + 2(x-1)H^+ + 2ADP + 2H_2O \quad (3.3)$$

Under normal resting conditions (pH = 7.4) x is approximately 1.3, resulting in a production of $2.4H^+$ during glycolysis [Lane et al., 2009]. Consequently, the H^+ increase from high energy phosphate turnover (ATP hydrolysis), as depicted in 2.2. Sufficient oxygenation enables the recovery of ATP metabolites in the respiratory chain of the mitochondria without acidosis [Bakker et al., 2013], [Fall and Szerlip, 2005], [Robergs et al.,

2004], [Vincent, 1995]. Here H^+ are needed to reduce molecular oxygen and P_i and ADP are recycled to form ATP. Metabolic acidosis is therefore the result of an energy (ATP) demand exceeding the ATP supply from the mitochondria and the resulting increasing turnover of non mitochondrial ATP, which leads to a H^+ build up in the cytosol [Robergs et al., 2004], [Vincent, 1995].

3.3 Hyperglycemia

As seen in figure 2.5, glucose is an important part of the Cori cycle and there are parallels and overlap between hyperlactatemia and hyperglycemia. Hyperglycemia and insulin resistance in critically ill patients is often observed (50%) and associated with metabolic stress [Van Cromphaut, 2009], [Mizock, 2001]. Additionally, hyperglycemia is often associated with a poor outcome for ICU patients by increasing the risk of e.g. myocardial infarction and multiple organ failure, which leads to increased morbidity and mortality [Pretty et al., 2010].

3.4 Hypoglycemia

An increased amount of amino acids in the blood stream, induced by e.g. parenteral nutrition, stimulates the insulin secretion and might result in hypoglycemia, with the effect potentially being enhanced by a high amount of in the blood stream. If the BGL is dropping to less than 2 mmol/L the central nervous system (CNS) is inadequately supplied with glucose, resulting in coma and hypoglycemic shock [Lacherade et al., 2009], [Singer et al., 2009], [Despopoulos and Silbernagl, 2003]. Hypoglycemia triggers the secretion of glucagon, the main antagonist of insulin, from the pancreas to stimulate glycogenolysis for compensation [Despopoulos and Silbernagl, 2003]. Hypoglycemia aggravates the outcome of an ICU patient by an increased risk of e.g. myocardial infarction, multiple organ failure, or polyneuropathy - all conditions increasing the patient mortality. To effectively prevent this scenario the BGL of the patient is kept between approximately 6 mmol/L and 8 mmol/L [Pretty et al., 2010]. Moreover, hypoglycemia seems to be preventable when associated with high-calorie parenteral feeding [Kavanagh and Goodship, 2010].

3.5 Lactate Models

The carbohydrate metabolism in general and lactate metabolism in particular is of interest for several branches of medicine. In sports medicine the anaerobic threshold is a central area of interest e.g. to assess exercise performance [Proshin and Solodyannikov, 2013], [Billat, 1996]. In emergency medicine, intensive care, trauma medicine and anesthesiology on the other hand, whole blood lactate level of a patient is measured for initial evaluation or e.g directing the resuscitation of trauma patients, [Bolton, 2007].
There are several models in existence, that describe a wide range of aspects regarding the lactate metabolism. Some describe the whole human organism, some subsystems

(e.g. carbohydrate metabolism of red blood cells), others even cancer cells, [Proshin and Solodyannikov, 2013], [Mendoza-Juez et al., 2012], [Wahl et al., 2011], [Brumen and Heinrich, 1984]. However, in sports medicine those models are not widely applied, which is ascribed to the non-individualized applicability of those models to e.g personal training [Proshin and Solodyannikov, 2013].

Chapter 4

Models

This chapter presents the reasoning behind modeling, specifies a special modeling technique (compartmental modeling), and describes applications of metabolic models. Finally an introductory algorithm on the modeling procedure is given.

4.1 Reasons for Modeling

A model is an abstraction from reality to a feasible or comprehensible level and thus generally involves some extend of simplification. Modeling methodology attempts to address the complexity usually found in natural systems. This complexity arises from various factors, such as hierarchy and interconnectivity of processes, as well as time-varying, nonlinear and stochastic properties of the system. In a physiological context hierarchy comprises the levels of molecules and chemical reactions, cell and organ structures, and finally the organism as a whole. Each level is controlled by complex processes of e.g. feedback and hormonal regulation. Feedback is especially important in the regulation of biochemical reactions. In these overlapping processes it is often impossible to directly measure aspects of interest, which therefore have to be deduced. An example for that is the measurement of hormones in the blood stream, when direct measurement of the secretion by the respective gland might often be inaccessible.
A model is distinctively influenced by its purpose, as is its quality. A model might be conceptual, statistical, mathematical or graphical and thus differently suited for different applications, such as the testing of hypotheses, examination of design or not least of all teaching. A mathematical description can be a very powerful and compact model and used to interpret data collections and subsequently predict the behavior of a system. The quality of the model can then be assessed by mapping theory with clinical data
There are different approaches to modeling. Empirical data driven models (black box models) make quantitative descriptions on systems based on their in- and output. The result is a mathematical description with only lose (implied) connection to the underlying process e.g. physiology. They are very useful when the underlying process is unknown or not understood and when knowledge about the system dynamic is needed without

knowing the specifics of a process. Opposite to data modeling there is system modeling, where detailed representation of the underlying process is pursued. The amount of detail in the representation is dependent on available prior knowledge about the system, the assumptions made, and also the purpose. The can be classified by their approaches into e.g. static/dynamic, deterministic/stochastic, lumped/distributed, linear/nonlinear and so on, with various combinations of each other.
Solving the model leads to simulation and examination of the output behavior often over time and of numerous variables. However, simulation can be used during the process of modeling, e.g. to clear up uncertainties and after completing the model, e.g. for making predictions based on the model output, [Carson and Cobelli, 2013].

4.2 Compartmental Models

Compartmental models can be used do deal with (nonlinear) dynamics in a System. They usually consider mass balances to quantitatively describe metabolites and their kinetic properties. A compartment is assumed to be a substantially and kinetically homogeneous amount of substance. The finite number of compartments possess specified connections (flux) that determine properties of e.g production, transport, distribution, use and interactions between the considered substances, may they be exo- or endogenous. The bloodstream is a prime example for a compartment, as is the blood glucose within it. Other substance in the bloodstream compartment e.g. blood lactate require a separate compartment, leading to multiple bloodstream compartments within one model. Similar substances can be lumped to reduce the dimensionality and thus complexity of the system, [Cobelli and Carson, 2008].

4.3 Steps of Physiological Modeling

A feasible approach to modeling physiological networks is summarized in the block diagram depicted in figure 4.1 and was used to develop the model presented in 8.

Step 1 has been discussed in chapter 2. Steps 2 and 3 are presented in chapters 6 and 8, respectively.

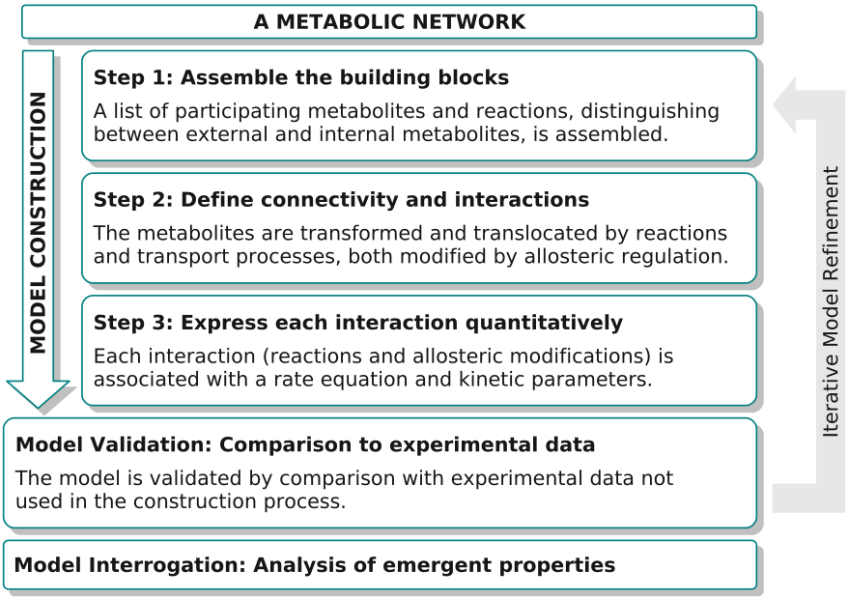

Figure 4.1: The figure shows an algorithm for successfully modeling physiological pathways. However, the larger the metabolic network, the more practical obstacles may arise in describing it mathematically, [Steuer and Junker, 2009].

4.4 Structural Modeling

Structural metabolic models only require knowledge of the system stoichiometry. As the stoichiometry characterizes all metabolite species (S), reaction rates (v), and their interactions, it forms the basis for any arbitrary depth the model shall possess. Branching and moiety-conserving reactions are a common sight in biochemistry and can be represented in a metabolic network as depicted in figure 4.2 [Rohwer, 2012].

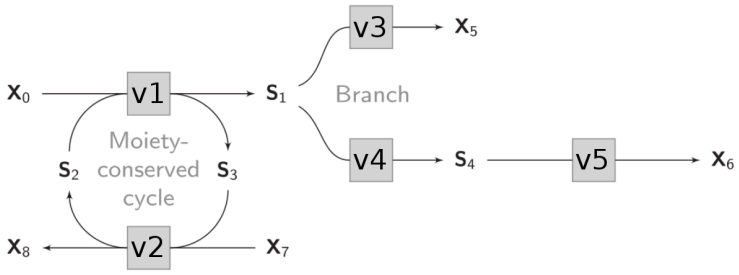

Figure 4.2: The figure shows a basic metabolic network with no particular grounding in reality. The frequently encountered branching and moiety-conserving reactions are incorporated. In this network the summarized amount of species S_2 and S_3 remains constant. The species x mark external (outside e.g. the cell membrane) metabolites that are not considered for the model description of the (internal) metabolism in the stoichiometric matrix given by figure 4.3 [Rohwer, 2012], [Steuer and Junker, 2009]. Edited from [Rohwer, 2012].

The stoichiometric coefficients, determining how many molecules are involved in any given reaction, can be summarized in a stoichiometric matrix $\mathbf{N} = \mathrm{m} \times \mathrm{r}$ (metabolites $\times$ reactions), depicted in figure 4.3 [Rohwer, 2012], [Steuer and Junker, 2009].

Multiplying the stoichiometric matrix with a vector $\mathbf{s} = [\mathrm{S}_1, ..., \mathrm{S}_\mathrm{n}]^T$, containing all species S_1 to S_n, and a vector $\mathbf{v} = [\mathrm{v}_1, ..., \mathrm{v}_\mathrm{n}]^T$, containing all reaction rates, leads to a system

$$\mathbf{N} = \begin{array}{c} \\ S_1 \\ S_2 \\ S_3 \\ S_4 \end{array} \begin{array}{c} \begin{array}{ccccc} \text{v}1 & \text{v}2 & \text{v}3 & \text{v}4 & \text{v}5 \end{array} \\ \begin{pmatrix} 1 & 0 & -1 & -1 & 0 \\ -1 & 1 & 0 & 0 & 0 \\ 1 & -1 & 0 & 0 & 0 \\ 0 & 0 & 0 & 1 & -1 \end{pmatrix} \end{array}$$

Figure 4.3: The figure shows the stoichimetric matrix corresponding to the basic network of figure 4.2. Species are assigned to the rows, while the reactions are assigned to the columns. The values of the matrix elements are completely arbitrary but correctly represents the consumed and produced metabolites by negative and positive coefficients, respectively [Rohwer, 2012]. Edited from [Rohwer, 2012].

of ordinary differential equation (ODE), as given in equation 4.1. The ODE describe the change in concentration of all metabolites over the entire network [Rohwer, 2012], [Steuer and Junker, 2009]. The complete procedure is summarized in figure 4.4.

$$\frac{d\mathbf{s}}{dt} = \mathbf{N}\mathbf{v} \tag{4.1}$$

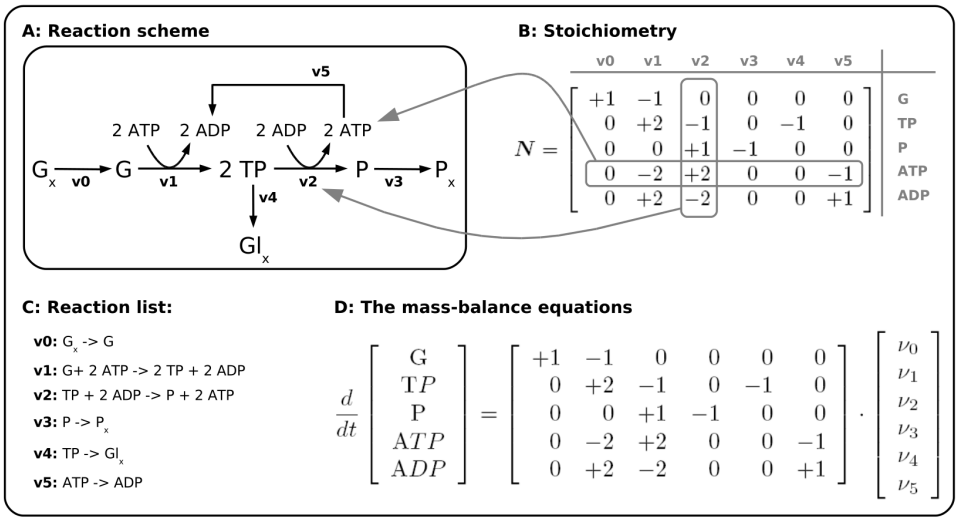

Figure 4.4: The figure shows the steps of developing the equations to describe, in this case, a metabolic model of glycolysis in a single cell organism, as well as the representation of those steps [Steuer and Junker, 2009].

In structural models $\mathbf{v}$ contains unknown kinetic properties. However, equation 4.1 can be set to zero and attempted to be solved for the unknowns, generally yielding only flux values or flux ratios. In case knowledge of kinetic properties is available $\mathbf{v}$ is considered to be a set of functions of the metabolite concentrations $\mathbf{s}$. Thus the entire development of the system over time for both concentrations and fluxes can be calculated, transforming the structural into a kinetic model [Rohwer, 2012]. Assuming that $\mathbf{v}$ only contains linear or bilinear equations, the general solutions for the system of ODE can be found by computing first the eigenvalues (λ) and corresponding eigenvector of $\mathbf{N}$, which results in equation 4.2 with the eigenvector matrix $\mathbf{B} = [\mathrm{EV}_1, ..., \mathrm{EV}_\mathrm{n}]$ and the fundamental solving system $\mathbf{z} = [\mathrm{e}^{\lambda_1 \mathrm{x}}, ..., \mathrm{e}^{\lambda_1 \mathrm{x}}]^{T1}$ [Steuer and Junker, 2009], [Merziger, 2004].

[1] In case $\lambda_1 = \lambda_2 \longrightarrow \mathbf{z} = [\mathrm{e}^{\lambda \mathrm{x}}, \mathrm{xe}^{\lambda \mathrm{x}}]^T$

$$\mathbf{y} = \mathbf{Bz} \tag{4.2}$$

However, the structure of the model can generally be explored by computing a solution space (flux cone) for e.g. flux-balance analysis [Rohwer, 2012] [Kauffman et al., 2003]. This solution space describes the metabolic capacity an organism posses [Kauffman et al., 2003].

4.4.1 Flux-Balance Analysis

However, the key of flux-balance analysis is experimental data on the fluxes, which are not always obtainable, potentially leaving (some) kinetic equations undefined. This often results in a significant degree of freedom for the system, as there likely are more internal metabolites then boundary fluxes, which is emphasized by the number of independent vectors spanning the right Nullspace (kernel) $\mathbf{N}$ of [Rohwer, 2012], [Steuer and Junker, 2009]. Moreover, it is feasible to set up $\mathbf{N}$ as a square matrix to to facilitate the analysis and use e.g. the rank($\mathbf{N}$) to isolate conservation reactions and determine the dimensions of the right Nullspace $\mathbf{K}$, which is spanned by r-rank($\mathbf{N}$) column vectors that satisfy the relation $\mathbf{NK} = 0$ as depicted in 4.5 [Steuer and Junker, 2009].

$$\mathbf{v^0} = \begin{bmatrix} 1 \\ 1 \\ 2 \\ 2 \\ 0 \\ 2 \end{bmatrix} \alpha_1 + \begin{bmatrix} 1 \\ 1 \\ 1 \\ 1 \\ 1 \\ 0 \end{bmatrix} \alpha_2$$

Figure 4.5: The figure shows all feasible steady state vectors $\mathbf{v}^{\mathbf{0}}$=$\mathbf{v}(\mathrm{S}^0)$, which are described by two (r-rank($\mathbf{N}$)=2) linearly independent basis vectors that form the right Nullspace [Steuer and Junker, 2009]. The free parameters α_1 and α_2 represent the dependent fluxes as a linear combination of the independent fluxes [Rohwer, 2012], [Steuer and Junker, 2009]. The numbers are again arbitrary. Edited from [Steuer and Junker, 2009].

The system has to be optimized for the undetermined parameters using an objective function. This function can e.g. be maximized for growth of a certain metabolite or minimized for the uptake of a particular substrate, as depicted in figure 4.6 [Rohwer, 2012].

A large drawback of this method is that the models are only valid for the steady state they have been built for, limiting their applicability. Moreover, it is unpredictable how certain parameters have to be tweaked quantitatively (e.g. enzyme activity) to achieve a specific effect for the system, as no particular kinetic information contained within the models. A way to minimize this problem is to introduce additional constraints based on e.g. thermodynamics to determine the direction of reactions and make then consistent with measured metabolite concentrations to limit the solution space (hybrid model) [Rohwer, 2012].

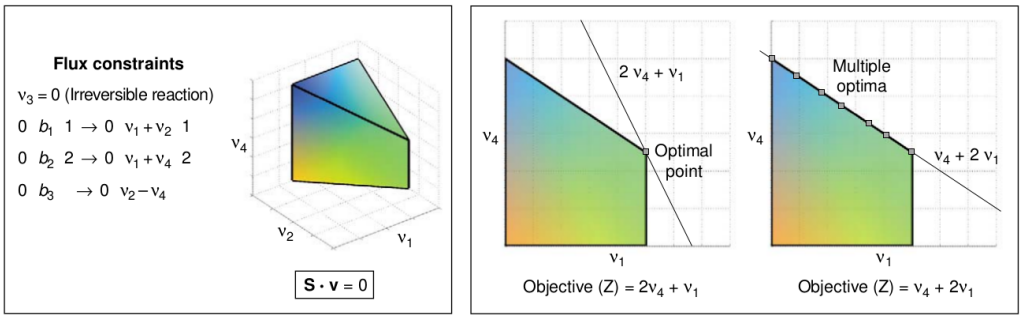

Figure 4.6: The left figure shows the flux constraint using experimental or other external, while the left figure shows the system optimization by using different objective functions [Kauffman et al., 2003].

4.5 Kinetic Modeling

Any kinetic model inherently implies a structural model as well and can therefore be subjected to a structural analysis as well. The system is usually reduced and simplified as far as possible without eliminating its core characteristics, as depicted in figure 4.9. The resulting models are quite specific in design, purpose, and applicability. Considering influences on the reaction rates by e.g. substrate concentrations or other effectors enables the model to exhibit dynamic behavior. This consideration is typically expressed by the Michaelis-Menten equation, as given in figure 4.7 [Rohwer, 2012]

$$v_4 = \frac{\frac{V_f}{K_1}\left(s_1 - \frac{s_4}{K_{\text{eq}}}\right)}{1 + \frac{s_1}{K_1} + \frac{s_4}{K_4}}$$

Figure 4.7: The figure shows a reversible reaction of one substrate and product, expressed in a Michaelis-Menten equation that corresponds to the basic network of figure 4.2. S_1 and S_4 denote the respective substrate concentrations, V_f denotes the maximum reaction velocity in the (forward) direction of the arrow, which equals to the limiting rate of the reaction [Rohwer, 2012]. K_1 and K_4 denote the Michaelis-Menten constants of the reaction, which are specific to the binding affinity metabolite and enzyme [Rohwer, 2012], [Gizak et al., 2008]. K_{eq} denotes the equilibrium constant for the reaction [Rohwer, 2012]. Edited from [Rohwer, 2012].

The rate laws should comprise the general behavior of the reaction and it is not necessary to cover every detailed aspect of the enzyme reaction to sufficiently describe the reaction behavior in dependence of the substrate concentrations. However there different underlying mechanism that describe an enzymatic reaction and influence the kinetic equations. The complexer the equation, the more terms and constants e.g. on inhibition have to be included. When further including transcription and translation, the enzyme concentrations are made into variables and the resulting differential equations have to be added to the existing differential equations for the network [Rohwer, 2012]

4.5.1 Bottom-Up Assembly of a Kinetic Model

The bottom-up approach to build a model is described by figure 4.9 The network structure is determined by the number of reactions included. Too many might potentially limit applicability of the system due to high processing power [Schallau and Junker, 2010] The

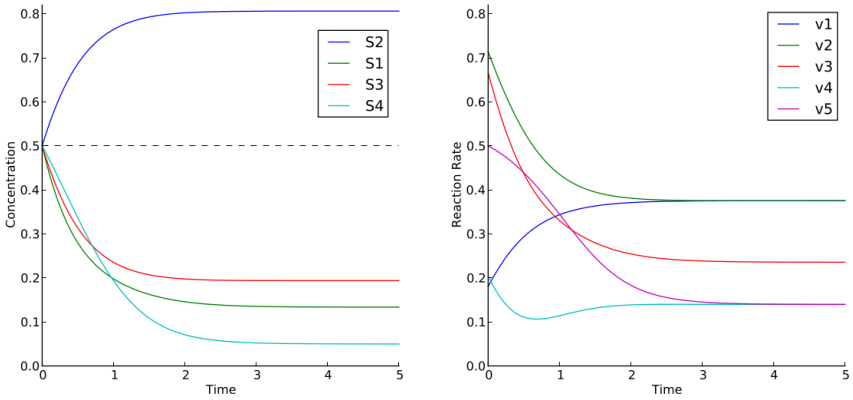

Figure 4.8: The left figure shows the change of metabolites over time, while the right figure shows the changing reaction rates in dependence of time. Corresponding to the network depicted in figure 4.2, the graphs show a simulation of reversible Michaelis-Menten kinetics and arbitrary values The initial metabolite concentration was set to 0.5 for all species. The moiety conservation of S_2 and S_3 can be observed, as their concentration graphs mirror around the symmetry axis 0.5 (dashed line) and the sum of their concentrations constantly yielding 1.0 [Rohwer, 2012].

stoichiometry of the reactions involved are generally well known for many organisms. Determining the enzyme kinetics include set up of representative rate laws, by considering e.g. enzyme activation or inhibition and the reaction mechanism. On the other hand it includes the parameter elimination of those rate laws e.g. inhibition, equilibrium and Michaelis-Menten constants. Gathering these data from literature is a time-consuming and cumbersome task, even with the help of enzyme databases like BRENDA [Rohwer, 2012]. It is common practice to substitute unavailable data for desired cells with data from (closely) related organisms, at best measured under in vivo conditions [Rohwer, 2012], [Lambeth and Kushmerick, 2002]. However, this is not necessarily a criterion met, as reaction mechanisms tend to be explored under environmental conditions optimal for the respective enzyme. These conditions might not be close to physiological conditions in a cell, concerning e.g. pH-value and temperature. There are, however, efforts for standardization [Rohwer, 2012]. Representative rate equations correspond to the underlying thermodynamics of a reaction Lambeth and Kushmerick [2002]. This means that the reversibility of a reaction has to be considered, otherwise the model behavior is influenced [Rohwer, 2012]. Moiety conserving metabolites are directly entered into the rate equations with their constraints as fixed parameters [Rohwer, 2012], [Wolf et al., 2000]. The moiety conserving reactions yield two non-independent equations, of which one can be ignored [Steuer and Junker, 2009]. Once initial concentrations of all metabolites are found the ODE system is integrated to yield the time-course or it is solved to obtain the steady state. To assess the model quality it subsequently needs to be validated. This is usually done by comparing the model output with independent data e.g. measurements of fluxes [Rohwer, 2012].

4.5.2 Top-Down Assembly of a Kinetic Model

In contrast to the bottom-up approach to modeling there is also the top-down approach, where the model parameters are iteratively adjusted to fit the model output to independent data (optimization). This technique, however, has the disadvantage of disjointing model

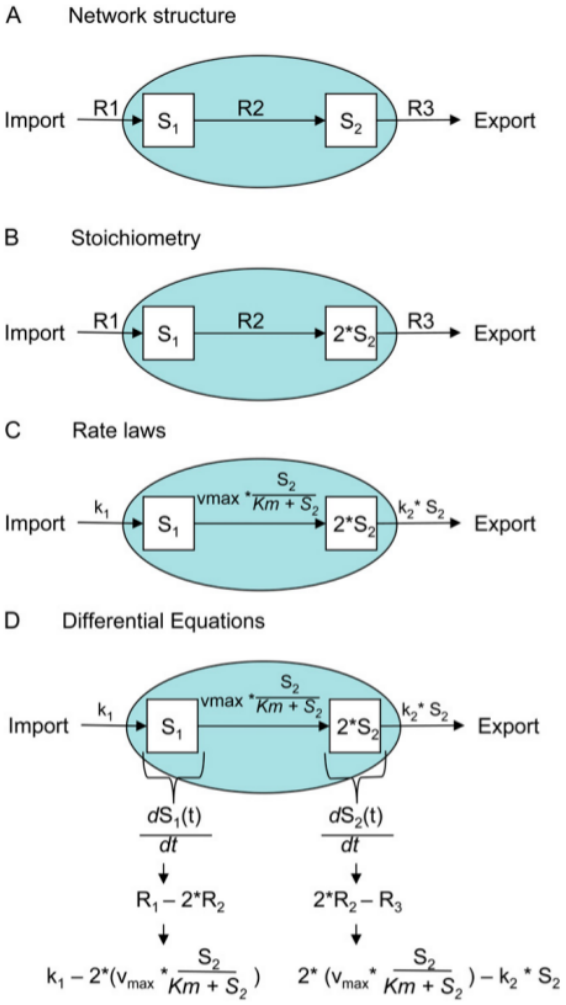

Figure 4.9: The figure shows the steps of putting together all available data. A describes the network connectivities. B introduces stoichiometric data that lead to numerical dependencies. C defines rate laws that govern the reaction velocity. D generates the ODE by combining stoiciometric data with the rate laws to describe time dependently changing concentration of a metabolite [Schallau and Junker, 2010].

parameters from e.g. enzyme properties that are grounded in reality. The connection to the process intended to model, is further weakened when empirical rate equations are used to build the model in the first place. Moreover, during this process it becomes increasingly unclear where model construction and validation begin and end, respectively. This has the inherent possibility of the model being inapplicable, as no physiological process is necessarily described by the tweaked parameters that therefore might not represent any physiological properties [Rohwer, 2012].

Chapter 5

Summary

This chapter will summarize the previously discussed topics as a transition to the problem statement at the end of this chapter.

5.1 Metabolism in Critical Illness

The physiological reactions to critical illness, such as sepsis and trauma, and acute stress are comparable to a large extent. They are both characterized by hormone induced catabolism and increased glucose production associated with insulin resistance and in case of critical illness infection and tissue damage. Increased levels of adrenalin and glucagon promote glycogenolysis and enhance the glucose output of the liver. An elevated level of cortisol in the blood induces increased muscle protein breakdown and gluconeogenesis. At the same time the muscular glucose uptake is reduced and leads to physiological stress hyperglycemia [Van Cromphaut, 2009], [Tappy, 2008]. This might exacerbate to hyperinsulinemia in combination with insensitivity to insulin mediated by the immune response, which also increases the glucose turnover. Moreover, these effects have time to build up and amplify over the duration of the illness. They are undoubtedly beneficial in the short term to provide highly demanded substrate for the body, but lead to increased protein breakdown, loss of body mass, and organ failure in the long term [Tappy, 2008].

5.2 Physiology

Glucose is an essential carbohydrate for the human metabolism and its primary energy source. Body structures like the brain are highly dependent on the direct consumption of glucose [Despopoulos and Silbernagl, 2003]. The Cori cycle is a metabolic feed back loop for BGL control. It involves the processes of glycolysis, gluconeogenesis, glycogenolysis, with their respective biochemical and hormonal regulation. The three processes are linked by exchanging the exchanging the main metabolites glucose, lactate and alanine and powered by the energy provided by the oxidation of fatty acids. Their hormonal

regulation is mainly accomplished by insulin and glucagon from the pancreas, which trigger interactions of organs such as liver and muscle. and interactions by [Baynes and Dominiczak, 2014], [Horn, 2009], [Despopoulos and Silbernagl, 2003].

5.3 Modeling and Metabolic Control

A physiological model is an approximation of reality expressed in mathematic formulas. Simplifications are made to reduce the mathematical complexity and focus on the relevant processes for a specific purpose, which can e.g. be of descriptive, explanatory, and predictive nature. Predicting the reaction of the human organism or organ systems to an input might be of general practical interest and can be simulated by the model to e.g. assess the pharmacokinetics and -dynamics of an administered drug [Cobelli and Carson, 2008].
Another application using the predictive character of mathematical equations is the control of certain metabolic factors, as is the case in glucose and insulin level control [Pielmeier, 2010], [Pretty et al., 2010]. Additionally, advice on how to adjust a parameter to reach a specified state may be derived from such a model [Pielmeier, 2010].

5.4 Problem Statement

Problem Statement Reflecting upon the described background information and aspects, the following problem statement was found:

How can a computerized model, within the scope of critically ill and possibly septic patients, sufficiently reflect the human lactate metabolism (Cori cycle) on the cellular level, to provide the basis for an application as a clinical decision support system in intensive medicine?

Premise Metabolic stress from either exhausting performance requirements (e.g. physical activity) or from critical illness (e.g. sepsis) represent a comparable metabolic problem for the organism and therefore result in similar physiological reactions of the body.

Objectives

- Devising a mathematical model that represents the relevant physiological processes of the Cori cycle based on the biochemical reactions of the glycogen metabolism, glycolysis, and gluconeogenesis
- Develop and test a computer program incorporating that model for validation purposes

Part II

Methods

Chapter 6

Quantification of the Cori Cycle

6.1 Central Metabolites of the Cori Cycle

6.1.1 Glucose (CID:79025)

The maximum glucose oxidation rate is 500g (2000$kcal$) per day for a 70kg adult. The rate of glucose production in sepsis, trauma, and burn injury patients is approximately $20 - 25\mu mol/kg * min$, which is roughly double the normal rate (approximately $10 - 12\mu$mol/kg*min) [Mitrakou, 2011], [Wolfe, 1999], [Consoli et al., 1990b]. Adrenalin doubles renal glucose production, increases glucose release of the liver by 50%, and overall glucose production by 60%. Moreover, adrenalin stimulated renal glucose release can be solely responsible for the increase in blood glucose after three hours [Stumvoll et al., 1997]. Glycogenolysis and glucoeogenesis each contribute approximately 50% to the normal glucose production [Mitrakou, 2011], [Stumvoll et al., 1997]. $75 - 80\%$ of the blood glucose in the postabsorptive state is released by the liver and the remaining $20 - 25\%$ by the kidneys. BGL peak $1 - 1.5$ hours after ingestion, before they return to normal within $3 - 4$ hours [Mitrakou, 2011]. Normoglycemia ranges between $3.3 - 7.8mmol/l$ but is around $5.6mmol/l$ over the day [Mitrakou, 2011], [Van Cromphaut, 2009]. During fasting a BLL of $4.4 - 6.7$ is maintained, which would be approximately $14g$ in an $70kg$ adult [Tappy, 2008]. Moreover, the glucose oxidation rate during exercise is approximately $0.7mmol/kg * min$ [Miller et al., 2002].

6.1.2 Lactate (CID:5460161)

Lactate can be released physiologically or pathophysiologically by any organ [De Backer et al., 1997]. The rate of lactate production under normal conditions ranges between $0.8 - 1mmol/kg * h$, which is approximately $1500mmol/l * d$ and results in a normal BLL of $0.6 - 2mmol/l$ [Garcia-Alvarez et al., 2014a], [Garcia-Alvarez et al., 2014b], [Bolton, 2007], [Levy, 2006], [Fall and Szerlip, 2005], [Levraut et al., 1998], [Meyer et al., 1998], [Consoli et al., 1990b]. However, lactate buildups occur e.g. in wounds ($4 - 15mmol/l$) [Hunt et al., 2007], [Trabold et al., 2003]. Lactate is oxidized at a rate of approximately

$7.8-8.5\mu mol/kg*min$, while Lactate-glucose conversion occurs at a rate of approximately $1.4-4.2\mu mol/kg*min$ [Consoli et al., 1990b], [Jenssen et al., 1990]. Gluconeogenesis from lactate is increased during exercise and exhibits a rate of approximately $0.2mmol/kg*min$ [Miller et al., 2002]. The combined conversion into glucose (34.2%) and oxidation of lactate (61.9%) is attributed to 96% of its turnover (approximately 100% use) [Bellomo, 2002], [Consoli et al., 1990b]. Alanine and lactate conversion is responsible for $60-80\%$ of gluconeogenesis [Consoli et al., 1990a]. Lactate clearance can reach $0.8-1.8mmol/min$ [Garcia-Alvarez et al., 2014a], [Fall and Szerlip, 2005], [Bellomo, 2002]. About 45% of the blood lactate originates from glycolysis of blood glucose, the rest from glycogenolysis [Consoli et al., 1990b]. During exercise lactate appearance and disappearance rate in the blood have been determined to be approximately $1mmol/kg*min$. The lactate oxidation rate under these conditions is approximately $0.8mmol/kg*min$ [Miller et al., 2002]. Lactate, as a gluconeogenetic precursor, contributes at a rate of $3.0\mu mol/kg*min$ to the BGL, which is approximately 24% of the lactate turnover in the blood. Moreover, lactate is oxidized at a rate of $4.2\mu mol/kg*min$, which makes 35% of its turnover. The combined oxidation (60%) and conversion into blood glucose is responsible for 90% of the lactate disappearance from the blood, generally limiting the lactate metabolism to those two processes [Consoli et al., 1990a]. Lactate producing tissues and their rate for an $70kg$ adult with a carbohydrate consumption of $300g$ and overall lactate production of $115g$ daily are given in detail in table 6.1 [Smith et al., 2005].

Tissue	Lactate Production (g/d)
Red Blood Cells	29
Skin	20
Brain	17
Skeletal Muscle	16
Kidneys	15
Gut	8
Other Tissues	10

Table 6.1: Lactate producing tissues and their rate

6.1.3 Alanine (CID:5950)

The combined amount of alanine, glutamine, and glutamate forms approximately 80% of the free amino acid pool, from which proteins can be synthesized [Rutten et al., 2005]. The alanine blood concentration amounts to $0.2-0.4mmol/l$ but only 30% originate from muscle catabolism [Mizock, 2001], [Meyer et al., 1998], [Consoli et al., 1990b], [Jenssen et al., 1990]. The rest is generated by pyruvate transamination (from glucose) in association with deamination of other amino acids Mizock [2001]. Alanine appears at a normal rate of approximately $4\mu mol/kg*l$ and is oxidized at a rate of approximately $1.3\mu mol/kg*min$, while alanine-glucose conversion occurs at a rate of approximately $1.8\mu mol/kg*min$. The combined conversion into glucose (44.2%) and oxidation of alanine (31.4%) is attributed to 75% of its turnover [Consoli et al., 1990b].

Glutamine (CID:5961)

Glutamine accounts for a 20% of all amino acids in the blood, which is double the amount of alanine. Both are the most important amino acids to serve as a precursor for gluconeogenesis. The postabsorptive basal alanine and glutamine turnover in the blood plasma amounts to $4.5\mu mol/kg * min$ and $5\mu mol/kg * min$, respectively. However, the glutamine plasma concentration is approximately double the concentration of plasma alanine at $0.6mmol/l$ and $0.3mmol/l$, respectively [Stumvoll et al., 1999], [Felig et al., 1970]. However, this relation is, if at all, only inversely reflected by the amount they occur in proteins (alanine 7.6% and glutamine 3.9%) Löffler et al. [2007]. Glutamine is produced by muscles ($19 - 168\mu mol/l$), lung ($56\mu mol/l$), and adipose tissue ($12\mu mol/l$). It is consumed by gut ($57\mu mol/l$), liver ($20\mu mol/l$), kidney ($35 - 110\mu mol/l$), and brain ($13\mu mol/l$) [Stumvoll et al., 1999].
Additionally, normal plasma glucagon and insulin have been measured as $84 - 186ng/l$ and $51 - 59pmol/l$, respectively [Meyer et al., 1998], [Consoli et al., 1990b].

6.2 Central organs of the Cori Cycle

6.2.1 Skeletal Muscles

Skeletal muscles represent about $20 - 32kg$ of the body mass and store approximately $200 - 1000g$ glycogen [Horn, 2009], [Tappy, 2008], [Blomstrand and Saltin, 1999], [Consoli et al., 1990b]. In the absorptive state the skeletal muscles consume approximately 30% of the supplied glucose for glycogen synthesis [Mitrakou, 2011]. In the postabsorptive human metabolism approximately 70% of the alanine and 40% of the lactate ($12mg/kg * min$) released into the bloodstream originate from skeletal muscles [De Backer et al., 1997], [Consoli et al., 1990a]. Moreover, they contribute to over 80% of total gluconeogenesis, which is responsible for more than 50% of their uptake from the blood. The skeletal muscles remove 30% of both alanine and lactate from the blood and about 80% in combination with the liver [Consoli et al., 1990a]. Combined blood lactate and glucose oxidation contribute approximately 60% to the overall carbohydrate oxidation during exercise, while the remainder is provided by muscle glycogen [Miller et al., 2002]. The normal oxidation of proteins and amino acids is attributed to $5 - 10\%$ of the overall energy production. The muscle degradation following depleted glycogen reserves during exercise has been determined to be approximately $7.3 - 12.0g/h$ [Blomstrand and Saltin, 1999]. This would translate to an overall muscle degradation of $26.3 - 43.2g/h$ during stress, which is more than 2% of the entire muscle mass a day [Griffiths and Hall, 2010], [Blomstrand and Saltin, 1999]. Moreover, in polytrauma patients approximately 25% of the available plasma proteins are used in in the overall protein synthesis of the body, which is increased from the normal 11% [Mansoor et al., 2007]. Sepsis increases the muscular glucose uptake by 67% [Mizock, 2001].

Alanine Alanine appears in the blood circulation at a rate of $4.2\mu mol/kg * min$. The alanine uptake rate by the skeletal muscles is approximately $1.6\mu mol/kg * min$ being

about 37% of its uptake from the blood. On the other hand skeletal muscles release alanine at a rate of approximately $2.9 - 3.0\mu mol/kg * min$, which accounts for $71 - 72\%$ of its appearance in the blood circulation [Consoli et al., 1990a], [Consoli et al., 1990b]. Alanine, as a gluconeogenetic precursor, contributes at a rate of $1.3\mu mol/kg * min$ to the BGL, which is approximately 30% of the alanine turnover in the blood. Moreover, alanine is oxidized at a rate of1.8μmol/kg*min, which makes 44% of its turnover. The combined oxidation (30%) and conversion into blood glucose is responsible for 75% of the alanine disappearance from the blood, leaving the rest for protein synthesis [Consoli et al., 1990a].

Lactate Lactate appears in the blood circulation at a rate of $12.7\mu mol/kg/min$ [Consoli et al., 1990b]. The lactate uptake rate by the skeletal muscles is approximately $3.3 - 3.9\mu mol/kg * min$ being about 27% of its uptake from the blood. On the other hand skeletal muscles release lactate at a rate of approximately $5.5 - 5.7\mu mol/kg * min$, which accounts for approximately $44 - 45\%$ of its appearance in the blood circulation [Consoli et al., 1990a], [Consoli et al., 1990b]. However during exercise the lactate release increases to $1.3mmol/min$ and the uptake to $0.6mmol/min$. Moreover, the lactate release is influenced by the glycogen reserves (low glycogen, increased lactate release) [Blomstrand and Saltin, 1999].

Glucose The Glucose uptake rate by the skeletal muscles is approximately $2.4\mu mol/kg * min$ being about 21% of its uptake from the blood [Grau and Bonet, 2009], [Van Cromphaut, 2009], [Consoli et al., 1990a], [Consoli et al., 1990b]. This would translate to a normal glucose uptake of $48 - 76\mu mol/min$ and $1.5 - 1.9mmol/min$ during exercise, when assuming an overall muscle mass of $20 - 32kg$ [Horn, 2009], [Blomstrand and Saltin, 1999], [Consoli et al., 1990b]

6.2.2 Liver

The liver weights around $1.5kg$ and stores approximately $70 - 120g$ glycogen [Horn, 2009], [Heinemann et al., 1999], [Tappy, 2008]. Blood glucose uptake by the liver is stimulated at a BGL of $> 6.7mmol/l$, while a BGL of $< 3.6mmol/l$ stimulates hepatic glucose secretion from both glycogenolysis and gluconeogenesis [Lacherade et al., 2009], [Wolfe, 1999]. The liver can remove blood lactate at a rate of approximately $800 - 1800mmol/min$ Garcia-Alvarez et al. [2014a], [Marko et al., 2004]

Glycogenolysis Glycogenolysis is generally attributed to 50% of the overall glucose production [Stumvoll et al., 1997]. In the absorptive state the liver consumes 45% of the supplied glucose for glycogen synthesis [Mitrakou, 2011]. Glycogenolysis rate in the liver is approximately $5.5 - 8.4\mu mol/kg * min$, being responsible for about 45% of the total glucose release into the bloodstream [Gerich et al., 2001], [Consoli and Nurjhan, 1990]. Glycogenolysis is accounted for approximately $50 - 90\%$ of the hepatic glucose output after over night fasting and ceases completely after $48 - 60$ hours of fasting, at which point the glycogen reserves are depleted [Mitrakou, 2011], [Van Cromphaut, 2009], [Wolfe, 1999], [Consoli and Nurjhan, 1990]. At this point glcogenolysis is completely replaced by

gluconeogenesis ($7.5\mu mol/kg * min$) for glucose production [Wolfe, 1999], [Consoli and Nurjhan, 1990]. The glycogen storage and glycogenolysis rate over time is given in more detail in table 6.2 [Smith et al., 2005].

Fasting (h)	Glycogen Storage ($\mu mol/g$ liver)	Glycogenolysis Rate (μmol/kg*min)
0	300	-
2	260	4.3
4	216	4.3
24	42	1.7
64	16	0.3

Table 6.2: Development of glycogeneolysis over time

Gluconeogenesis

Hepatic Uptake The combined liver and muscle metabolism removes 80% of alanine and 60% of lactate from the blood circulation [Levy, 2006], [Fall and Szerlip, 2005], [Consoli et al., 1990a]. The liver alone removes $45 - 55\%$ of the alanine and $35 - 50\%$ of the lactate from the blood [Consoli et al., 1990a]. Generally spoken the hepatic uptake of the four main precursors (lactate, alanine, glutamine, and glycerol) is attributed to 50% of overall gluconeogenesis [Stumvoll et al., 1997]. The hepatic blood flow is approximately $700ml/min$ (normal $1600ml/min$) while exercising with an lactate uptake rate of about $1.0mmol/min$ (normal $0.2-0.4mmol/min$) [van Hall, 2010], [Jenssen et al., 1990]. During sepsis the hepatic lactate uptake from the blood is increased two to threefold [Mizock, 2001].

Hepatic Output The normal glucose release rate by the liver is approximately $8 - 12\mu mol/kg * min$ and the combined alanine (10%) and lactate (20%) conversion in gluconeogenesis is approximately $3.6 - 3.9\mu mol/kg * min$, which is $17 - 25\%$ of the total hepatic glucose output in postabsorptive state of the body [Meyer et al., 1998], [Consoli et al., 1990a], [Consoli and Nurjhan, 1990]. Moreover, in the postabsorptive state (fasting) $25 - 55\%$ of the over all glucose release comes from hepatic gluconeogenesis [Gerich et al., 2001], [Consoli et al., 1990a], [Consoli and Nurjhan, 1990], [Consoli et al., 1990b].

6.2.3 Kidney

Catabolic processes generate acids (e.g. pyruvatic acid during glycolysis) and thus H^+ because they are dissociated. During metabolic acidosis those H^+ are eliminated in the renal cortex by synthesizing glucose from two acids, as described in section 2.2.3 [Baynes and Dominiczak, 2014], [Horn, 2009], [Gerich et al., 2001], [Stumvoll et al., 1997].

Renal Uptake Gluconeogenesis is the exclusive way for renal glucose production, which can increase considerably during fasting [Garcia-Alvarez et al., 2014b], [van Hall, 2010].

Lactate Although the liver is mostly responsible for the lactate uptake from the blood, approximately $20 - 30\%$ is attributed to the kidneys and occurs at a rate of approximately $160\mu mol/min$ [Garcia-Alvarez et al., 2014b], [van Hall, 2010], [Levy, 2006], [Bellomo, 2002]. At the same time the kidneys contribute 50% of the lactate conversion into glucose [Garcia-Alvarez et al., 2014b]. In contrast to the liver, this ability increases with acidosis ($6.7\mu mol/min$) [Garcia-Alvarez et al., 2014b], [Bellomo, 2002], [Gerich et al., 2001]. Over 50% of renal lactate uptake is used in renal gluconeogenesis. The total renal lactate removal increases from 16% (at a pH-value of 7.45) to 44% (at a pH-value of 6.75) [Bellomo, 2002]. Additionally, the kidneys contribute to approximately $4 - 5\%$ of the overall lactate release into the circulation [van Hall, 2010].

Glucose Normal renal glucose removal appears at a rate of 2.3μmol/kg*min and is approximately 20% of the overall glucose disappearance from the blood [Stumvoll et al., 1997]. The glucose uptake by the kidneys decreases in periods of metabolic stress while renal glucose uptake and release increase [Gerich et al., 2001]. However, it accounts for approximately $10 - 20\%$ of the overall glucose uptake from the blood, at a rate of $10\mu mol/min$ [Mitrakou, 2011], [Stumvoll et al., 1997].

Renal Output The renal blood flow is $1000 - 1800ml/min$ and the rate of normal renal glucose output is approximately $1.7 - 3.2\mu mol/kg * min$ which accounts for $20 - 25\%$ of the total glucose release of the organism [Gerich et al., 2001], [Stumvoll et al., 1997]. Under severe conditions the kidneys were reported to release glucose at a rate of $880\mu mol/min$, [Stumvoll et al., 1997]. Renal glucose release can increase threefold during hypoglycemia ($3.2mmol/l$), elevating its contribution to total glucose release to 36% [Mitrakou, 2011], [Meyer et al., 1998]. Consequently, the kidneys are responsible for approximately $40 - 50\%$ of total gluconeogenesis that accounts for $85 - 90\%$ of the renal glucose release [Mitrakou, 2011], [Gerich et al., 2001], [Stumvoll et al., 1997]. Additionally, about 50% of the in blood circulation available lactate, 70% of glutamine, and $17 - 35\%$ of glycerol are metabolized in renal gluconeogenesis. Mediated by fatty acids, elevated insulin concentrations increase glucose uptake and equally reduce renal and hepatic glucose release. Adrenalin on the other hand stimulates renal gluconeogenesis (twofold) and also more than hepatic gluconeogenesis. Moreover, renal glucose release is reported to compensate for $50 - 100\%$ of hepatic glucose release e.g. in sepsis [Bellomo, 2002], [Gerich et al., 2001].

Urinary Disposal Urinary lactate elimination is usually 2%, even hat high BLL ($> 20mmol/l$) resulting from exercise [Fall and Szerlip, 2005], [Bellomo, 2002]. Higher urinary lactate excretion ($10 - 12\%$) has been observed when the BLL is artificially kept at $10mmol/l$, though [Bellomo, 2002]. Renal glomerular filtration of the blood is capable of filtering $180l/d$ [Mitrakou, 2011], [Bellomo, 2002]. Consequently approximately $180g$ of glucose is filtered and reabsorbed into the organism [Mitrakou, 2011]. However, renal glucose reabsorption is inhibited at a BGL of $12 - 13mmol/l$ because all Na^+-glucose symporters are occupied [Vivian, 2014], [Hick and Hick, 2000].

6.2.4 Blood

Erythrocytes Red blood cells (erythrocytes) constantly consume approximately $40g$ glucose per day under most conditions [Horn, 2009], [Wolfe, 1999]. Moreover, they release lactate at at rates between $4.1mg/min$ and $16mg/min$ [De Backer et al., 1997], [Chapman et al., 1962]. However, the lactate production from glycolysis in the red blood cells increases with the pH-value. At $pH = 7.5$ they produce approximately $15mmol/l$, which increases to $20mmol/l$ and at $pH = 8.0$. [Chapman et al., 1962].

Leukocytes White blood cells (leukocytes) release lactate at a rate of $11mg/min$ [De Backer et al., 1997].

6.2.5 Heart

Myocardium primarily relies on fatty acids for energy supply. However, during periods of stress (e.g. fasting or physical exercise) the heart switches to carbohydrate metabolism and oxidizes lactate [Lacherade et al., 2009], [Gladden, 2008]. An increased stress level, expressed by increased BLL, blood flow, and myocardial oxygenation, the heart covers up to 60% of its energy demand with lactate [Gladden, 2008]. Cardiac lactate and glucose oxidation at rest is approximately $10 - 15\%$ and 8%, respectively. During exercise it is increased to approximately 30% and 14%, respectively [van Hall, 2010]. A cardiac lactate oxidation rate of $16.3 - 24.4nmol/min$ has been observed in animals [Liu and Spitzer, 1978].

6.2.6 Brain

Lactate It has been theorized that lactate was the main product of glycolysis in the brain and therefore an important metabolic precursor in its metabolism, as is the case in skeletal muscles [Gladden, 2008]. Cerebral lactate consumption was considered to be insignificant on the overall body scale and that there was no net uptake or release of cerebral lactate under normal conditions [Gladden, 2008], [Quistorff et al., 2008]. More recent insight shows that lactate can cover approximately $7 - 8\%$ of the cerebral energy demand under normal conditions, which increases to $20 - 25\%$ as the BLL rises. Normally the brain releases lactate at a rate of $50 - 60\mu mol/min$ and contributes 8% to the overall lactate production, which increases to 13% during exercise. However, an artificially increased BLL ($7mmol/l$) resulted in a cerebral lactate uptake of approximately $160\mu mol/min$ at rest, which increased even more during exercise ($280\mu mol/min$) and was associated with a decreased glucose uptake [van Hall, 2010], [van Hall et al., 2009]. Cerebral lactate uptake from the blood is $1 - 1.3$mmol/min during exercise. [Quistorff et al., 2008]. Additionally, cerebral lactate uptake amounts to 11% during exercise [van Hall, 2010].

Glucose In the absorptive state the brain consumes approximately 15% of the supplied glucose and it constantly consumes approximately $120g$ ($1mg/kg * min \approx 1.5g/kg * d$)

glucose per day [Mitrakou, 2011], [Horn, 2009], [Tappy, 2008], [Berg et al., 2002], [Wolfe, 1999]. At rest the CNS contributes to 80% of the blood glucose uptake in the body. Cerebral glucose uptake from the blood is $0.5mmol/min$ during exercise. [Quistorff et al., 2008]. Half of the glucose uptake of CNS and muscles is mediated by insulin [Van Cromphaut, 2009]. The large energy requirements of the CNS cannot be met by perfusion at a BGL below $2.0mmol/l$, where it relies on substitution with lactate for energy supply [Lacherade et al., 2009]. Moreover, the cerebral glycogen reserves have been estimated to last approximately $3.5min$ at normal energy consumption, assuming a glycogen and phosphocreatin store of 10 and $5mmol/kg$, respectively. Under hypoxia this would produce $20mmol$ of lactate, when assuming an oxygen consumption of $2\mu mol/g$ [Quistorff et al., 2008].

6.2.7 Gut

The epithelium of the small intestine converts some amino acids into glucose during digestion, since ATP is available in abundance during ingestion and allows for anabolism [Horn, 2009].

6.2.8 Lungs

The contribution of pulmonary lactate uptake and release is usually negligible [van Hall, 2010], [De Backer et al., 1997]. However, normal lactate release at a rate of $80-300\mu mol/l$ has been reported, as well as a lactate production rate of $12000mmol/min$ in patients with acute pulmonary disease van Hall [2010], [Marko et al., 2004].

6.2.9 Adipose Tissue

Glycerol Glycerol in the bloodstream is by and large produced by adipose tissue breakdown. In the postabsorptive state 50% of the blood glycerol is converted into glucose [Nurjhan et al., 1992]. Normal blood glycerol concentration is approximately $50\mu mol/l$ [Jenssen et al., 1990]. Glycerol contributes to approximately 3% of hepatic glucose output and approximately 10% of renal and total gluconeogenesis [Stumvoll et al., 1997], [Nurjhan et al., 1992]. However, this is increased in prolonged fasting and stress, where glycerol contributes to 60% of the hepatic glucose output and $20-30$% of overall glucose production [Mizock, 2001], [Nurjhan et al., 1992]. Glycerol is released at a rate of approximately $6\mu mol/min$ and $49-77\mu mol/min$ [Blomstrand and Saltin, 1999].

Fatty Acid A $70kg$ adult may store about $15kg$ of fat in his body [Baynes and Dominiczak, 2014]. The rate of fatty acid release into the blood in sepsis, trauma, and burn injury patients is approximately $12-15\mu mol/kg*min$, which is roughly double the normal rate [Wolfe, 1999]. Normally fatty acids are released at a rate of approximately $10\mu mol/min$ and removed from the blood at a rate of $175\mu mol/min$ during exercise

[Blomstrand and Saltin, 1999]. In the absorptive state the adipose tissue takes up approximately 5% of the supplied glucose [Mitrakou, 2011].

Lactate The skin produces the largest amount of lactate at $20mg/min$ [De Backer et al., 1997]. Lactate release from the adipose tissue has been reported to occur at a rate of $60 - 150$ and $30 - 40\mu mol/min$ for the overall body fat mass, which is $4 - 10$ and $2\mu mol/kgfattissue/min$, respectively. Additionally, it is said to increase during exercise [van Hall, 2010].

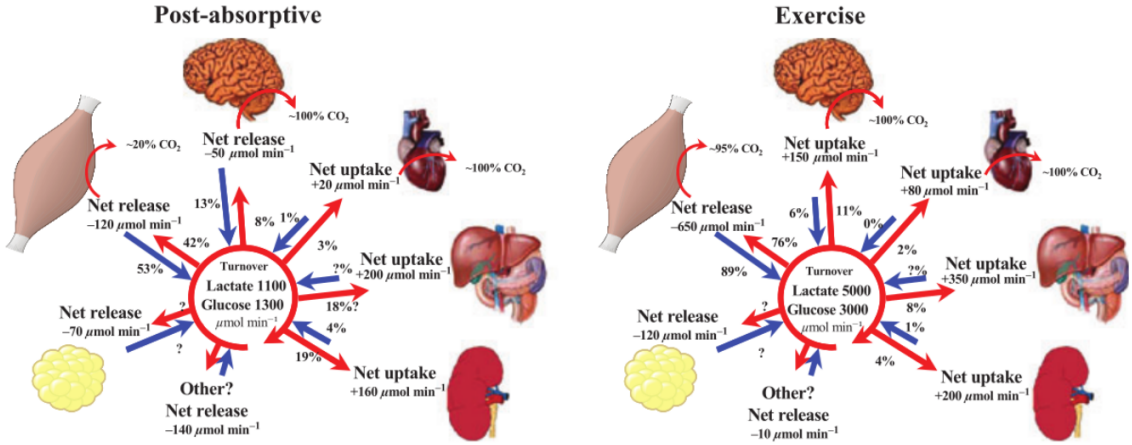

Figure 6.1: The figure summarizes this chapter by illustrating the turnover of glucose and lactate from the contribution of each discussed tissue. Edited from [van Hall, 2010].

Chapter 7

Assumptions and Constraints

This chapter presents the main simplifications, generalizations and assumptions used to model the Cori cycle. Assumptions discussed in this chapter generally comprise the abstractions specifically used for the model e.g. a standard body mass of 70kg or simplified chemical reactions.

7.1 Scales, Dimensions and Magnitudes

7.1.1 Proportions

The naked eye is able to see structures of 100μm, a light microscope has a resolution of up to 0.3μm at a zoom of 1000, limited by the wavelength of light. An electron microscope has a resolution boundary of 0.3nm, where even large biomolecules like glycogen may be identified. Table 7.1 illustrates the proportions and magnitude of different cells [Welsch and Sobotta, 2003].

Structure	Diameter
Human egg cell	$250 - 300\mu m$
Intestinal epithelium (hight)	$20 - 25\mu m$
Liver cell	$25\mu m$
Red blood cell	$7.6\mu m$
Hypochondrion (length)	$2 - 5\mu m$
Bacteria	$1 - 2\mu m$
Viruses	$10 - 100nm$
Glycogen (β particle)	$20nm$

Table 7.1: Scale of relevant structures

7.1.2 General Assumptions on the Human Body

The conventional 70kg (male) adult is a frequently made assumption, especially in text books, which can occasionally be validated by cohorts of several studies [Baynes and Dominiczak, 2014], [Horn, 2009], [Tappy, 2008], [Löffler et al., 2007], [Smith et al., 2005], [Despopoulos and Silbernagl, 2003], [Berg et al., 2002], Heinemann et al. [1999]. A body mass of 70kg is therefore used throughout the modeling process as a reference. The processes described by the model occur in one cell and have to be scaled up to the dimensions of the whole body.
The overall density of the human body should, due to its large water portion, measure slightly above $1g/ml = 1g/cm^3 = 1kg/l$ and has been determined to vary around $1.02-1.1g/ml$ with a mean of approximately $1.06g/ml$ [Jackson and Pollock, 1978]. There is, however, variation between organs, as fat tissue has a density of $0,9g/ml$ and visceral organs of $1,05g/ml$ [Müller et al., 2007].
Additionally it is assumed that the use of only two decimals in a final assumption will be a sufficient degree of precision, especially when considering the at times large margin of tolerances included in the premises.

7.1.3 Skeletal Muscles and Heart

The entire skeletal muscle mass of the body amounts to approximately $25-30$kg for a 70kg adult, which is about 40% of the mass [Horn, 2009], [Hick and Hick, 2000], [Consoli et al., 1990b]. Typical skeletal muscle cells (muscle filaments) measure in the magnitude of a few μm in diameter ($10-100\mu$m [Aumüller et al., 2007], $40-100\mu$m (rarely $500\mu m$) [Welsch and Sobotta, 2003], $15-200\mu m$ [Hick and Hick, 2000]) and several cm in length ($15cm$ [Hick and Hick, 2000], $20cm$ [Aumüller et al., 2007]) [Aumüller et al., 2007], [Welsch and Sobotta, 2003], [Hick and Hick, 2000]. Hand muscles may contain $100-300$ muscle filaments and arm and leg muscles $600-1700$. Muscles consist of several types of muscle cells, each with different contraction properties [Welsch and Sobotta, 2003].
Since the measurements exhibit quite a spread, and the distribution of those measurements is not given, as is their relation to a particular muscle, the heart is used as the basis for scaling the properties of one muscle cell to the muscle mass of the body.

Heart Although not being defined as a skeletal muscle per se, myocardium bears strong structural resemblance to skeletal muscles and considered to be a special type of skeletal muscle [Aumüller et al., 2007], [Welsch and Sobotta, 2003]. Heart muscle cells (cardiomyocytes) measure $10-20\mu m$ in diameter and $50-100\mu m$ in length [Welsch and Sobotta, 2003].
Heart mass and volume are strongly dependent on the individual fitness level. The normal mass of 300, which corresponds to $0.4-0.45$% of the body weight, and volume of 785ml can increase to $500g$ and $1440ml$, respectively, in athletes [Aumüller et al., 2007]. Considering the scope of application for the model it seems reasonable to start scaling from at the lower end of the available data.
The heart measures $12-14cm$ from the apex to the basis, with a largest width of $8-9cm$, and a sagittal diameter of $6cm$ at the basis. It is subdivided into right and left atrium

(atrium cordis dexter and sinister) and right and left ventricle (ventriculus cordis dexter and sinister) by valves and septa (septum interatriale and interventriculare), as depicted in figure 7.1 [Aumüller et al., 2007].

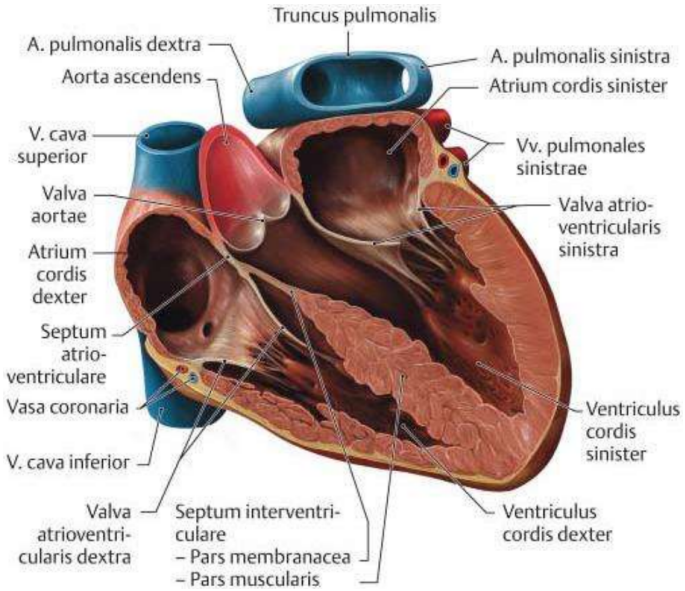

Figure 7.1: The figure shows the opened heart in its physiological position. The direct axis from the apex to the basis is inclined by an angle of approximately 45° to the three main planes [Aumüller et al., 2007].

To relate the activity of one cell to the whole organ it is necessary to estimate how many cells are contained within that organ. The rather complex geometry of the heart can is simplified to a cube for simpler approximation of its properties regarding the number of heart muscle cells that build up the organ. Using formula 7.1 with a cube length $a = 9.22479cm$ delivers a volume of $V_a = 784.99965cm^3 = 784.99965ml \approx 785ml$ [Becker, 2003].

$$V = a^3 \tag{7.1}$$

A cube volume has the advantage of being solely dependent on the cube length to the power of three. This results in small adjustments to the cube length being strongly reflected in the volume of the cube. Moreover, the approximation of, at least parts, of the heart as a cube is an excepted simplification [Devereux and Reichek, 1977].
However, the heart is hollow, the cardiac wall (myocardium) is not equally thick in all regions (figure 7.1) and there is also the septum to be considered for calculating the volume and subsequent the density of the heart muscle tissue. Data on the heart wall is given in table 7.2 [Aumüller et al., 2007]. Additionally, the muscle mass of the left ventricle alone has been measured in the range of $105 - 505g$, with an internal dimension of $3.3 - 7.5cm$, posterior wall thickness of $0.8 - 2.2cm$, and intervestibular septum thickness of $0.7 - 2.3cm$, in a rather heterogeneous cohort of healthy and ill [Devereux and Reichek, 1977].

Part of the cardiac wall	Thickness (mm)
Atrium (right)	3
Atrium (left)	3-4
Ventricule (right)	3-4
Ventricule (left)	10-12
Interatrial septum	-
Interventricular Septum	5-10

Table 7.2: Cardiac muscle tissue thickness

This leads to the sketch depicted in figure 7.2, where averaged values from table 7.2 are used for the calculations.

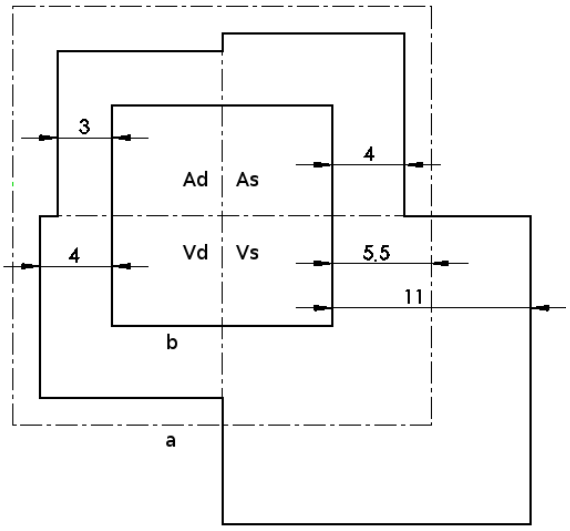

Figure 7.2: The figure shows the base square of the approximation of the heart as a cube. Ad = atrium cordis dexter, As = atrium cordis sinister, Vd = ventriculus cordis dexter, Vs = ventriculus cordis sinister, measurements in mm

In the sketch atria and ventricles are considered to be of equal size and an average cardiac wall thickness of $w = 0.55cm$ (dashed line) is assumed. The volume of the resulting hollow cube can be calculated by subtracting twice the wall thickness (w) from the length (a) of the cube and use the resulting length (b) to determine the volume (V_b) of a smaller cube to subtract from the initial volume (V_a).

$$b = 9.22479cm - 2(0.55)cm = 8.12479cm \rightarrow V_b = 536.33536cm^3 \approx 536ml$$

The resulting volume $V_w = 248.66429cm^3 = 249ml$ represents the heart muscle volume of the heart wall. However, this does not include the septa yet. They are considered to be one single structure, idealized as a cuboid, spanning the inner cube at the length and hight ($b = 8.12479cm$). Since no other data is available the interatrial septum is assumed to have a thickness of 3.5mm, based on the wall thickness of the atria and span half the cube, where it merges with the interventricular septum with an average thickness

of 7.5mm. The resulting structure is assumed to have an average thickness of $s = 0.55$mm over the entire length and hight of the inner cube. The septum cuboid thus has a volume of $V_s = 36.30672cm^3 \approx 36ml$. Adding the septum volume (V_s) to the volume of the hollow cube (V_w) results in an overall heart muscle volume of $V_H = 285ml$, which is roughly a third of the reference volume of $785ml$. After correcting for the volume, a density of $\varrho_m = \frac{300g}{285ml} = 1.05g/ml$ can be established for muscle tissue that corresponds with those given in the literature Müller et al. [2007], [Devereux and Reichek, 1977].
Using equation 7.2 to calculate the volume of a single heart muscle cell, assuming a diameter $d_{mc} = 15\mu m$, and a hight of $h_{mc} = 75\mu m$, the volume of a heart muscle cell amounts to $V_{mc} = 13253.6\mu m^3 = 13.2536nl$ [Becker, 2003].

$$V = \pi \cdot \left(\frac{d}{2}\right)^2 \cdot h \tag{7.2}$$

Dividing by $\varrho_m = 1.05g/ml$, the mass of one heart muscle cell is assumed to be $m_{mc} = 12.6 \cdot 10^{-9}g = 12.6ng$. A heart ($m_H = 300g$) therefore consists of $2.38 \cdot 10^{10}$ heart muscle cells. Since the heart represents 0.4% of the entire muscle mass, $750g$ represent 1% of the entire muscle mass of the body and $30000g = 30kg$ represent 40%. According to this, a $30kg$ muscle mass consist of $2.38 \cdot 10^{12}$ cells, $25kg$ consist of $1.98 \cdot 10^{12}$ cells.
The entire muscle mass of the body (m_M)is assumed to be composed by $2 \cdot 10^{12}$ muscle cells, which translates to an overall muscle mass of $m_M = 25.25kg$ and volume of $V_M = 26.51l$. However, this might be a little of an overestimation, as heart muscle cells tend to be a little shorter than those of the extremities. On the other hand, heart muscle cells might have a little less mass than skeletal muscle cells of the extremities, as they possess less nuclei and the overestimation in quantity could be compensated, to some degree, by the underestimation in mass [Welsch and Sobotta, 2003].
The results of the muscle approximation are summarized in 7.3

Structure	Symbol	Value
Heart dimensions(cube)	a	$9.22479cm$
Heart volume (cube)	V	$785ml$
Heart cell dimensions (average)	d_{mc}, h_{mc}	$15\mu m$, $75\mu m$
Volume of a heart cell	V_{mc}	$13.2536nl$
Mass of a heart cell	m_{mc}	$13.9pg$
Density of a heart cell	ϱ_m	$1.05g/ml$
Heart wall volume (hollow cube)	V_w	$249ml$
Septum volume (cuboid)	V_s	$36ml$
Number of cells in the heart	-	$2.38 \cdot 10^{10}$
Volume of the heart (hollow cube)	V_H	$285ml$
Mass of the heart	m_H	$0.3kg$
Number of cells in the muscle mass of the body	-	$2 \cdot 10^{12}$
Volume of the muscle mass of the body	V_M	$26.51l$
Muscle mass of the body	m_M	$25.25kg$

Table 7.3: Scaling of the heart muscle - one heart muscle cell represents all skeletal muscle cells of the body

7.1.4 Liver

The liver mass is often given in the magnitude of approximately 2.3% of the body mass ($1.5kg$ [Horn, 2009], $1.4 - 1.8kg$ [Aumüller et al., 2007], $1.4 - 1.8kg$, [Welsch and Sobotta, 2003], $1.6 - 1.7kg$ [Heinemann et al., 1999]), with an average tissue density of $1.08g/ml$ [Heinemann et al., 1999]. To the liver attached tissue (gallbladder, ligaments) amounts to an average $41.3g$ and has been excluded. For a liver of the mass $m_L = 1.6kg$ these measurements lead to a volume $V_L = 1.73l$ ($1862ml$ for $1724g$ liver [Heinemann et al., 1999]).
Liver cells (hepatocytes) measure $d_{lc} = 25\mu m$ in diameter and are organized in hexagonal lobules (lobuli hepatis), as depicted in figure 7.3. One hepatic lobule measures $0.7 - 2mm$ in diameter and contains approximately 10^6 cells [Welsch and Sobotta, 2003].

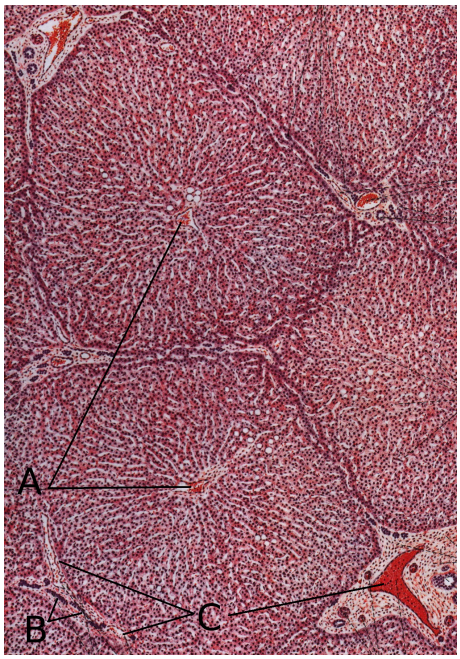

Figure 7.3: The figure shows how the hepatocytes are organized in the hepatic lobules (70× zoom). A = v. centralis, B = ductuli interlobulares, C = v. portae (vv. interlobulares) Artery, vein, and bile duct form the portal triad (trias hepatica) [Welsch and Sobotta, 2003]. Edited from [Welsch and Sobotta, 2003].

A liver cell is assumed to be spherical with the diameter $d_{lc} = 25\mu m$ and thus have a volume of $V_{lc} = 8181.23\mu m^3 = 8.81823 \cdot 10^{-12}ml = 8.81823pl$, using formula 7.3 [Becker, 2003]. One hepatic lobule therefore contains $1 \cdot 10^6$ cells and has a volume of $V_l = 8.18123 \cdot 10^{-3}ml = 8.18123\mu l$. A liver with a volume of $V_L = 1.73l$ thus contains $2.11 \cdot 10^5$ hepatic lobules and therefore $2.11 \cdot 10^{11}$ liver cells.

$$V = \frac{1}{6} \cdot \pi \cdot d^3 \tag{7.3}$$

The results of the liver approximation are summarized in 7.4

Structure	Symbol	Value
Liver cell dimensions (average)	d_{lc}	$25\mu m$
Volume of a liver cell	V_{lc}	$8.81823pl$
Mass of a liver cell	m_{lc}	$8.2ng$
Density of a liver cell	ϱ_l	$1.08g/ml$
Hepatic lobule volume	V_l	$8.18123\mu l$
Number of cells in the liver	-	$2.11 \cdot 10^{11}$
Volume of the liver	V_L	$1.73l$
Mass of the liver	m_L	$1.6kg$

Table 7.4: Scaling of the liver cell

7.1.5 Kidney

The kidneys weigh combined in the magnitude of $300g$ ($120-180g$ [Aumüller et al., 2007], $120-300g$ [Welsch and Sobotta, 2003]) and measure $10-12cm$ in hight, $5-6cm$ in width, and $3-4cm$ in depth [Aumüller et al., 2007], [Welsch and Sobotta, 2003]. The right kidney may be smaller than the left one [Aumüller et al., 2007]. Although, the renal medulla produces lactate, the renal cortex is solely responsible for renal gluconeogenesis [Baynes and Dominiczak, 2014], [Stumvoll et al., 1997]. The renal cortex is $6-10mm$ thick ($10mm$ [Behrends, 2010], $10mm$ [Hick and Hick, 2000]), as depicted in figure 7.4 [Welsch and Sobotta, 2003].

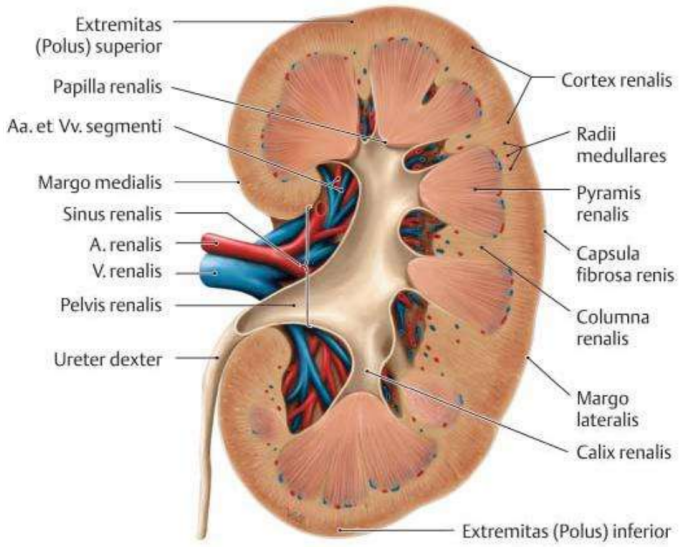

Figure 7.4: The figure shows the dorsal view on the frontal half of the right kidney [Aumüller et al., 2007].

The size and shape of liver cells is assumed for the cells of the renal cortex ($d_{kc} = 25\mu m$, spherical). Moreover the cortex of one kidney is assumed to be shaped as a hollow cuboid with the dimensions $l \times w \times d = 11cm \times 5.5cm \times 3.5cm$ and a wall thickness of $c = 0.8cm$. A renal cortex volume of two equally sized kidneys $V_K = 2(82.3ml) = 164.6ml$ is assumed. The density of the renal cortex is assumed to be similar to that of muscle and liver [Müller et al., 2007]. A reference to the kidney density of pigs could be found at approximately

$1.06 g/ml$ [Klein, 1998]. Thus a mass of the renal cortex is assumed to be $m_K = 155.28g$, which represents approximately half of the total kidney mass.

Structure	Symbol	Value
Kidney cell dimensions (assumed)	d_{kc}	$25\mu m$
Volume of a kidney cell	V_{kc}	$8.83191pl$
Mass of a kidney cell	m_{lc}	$8.3ng$
Density of a renal cortex cell	ϱ_l	$1.06g/ml$
Number of cells in the kidney cortex	-	$2.11 \cdot 10^{11}$
Volume of the kidney cortex	V_K	$164.6ml$
Mass of the kidney cortex	m_K	$155.28g$

Table 7.5: Scaling of the renal cortex

7.1.6 Blood

The hematocrit describes the volume of cells in the blood volume. The blood volume is usually in the magnitude of $5l$ ($5l$ [Baynes and Dominiczak, 2014], $4-6l$ [Aumüller et al., 2007], $4-5l$ [Despopoulos and Silbernagl, 2003], $3.7-4.5l$ [Welsch and Sobotta, 2003]) and consists of $54-56\%$ plasma and $44-45\%$ of cells [Aumüller et al., 2007], [Welsch and Sobotta, 2003]. The blood density is approximately $1.05 g/ml$ [Kenner, 1989].

Erythrocytes The major part of the cellular volume is comprised by red blood cells, of which there are $4000-6000 \cdot 10^3/\mu l = 4-6 \cdot 10^12/l$ ($4000-6000 \cdot 10^9/l$ [Aumüller et al., 2007], $4.15-4.9 \cdot 10^6/\mu l$ [Welsch and Sobotta, 2003]). They are shaped like biconcave discs with a diameter of $7.5-8\mu m$ ($7.7\mu m$ [Aumüller et al., 2007], $7.5\mu m$ [Welsch and Sobotta, 2003], $8.0\mu m$ [Jay, 1975], $7.8-8\mu m$ [Evans and Fung, 1972], $8.1\mu m$ [Canham and Burton, 1968]) and a thickness $t_e = 2\mu m$ on the edge and a thickness $t_c = 1\mu m$ in the center [Aumüller et al., 2007], [Welsch and Sobotta, 2003]. One red blood cell has a surface area of $140\mu m^2$ ($134\mu m^2$ [Jay, 1975], $135\mu m^2$ [Evans and Fung, 1972], $134-138.1\mu m^2$ [Canham and Burton, 1968]), which implies the total surface area for all red blood cells to be $3800m^2$ [Welsch and Sobotta, 2003]. Moreover, a red blood cell volume of $107.5\mu m^3$ ($99\mu m^3$ [Jay, 1975], $94\mu m^3$ [Evans and Fung, 1972]) has been established [Canham and Burton, 1968]. However, only $71\% = 76\mu m^3$ is considered to be cytoplasm [Brumen and Heinrich, 1984].

Leukocytes White blood cells come in a ratio of approximately 1:10000 with red blood cells and comprise about 1% of the blood cells [Aumüller et al., 2007], [Welsch and Sobotta, 2003]. The most common among this heterogeneous group of cells are the neutrophil granulocytes with a diameter of $8.5-15\mu m$ ($12-15\mu m$ [Aumüller et al., 2007], $8.5-10\mu m$ [Welsch and Sobotta, 2003]). Their number can rise from 60% to 80% of the white blood cells during infection with a normal number of $1.7-7 \cdot 10^3/\mu l$ [Welsch and Sobotta, 2003]. There are also lymphocytes as part of the white blood cells, which

have a diameter of $6 - 12\mu m$ ($6 - 10\mu m$ [Aumüller et al., 2007], $6 - 12\mu m$ [Welsch and Sobotta, 2003]) and measure $1 - 3 \cdot 10^3/\mu l$ in their numbers [Aumüller et al., 2007]. However, due to their low number, which is even below blood plates (thrombocytes) by approximately a factor of 100, their contribution to e.g. lactate production is assumed to be negligible and their are metabolic properties (e.g. lactate production) are well represented by red blood cells [Aumüller et al., 2007], [De Backer et al., 1997].

Assuming the volume of a single red blood cell to be $100\mu m^3$, their number in the blood at $5 \cdot 10^{12}/l$, and a blood volume of $5l$, the overall volume of the red blood cells is $V_{RBC} = 2500ml$ for $25 \cdot 10^{12}$ cells, which corresponds to 95% of all blood cells [Behrends, 2010]. A density $\varrho_{rbc} = 1.1g/ml$ of red blood cells is assumed and thus a mass for all blood cells of $m_RBC = 2273 \approx 2.27kg$ [Kenner, 1989].

Structure	Symbol	Value
Red blood cell dimensions (average)	d_{rbc}	$7.7\mu m$
Volume of a red blood cell	V_{rbc}	$0.1pl$
Density of a red blood cell	ϱ_{rbc}	$1.1g/ml$
Number red blood cells	-	$25 \cdot 10^{12}$
Volume of all red blood cells	V_B	$2.5l$
Mass of all red blood cells	m_B	$2.27kg$

Table 7.6: Scaling of the red blood cells -one red blood cell represents all blood cells of the body

7.1.7 Brain

The CNS contains $1 \cdot 10^{10} - 1 \cdot 10^{11}$ neurons ($1 \cdot 10^{10} - 1 \cdot 10^{11}$ [Aumüller et al., 2007], $1 \cdot 10^{11} - 1 \cdot 10^{12}$ [Welsch and Sobotta, 2003]) and about $3 - 10$ times as much glial cells [Aumüller et al., 2007]. A spherical neuron of the diameter $d_n = 20\mu m$ is assumed based on shape and relative size to other tissues [Zhang et al., 2014], [Welsch and Sobotta, 2003]. Using formula 7.3 and assuming $1 \cdot 10^{11}$ neurons in the CNS, this would translate to a volume of $V_n = 419ml$ and by assuming a density of $1.05g/ml$, a mass of $m_n = 399g$ for all neurons of the CNS, which correlates with the literature, when multiplied by 3.5 for the glial cells of assumed identical size [Aumüller et al., 2007], [Franceschini et al., 2007], [Ankney, 1992]. The total volume $V_C = 1467ml \approx 1.47l$ of the CNS is therefore assumed, which translates to a total mass $m_C = 1397g \approx 1.4kg$.

Structure	Symbol	Value
Neuron dimensions (assumed)	d_n	$20\mu m$
Volume of a neuron	V_n	$4.2nl$
Mass of a neuron	m_n	$4ng$
Density of neurons	ϱ_b	$1.05g/ml$
Number neurons	-	$1 \cdot 10^{11}$
Volume of the CNS	V_C	$1.47l$
Mass of the CNS	m_C	$1.4kg$

Table 7.7: Scaling of the neurons

7.1.8 Blood Flow

Considering large blood vessels like the superior and inferior vena cava at a diameter of approximately $3cm$, which equals a cross-sectional area of $7cm^2$ and a measured blood velocity of roughly $14cm/min$ in those vessels, the venous blood flow is $5.8l/min$. This can increase tenfold during exercise [Wexler et al., 1968].

Muscles The blood perfusion of the muscles is very dependent on physical activity [Behrends, 2010], [Hick and Hick, 2000]. At rest the perfusion the skeletal muscles is approximately $2-3ml/min * dl$ ($3ml/min * 100g$ tissue), which corresponds to about $15-21\% = 0.75-1l/min$ oft the cardiac output [Behrends, 2010], citepHick2000. This can increase 20-fold at maximum physical activity to $15l/min$ ($100ml/min * 100g$ tissue citepHick2000) [Behrends, 2010]. At rest a muscle blood flow of $757.5ml/min$ is assumed.

Heart Coronary perfusion at rest is approximately $70-80ml/min * 100g$ tissue, which corresponds to approximately 5% of the cardiac output and can increase $4-5$ fold during stress to approximately $300ml/min * 100g$ tissue [Behrends, 2010], [Hick and Hick, 2000]. The normal cardiac output is assumed to be $5l/min$, so that 20% of the cardiac output translate to $1l/min$ [Behrends, 2010]. At rest a coronary blood flow of $225ml/min$ is assumed.

Liver Normal liver perfusion in an adult is approximately $1500 \pm 300ml/min$, which corresponds to about 25% of the cardiac output and $100ml/min * 100g$ tissue [Stein and Schröder, 2006], [Hick and Hick, 2000]. A hepatic blood flow of $1600ml/min$ is assumed.

Kidneys Normal kidney perfusion is approximately $1000-1800ml/min$ [Gerich et al., 2001]. At rest the contain $20-25\%$ of the blood from the cardiac output ($1-1.2l$), which corresponds to a perfusion of $400ml/min * 100g$ tissue [Behrends, 2010], [Hick and Hick, 2000]. A blood flow of $311ml/min$ is assumed for the renal cortex.

Brain Normal CNS perfusion is approximately $750ml/min$ ($50ml/min * dl$), which corresponds to about $13 - 15\%$ of the cardiac output [Behrends, 2010], [Hick and Hick, 2000]. The perfusion varies between cortex ($100ml/min * 100g$ tissue) and medulla ($20ml/min * 100g$ tissue) and may increase up to 50% at increased neuronal activity [Hick and Hick, 2000]. A normal cerebral blood flow of $735ml/min$ is assumed

Skin At normal room temperature skin perfusion amounts to approximately $10\% = 0.5l/min$ but is largely dependent on the thermo-regulation. It can increase from about $100ml/min * m^2$ body surface area to $2l/min * m^2$ body surface area at physical activity [Behrends, 2010]. This translates to $150 - 500ml/min * 100g$ tissue [Hick and Hick, 2000].

7.2 Kinetics

7.2.1 Metabolic Reactions

The metabolic reactions considered are generally assumed to follow Michaelis-Menten kinetics (only occasionally mass-action kinetics) as the metabolite concentrations yielded from the network are of interest for the model. This implies, that the amount of enzyme in a cell remains constant over time. Solving equation 4.1 for zero tends to generally result in information about flux values or flux ratios but not concentrations [Rohwer, 2012]. Moreover, the metabolic reactions are generally assumed to be reversible (unless it does not fit observations (e.g. glucose export from muscle cells)), because antagonistic metabolic pathways are modeled realistic behavior is aspired to [Imperial and Centelles, 2014], [Schallau and Junker, 2010], [Horn, 2009], [Chalhoub et al., 2007], [Lambeth and Kushmerick, 2002]. The reactions of those pathways depend on their intermediate concentrations and can be redirected to reactants or products [Imperial and Centelles, 2014]. General assumptions for uni-uni and bi-bi reaction mechanisms are summarized in table 7.8 [Imperial and Centelles, 2014], [Lambeth and Kushmerick, 2002]. The reversible uni-uni mechanism assumes a competitive enzyme inhibition, which is expressed by the [B] in the denominator of the equation. For multiple substrates, the bi-bi mechanism involving a (random or ordered) ternary complex mechanism is the most frequently found. The main difference in comparison to the uni-uni mechanism are the independent terms in the denominator. However, there are also uni-bi or bi-uni reaction mechanisms. The equations irreversible reactions are identical with the irreversible reactions of uni-uni and bi-bi, respectively, as no products are considered. The denominators have to be adjusted for the reversible reactions by using the uni positive and bi negative factor in uni-bi reactions and vice versa [Imperial and Centelles, 2014]. Moreover, all equations can be modified with factors that represent inhibition or cooperative behavior in the enzyme reaction [Chalhoub et al., 2007], [Lambeth and Kushmerick, 2002].

$A \longrightarrow B$	Irreversible	Reversible
Michaelis-Menten	$v = \frac{V_f \cdot \frac{[A]}{K_{mA}}}{1 + \frac{[A]}{K_{mA}}}$	$v = \frac{V_f \cdot \frac{[A]}{K_{mA}} - V_r \cdot \frac{[B]}{K_{mB}}}{1 + \frac{[A]}{K_{mA}} + \frac{[B]}{K_{mB}}}$
$A + B \longrightarrow C + D$		
Ternary complex mechanism	$v = \frac{V_f \cdot \frac{[A][B]}{K_{mA}K_{mB}}}{1 + \frac{[A]}{K_{mA}} + \frac{[B]}{K_{mB}} + \frac{[A][B]}{K_{mA}K_{mB}}}$	$v = \frac{V_f \cdot \frac{[A][B]}{K_{mA}K_{mB}} - V_r \cdot \frac{[C][D]}{K_{mC}K_{mD}}}{1 + \frac{[A]}{K_{mA}} + \frac{[B]}{K_{mB}} + \frac{[A][B]}{K_{mA}K_{mB}} + \frac{[C]}{K_{mC}} + \frac{[D]}{K_{mD}} + \frac{[C][D]}{K_{mC}K_{mD}}}$

Table 7.8: General reaction kinetics

Units

To facilitate calculations, the variables of the kinetic equations are converted to SI-Units as summarized in table 7.9 [Scheer et al., 2010][1], [Holmes, 2007], [Hynne et al., 2001], [Wolf et al., 2000].

Parameter	Symbol	Unit
Concentration	[ ]	$\frac{mmol}{l} = mM$
Maximum velocity	V	$\frac{mM}{min}$
Michaelis-Menten constant (Individual binding constant)	K_m	mM
Inhibition constant	K_i	mM
Equilibrium constant	K_{eq}	dimensionless
Rate constant	k	$\frac{mM}{min}, \frac{1}{min}, \frac{1}{mMmin}$ *
Hill-coefficient	n	dimensionless
Correction factor for insulin	α	dimensionless
		* $0^{th}, 1^{st}, 2^{nd}$ order, respectively

Table 7.9: Units for variables in kinetic equations

Parameters

There exists a large variety of measured values for the parameters of table 7.9, often with a span of several orders of magnitude, as can be seen e.g. at the Michaelis-Menten constants listed in BRENDA [Scheer et al., 2010]. Therefore, parameter values of cells closest to

[1] This reference is used to reference the BRENDA enzyme database in general

those mentioned in 7 and species closest to human were preferred as as substitute and in general averaged [Rohwer, 2012]. Thus the used value might not so necessarily reflect a specific measurement result but an order of magnitude, which can be confirmed by other referenced sources. The variables are given together with the assumed kinetic equation they are used in.

7.2.2 Variables

Variables are designated according to their classification:

- Transporters, four capital letters
- Enzymes, two to three capital letters and -ase suffix
- Metabolites, three capital letters
- Nucleotides, one capital letter and index

The assumed steady state concentrations of the metabolites, nucleotides, and coenzymes in a cell are given in table 7.10. A general trend can be observed when comparing models using single cell organisms with those aiming to describe different organs of mammals: The measured steady state concentrations of metabolites tend to have higher values in the range of one to two orders of magnitude in single cell organisms [Chalhoub et al., 2007], [Chassagnole et al., 2002], [Lambeth and Kushmerick, 2002], [Hynne et al., 2001], [Teusink et al., 2000], [Wolf et al., 2000], [Mulquiney and Kuchel, 1999], [Schuster et al., 1988], [Scopes, 1973].
Some of those initial values already reflect a stressed metabolism. This can be derived from e.g. the lactate-pyruvate ratio of 16 : 1, which is increased in comparison to the normal, but well within range of the stress related ratio mentioned in chapter 2. Moreover, the NADH + H^+-NAD^+ ratio indicates a metabolic situation closer to starvation [Williamson et al., 1967].

Metabolite	Concentration (mM)	Reference
$[GLU_x]$	5	[Chalhoub et al., 2007], [Meyer et al., 1998]
$[LAC_x]$	1	[Chalhoub et al., 2007], [Bolton, 2007], [Fall and Szerlip, 2005]
$[ALA_x]$	0.3 (alanine) 0.6 (glutamine)	[Chalhoub et al., 2007], [Jenssen et al., 1990], [Stumvoll et al., 1999], [Felig et al., 1970]
[GLU]	5	[Chalhoub et al., 2007]
[G6P]	0.1	[Chalhoub et al., 2007], [Damsbo et al., 1991]
$[GLG_x]$	162.2 (liver) 15.8 (muscles)	[Chalhoub et al., 2007], [Lambeth and Kushmerick, 2002], [Horn, 2009], [Löffler et al., 2007], tables 7.4 and 7.3
[F6P]	0.05	[Chalhoub et al., 2007], [Lambeth and Kushmerick, 2002], [Mulquiney and Kuchel, 1999], [Schuster et al., 1988]
[FBP]	0.02	[Chalhoub et al., 2007], [Lambeth and Kushmerick, 2002], [Mulquiney and Kuchel, 1999], [Schuster et al., 1988]
[GAP]	0.02	[Chalhoub et al., 2007], [Lambeth and Kushmerick, 2002], [Mulquiney and Kuchel, 1999], [Schuster et al., 1988]
[PEP]	0.02	[Lambeth and Kushmerick, 2002], [Hynne et al., 2001], [Teusink et al., 2000], [Mulquiney and Kuchel, 1999], [Schuster et al., 1988]
[PYR]	0.08	[Chalhoub et al., 2007], [Lambeth and Kushmerick, 2002], [Mulquiney and Kuchel, 1999], [Schuster et al., 1988]
$[ACA_x]$	0.14	[Chalhoub et al., 2007]
[LAC]	1.3	[Chalhoub et al., 2007], [Lambeth and Kushmerick, 2002], [Mulquiney and Kuchel, 1999], [Schuster et al., 1988]
[ALA]	0.5	[Chalhoub et al., 2007]
$[A_3]$	3.7	[Chalhoub et al., 2007], [Chassagnole et al., 2002], [Lambeth and Kushmerick, 2002], [Mulquiney and Kuchel, 1999], [Schuster et al., 1988], [Scopes, 1973]
$[A_2]$	0.3	[Chalhoub et al., 2007], [Chassagnole et al., 2002]
[A]	4	[Chalhoub et al., 2007], [Wolf et al., 2000], [Hynne et al., 2001], [Teusink et al., 2000]
$[N_2]$	0.002	[Chalhoub et al., 2007], [Schuster et al., 1988]
$[N_1]$	0.5	[Yang et al., 2007], [Yamada et al., 2006], [Lambeth and Kushmerick, 2002], [Hynne et al., 2001], [Scopes, 1973]
[N]	0.502	[Wolf et al., 2000], [Williamson et al., 1967]

Table 7.10: Steady state metabolite concentrations

Lactate

The lactate producing tissues red blood cells, skeletal muscles and brain combined are responsible for roughly two thirds (65% (chapter 2)) of the entire lactate production and are specifically modeled by the different metabolic pathways. The 10% of the intestine are ignored, justified with the scope of application and the assumption that there is no digestion (postabsorptive state (chapter 1)). The remaining 25% generated by the adipose tissue is assumed to be of the constant rate of $0.05 mmol/min$ for the entire body fat mass [van Hall, 2010].

Nucleotides

Although, frequently encountered ATP is not the only nucleotides found in the body. guanosine triphosphate (GTP) is used e.g. in the glycogen metabolism [Horn, 2009]. However, for the model it is generally assumed that behave similarly and can be expressed by ATP and ADP, respectively. The same is assumed for the respective variations of the redox coenzymes NAD^+ and $NADH + H^+$. The nucleotides and redox coenzyme concentrations are constraint by equations 7.4a and b, as their overall amount is assumed to remain constant over time [Wolf et al., 2000].

$$[\mathrm{A}] = [\mathrm{A_3}] + [\mathrm{A_2}] \tag{7.4a}$$

$$[\mathrm{N}] = [\mathrm{A_2}] + [\mathrm{A_1}] \tag{7.4b}$$

pH-Value

The pH-value inside a cell is assumed to remain constant at e.g. 7.4 because it is further assumed that pH-value influencing metabolites e.g. lactate are released into the blood stream, by which the cell self-regulates its pH-value. This ties in with the assumption of ATP production being a major contributor to a reduced pH-value, as outlined in chapter 3, and is reflected by the constraint of the total nucleotide concentration to $2.8 mM$, as given in table 7.10.

Amino acids

As outlined in chapter 6 and shown in table 7.10, the alanine-glutamine ratio in the blood is 1 : 3. The normal combined alanine and glutamine concentration should therefore translate to approximately $0.9 mM$. Moreover, the stress related amino acid release into the blood is assumed to follow a linear function, which is derived from the loss of 2% muscle mass daily adding up to 20% over approximately 10 days, as outlined in chapter 1. Assuming the $25.25 kg$ total muscle mass from table 7.3 that would translate to the loss of $505 g$ of total muscle mass per day. For a rough estimate the muscle is assumed to be pure protein and made of the 21 proteinogenic amino acids in equal shares (4.76%), which leads to approximately $24 g$ of muscle per amino acid [Löffler et al.,

2007], Despopoulos and Silbernagl [2003]. The one used for the model is alanine with a molecular weight of $89g/mol$, according to PubChem [Wang et al., 2010][2]. Thus dividing $24g$ by the molecular weight of alanine yields a rate of about $0.2mmol/min$ or $0.3mmol/min$, when additionally considering glutamine with a molecular weight of $146g/mol$ [Wang et al., 2010]. This can be confirmed by considering a more specific percentage of alanine ($\approx 8\%$) and glutamine ($\approx 4\%$) in the pure protein muscle, which translates to a muscle degradation of approximately $40g/d$ ($0.3mmol/min$) and $20g/d$ ($0.1mmol/min$) for alanine and glutamine, respectively [Löffler et al., 2007]. Combined this amounts to $42mg/min$ ($0.4mmol/min$). However, since the muscle breakdown only accounts for 30% of the overall alanine production, the total alanine production is higher then that [Mizock, 2001].
The combined share of alanine and glutamine in the all protein muscle is approximately 10%. Based on this, the model will use an alanine production rate of $35mg/min = 0.4mmol/min$, which incorporates both alanine and glutamine, and will be added as 30% to the alanine production from muscle glycolysis (70%) to generate the total alanine concentration in the blood (alanine compartment). To address the renal preference for glutamine over alanine as a precursor in gluconeogenesis, the alanine compartment will be drained at the combined alanine uptake rates of liver (1/3) and kidney (2/3). 30% of the muscular alanine production can hence be used to rebuild muscle tissue (all protein muscle approximation). This tissue synthesis is modeled in dependency of the correction factor for insulin (α), which ensures that muscle tissue is regenerated at the same time that glycogen is stored, which indicates a less stressed metabolic situation.

[2]This reference is used to reference the PubChem database for chemical structures in general

Part III

Problem Solution

7.3 Equations and Constants

7.3.1 Membrane Transporters

There generally exists a large variety of different membrane transporters in the body [Alexander et al., 2013]. For the model it is generally assumed that the metabolite transport across the cell membrane is carried out by various kinds of transporters e.g. types of glucose transporter (GLUT) and monocarboxylate transporter (MCT), which are assumed to follow saturation kinetics. Moreover, those transporters are assumed to generally work bidirectional [Richter and Hargreaves, 2013], [Chalhoub et al., 2007][3].

GLUT: $GLU_x \longleftrightarrow GLU$ There are several transporters, with different properties, to transport glucose (GLU) in and out of the cell [Uldry and Thorens, 2004]. GLUT1 is responsible for the basal uptake and will be used in neurons and red blood cells, GLUT2 is found in liver and kidneys, and GLUT4 is insulin dependent and found in skeletal and cardiac muscle [Arleth et al., 2000]. The kinetic equation to describe GLUT1 and GLUT2 is assumed to be of the form given in table 7.11 [Imperial and Centelles, 2014], [Chalhoub et al., 2007].

$$
\begin{aligned}
v_{\mathrm{GLUTX}} &= \frac{V_{\mathrm{GLUTX}} \cdot \frac{[GLU_x]}{K_{\mathrm{mGLUTX}}} - V_{\mathrm{GLUTX}} \cdot \frac{[GLU]}{K_{\mathrm{mGLUTX}}}}{1 + \frac{[GLU_x]}{K_{\mathrm{mGLUTX}}} + \frac{[GLU]}{K_{\mathrm{mGLUTX}}}} \\
&= \frac{V_{\mathrm{GLUTX}} \cdot ([GLU_x] - [GLU])}{K_{\mathrm{mGLUTX}} + [GLU_x] + [GLU]}
\end{aligned}
$$

Parameter	Value	Reference
V_{GLUT1}	$0.5\frac{mM}{min}$	[Hughes et al., 1993]
K_{mGLUT1}	$1mM$	[Berg et al., 2002], [Arleth et al., 2000]
V_{GLUT2}	$19.22\frac{mM}{min}$	[Chalhoub et al., 2007], [Hughes et al., 1993]
K_{mGLUT2}	$17mM$	[Uldry and Thorens, 2004], [Berg et al., 2002], [Arleth et al., 2000], [Hughes et al., 1993]

Table 7.11: GLUT kinetics

The differential equations that describe the model have to be solved for the respective metabolite to represent its concentration over time, as mentioned in chapter 4. Using the GLUT1 equation as an example, table 7.12 briefly illustrates the basis for the

[3] All referenced values have been corrected with the liver density ($1.08g/ml$ (table 7.4)) for unit conversion to mM/min

implementation of the differential equations in the computerized model presented in chapter 9, where the equation will be numerically integrated by LabVIEW.

$$
\begin{aligned}
\mathrm{v_{GLUT1}} = \dot{\mathrm{GLU}} = &\quad \frac{0.5\frac{mM}{min}\cdot[\mathrm{GLU_x}]}{1mM+[\mathrm{GLU_x}]+[\mathrm{GLU}]} - \frac{0.5\frac{mM}{min}\cdot[\mathrm{GLU}]}{1mM+[\mathrm{GLU_x}]+[\mathrm{GLU}]} \\
\frac{\mathrm{dGLU}}{\mathrm{dt}} = &\quad \frac{0.5\frac{mM}{min}\cdot[\mathrm{GLU_x}]}{1mM+[\mathrm{GLU_x}]+[\mathrm{GLU}]} - \frac{0.5\frac{mM}{min}\cdot[\mathrm{GLU}]}{1mM+[\mathrm{GLU_x}]+[\mathrm{GLU}]} \\
\int 1d\mathrm{GLU} = &\quad \int \left(\frac{0.5\frac{mM}{min}\cdot[\mathrm{GLU_x}]}{1mM+[\mathrm{GLU_x}]+[\mathrm{GLU}]} - \frac{0.5\frac{mM}{min}\cdot[\mathrm{GLU}]}{1mM+[\mathrm{GLU_x}]+[\mathrm{GLU}]} \right) \cdot dt \\
\mathrm{GLU} = &\quad \int_0^t \left(\frac{0.5\frac{mM}{min}\cdot[\mathrm{GLU_x}]}{1mM+[\mathrm{GLU_x}]+[\mathrm{GLU}]} - \frac{0.5\frac{mM}{min}\cdot[\mathrm{GLU}]}{1mM+[\mathrm{GLU_x}]+[\mathrm{GLU}]} \right) \cdot dt
\end{aligned}
$$

Table 7.12: GLUT kinetics

GLUT4: $GLU_x \longrightarrow GLU$ GLUT4 is considered to be a unidirectional transporter, corresponding to a modified Michaelis-Menten equation. The kinetic equation to describe GLUT4 is assumed to be of the form given in table 7.13 [Richter and Hargreaves, 2013], [Pielmeier, 2010]. However, when ignoring α the equation can also be used to model a unidirectional GLUT1, GLUT2 or MCT for lactate transport, as presented in table 7.15.

$$
\begin{aligned}
\mathrm{v_{GLUT4}} = &\quad \frac{\mathrm{V_{GLUT4}}\cdot\frac{[\mathrm{GLU_x}]}{\mathrm{K_{mGLUT4}}}}{1+\frac{[\mathrm{GLU_x}]}{\mathrm{K_{mGLUT4}}}}\cdot\alpha \\
= &\quad \frac{\mathrm{V_{GLUT4}}\cdot[\mathrm{GLU_x}]}{\mathrm{K_{mGLUT4}}+[\mathrm{GLU_x}]}\cdot\alpha
\end{aligned}
$$

Parameter	Value	Reference
$\mathrm{V_{GLUT4}}$	$0.09\frac{mM}{min}$	[Pielmeier, 2010]*
$\mathrm{K_{mGLUT4}}$	$5mM$	[Richter and Hargreaves, 2013], [Chalhoub et al., 2007], [Uldry and Thorens, 2004], [Arleth et al., 2000]

*corrected with muscle density ($1.05g/ml$ (table 7.3)) for unit conversion to mM/min

Table 7.13: GLUT4 kinetics

LACT: $LAC_x \longleftrightarrow LAC$ Different active and passive lactate (LAC) transport mechanisms through the cell membrane are known and involve a H^+ cotransport, when LAC is released into the blood [Dienel, 2014], [Brooks, 2009], [Horn, 2009], [Juel, 2004], [Brooks, 2002], [von Grumbckow et al., 1999], [Juel, 1997], [Balkovetz et al., 1988]. The bidirectional lactate transport by e.g.MCT4 in the model is assumed to be described by the equation in table 7.14 [Chalhoub et al., 2007], [Fox et al., 2000]. The unidirectional lactate transport is assumed to follow the equation in table 7.15 [Chalhoub et al., 2007]. The required concentration of intra- or extracellular lactate depends on the desired transport direction.

$$v_{LACT} = \frac{V_{LACT} \cdot \frac{[LAC_x]}{K_{mLACT}} - V_{LACT} \cdot \frac{[LAC]}{K_{mLACT}}}{1 + \frac{[LAC_x]}{K_{mLACT}} + \frac{[LAC]}{K_{mLACT}}}$$

Parameter	Value	Reference
V_{LACT}	$24.3\frac{mM}{min}$	[Chalhoub et al., 2007]
K_{mLACT}	$28mM$	[Fox et al., 2000]

Table 7.14: LACT kinetics

$$v_{LACTu} = \frac{V_{LACT} \cdot \frac{[LAC_x]}{K_{mLACT}}}{1 + \frac{[LAC_x]}{K_{mLACT}}}$$

Table 7.15: Unidirectional LACT kinetics

ALAT: $ALA_x \longleftrightarrow ALA$ The bidirectional alanine (ALA) transport through the cell membrane is assumed to be of the form given in table 7.16. The unidirectional alanine transport is assumed to follow the equation given in table 7.17 [Chalhoub et al., 2007]. The required concentration of intra- or extracellular lactate depends on the desired transport direction.

$$v_{ALAT} = \frac{V_{ALAT} \cdot \frac{[ALA_x]}{K_{mALAT}} - V_{ALAT} \cdot \frac{[ALA]}{K_{mALAT}}}{1 + \frac{[ALA_x]}{K_{mALAT}} + \frac{[ALA]}{K_{mALAT}}}$$

Parameter	Value	Reference
V_{ALAT}	$12.96 \frac{mM}{min}$	[Chalhoub et al., 2007]
K_{mALAT}	$0.6mM$	[Chalhoub et al., 2007]

Table 7.16: ALAT kinetics

$$v_{ALATu} = \frac{V_{ALAT} \cdot \frac{[ALA_x]}{K_{mALAT}}}{1 + \frac{[ALA_x]}{K_{mALAT}}}$$

Table 7.17: Unidirectional ALAT kinetics

7.3.2 Metabolic Reactions

The equations and parameters describing the metabolite conversion during the reaction chains have been adapted and evaluated from different sources, most importantly [Imperial and Centelles, 2014], [Chalhoub et al., 2007], [Lambeth and Kushmerick, 2002], [Hynne et al., 2001], [Wolf et al., 2000], and the enzyme database BRENDA.

GKase-G6Pase: $GLU \xleftrightarrow[ATP \curvearrowright ADP]{} G6P$ The conversion of hexoses (e.g. GLU) into glucose-6-phosphate (G6P) is generally catalyzed by the hexokinase (HKase) enzymes (EC 2.7.1.1) and in the liver by HKase IV, which is also named glucokinase (GKase) (EC 2.7.1.2) and specific to D-glucose [Molnes et al., 2011], [Scheer et al., 2010], [Xu et al., 1995]. For this conversion to be reversible, glucose-6-phosphatase (G6Pase) is required, which is found in organs conducting gluconeogenesis, so mostly liver and kidney cortex [Horn, 2009]. The reversible reaction in those organs is assumed to be of the form given by the equation in table 7.18. The GKase reaction is assumed to follow a bi-bi ternary complex mechanism and the G6Pase is assumed to follow Michaelis-Menten kinetics. [Imperial and Centelles, 2014], [Scheer et al., 2010], [Chalhoub et al., 2007], [Liebermeister and Klipp, 2006], [Kelmer-Bracht et al., 2003] [Hynne et al., 2001].

$$v_2 = \frac{V_{GKase} \cdot \frac{[GLU][A_3]}{K_{m2GLU}K_{m2A_3}} - V_{G6Pase} \cdot \frac{[G6P]}{K_{m2G6P}}}{1 + \frac{[GLU]}{K_{m2GLU}} + \frac{[A_3]}{K_{m2A_3}} + \frac{[G6P]}{K_{m2G6P}} + \frac{[GLU][A_3]}{K_{m2GLU}K_{m2A_3}}}$$

Parameter	Value	Reference
V_{GKase}	$2.37\frac{mM}{min}$	[Cloutier et al., 2009], [Chalhoub et al., 2007], [Oakes et al., 1997]
V_{G6Pase}	$6\frac{mM}{min}$	[Oakes et al., 1997], [Minassian et al., 1995]
K_{m2GLU}	$6.75mM$	[Chalhoub et al., 2007], [Smith et al., 2005], [Berg et al., 2002], [Xu et al., 1995]
K_{m2A_3}	$0.16mM$	[Molnes et al., 2011], [Hynne et al., 2001]
K_{m2G6P}	$2mM$	[Minassian et al., 1995]

Table 7.18: GKase-G6Pase kinetics

HKase: $GLU + ATP \longrightarrow G6P + ADP$ HKase is used for describing the metabolic pathways of e.g. red blood cells and assumed to be of the form given by the equation in table 7.19 [Liebermeister and Klipp, 2006], [Hynne et al., 2001].

$$v_{2u} = \frac{V_{HKase} \cdot \frac{[GLU][A_3]}{K_{m2uGLU}K_{m2uA_3}}}{1 + \frac{[GLU]}{K_{m2uGLU}} + \frac{[A_3]}{K_{m2uA_3}} + \frac{[GLU][A_3]}{K_{m2uGLU}K_{m2uA_3}}}$$

Parameter	Value	Reference
V_{HKase}	$2.37\frac{mM}{min}$	[Cloutier et al., 2009], [Chalhoub et al., 2007], [Oakes et al., 1997]
K_{m2uGLU}	$0.1mM$	[Hynne et al., 2001], [Xu et al., 1995]
K_{m2uA_3}	$0.16mM$	[Molnes et al., 2011], [Hynne et al., 2001]

Table 7.19: HKase kinetics

storage-consum: $G6P \xleftrightarrow[ATP \curvearrowright ADP]{} GLG$ The glycogen (GLG) metabolism is lumped into the form given by the equation in table 7.20. The conversion of GTP into guanosine diphosphate (GDP) during the reaction is assumed to to be equivalent to the conversion of ATP into ADP, which is used instead. The GLG production is described by a 2^{nd} order rate law (storage) and its consumption is assumed to follow a 0^{th} order rate law (consum) [Tian et al., 2013], [Chalhoub et al., 2007], [Hynne et al., 2001]. Both are modified with

a correction factor for insulin, to signify the insulin dependence of those pathways [Horn, 2009].

$$v_3 = k_{storage}[G6P][A_3] \cdot \alpha - k_{consum} \cdot \frac{1}{\alpha}$$

Parameter	Value	Reference
$k_{storage}$	$2.26 \frac{1}{mMmin}$	[Tian et al., 2013], [Hynne et al., 2001]
k_{consum}	$0.04 \frac{mM}{min}$	[Chalhoub et al., 2007]

Table 7.20: GLG kinetics

GPIase: $G6P \longleftrightarrow F6P$ The reversible conversion of G6P into fructose-6-phosphate (F6P) is catalyzed by glucose-6-phosphate isomerase (GPIase) (EC 5.3.1.9), assumed to follow Michaelis-Menten kinetics and be of the form given by the equation in table 7.21 [Imperial and Centelles, 2014], [Tian et al., 2013], [Rohwer, 2012], [Scheer et al., 2010], [Chalhoub et al., 2007], [Lambeth and Kushmerick, 2002], [Hynne et al., 2001].

$$v_4 = \frac{V_{GPIase} \cdot \frac{[G6P]}{K_{m4G6P}} - V_{GPIase} \cdot \frac{[F6P]}{K_{m4F6P}}}{1 + \frac{[G6P]}{K_{m4G6P}} + \frac{[F6P]}{K_{m4F6P}}}$$

$$= \frac{V_{GPIase} \cdot (K_{m4F6P}[G6P] - K_{m4G6P}[F6P])}{K_{m4G6P}K_{m4F6P} + K_{m4F6P}[G6P] + K_{m4G6P}[F6P]}$$

Parameter	Value	Reference
V_{GPIase}	$35.42 \frac{mM}{min}$	[Cloutier et al., 2009], [Chalhoub et al., 2007]
K_{m4G6P}	$0.11mM$	[Chalhoub et al., 2007], [Lambeth and Kushmerick, 2002]
K_{m4F6P}	$0.05mM$	[Cloutier et al., 2009], [Chalhoub et al., 2007], [Lambeth and Kushmerick, 2002], [Mulquiney and Kuchel, 1999], [Van Beneden and Powers, 1989]

Table 7.21: GPIase kinetics

PFKase-FBPase: $F6P \xleftrightarrow[ATP \curvearrowright ADP]{} FBP$ The conversion of F6P into fructose-1,6-biphosphate (FBP) is calalyzed by phosphofructokinase (PFKase) (EC 2.7.1.11). The reverse reaction requires fructose-1,6-biphosphatase (FBPase) (EC 3.1.3.11) [Scheer et al., 2010], [Horn, 2009]. For simplicity reasons a two-substrate allosteric inhibition is assumed to lump both reactions into the form given by the equation in tab 7.22. This translates to a reversible, noncompetitive, random order, bi-uni reaction mechanism [Imperial and Centelles, 2014], [Tian et al., 2013], [Scheer et al., 2010], [Steuer and Junker, 2009],

[Liebermeister and Klipp, 2006], [Madison and Madison, 2006], [Lambeth and Kushmerick, 2002], [Hynne et al., 2001], [Gilbert, 2000], [Termonia and Ross, 1981]. However, since PFKase exhibits an unusual behavior this equation does not comprise all its aspects, e.g. the stimulating effect of ADP or adenosine monophosphate (AMP) [Tian et al., 2013], [Horn, 2009], [Termonia and Ross, 1981]. Moreover, the inhibiting effect of citrate was ignored, while the inhibiting effect of ATP was included with a factor in the denominator [Lambeth and Kushmerick, 2002].

$$v_5 = \frac{V_{PFKase} \cdot \frac{[F6P][A_3]}{K_{m5F6P} K_{m5A_3}} - V_{FBPase} \cdot \frac{[FBP]}{K_{m5FBP}}}{\left(1 + \frac{[F6P]}{K_{m5F6P}} + \frac{[A_3]}{K_{m5A_3}} + \frac{[FBP]}{K_{m5FBP}} + \frac{[F6P][A_3]}{K_{m5F6P} K_{m5A_3}}\right)\left(1 + \frac{[A_3]}{K_{m5A_3}}\right)}$$

Parameter	Value	Reference
V_{PFKase}	$45\frac{mM}{min}$	[Tian et al., 2013], [Lambeth and Kushmerick, 2002], [Hynne et al., 2001]
V_{FBPase}	$21.6\frac{mM}{min}$	[Chalhoub et al., 2007], [Westermark and Lansner, 2003]
K_{m5F6P}	$0.05mM$	[Mulquiney and Kuchel, 1999], [Durante et al., 1995]
K_{m5A_3}	$0.05mM$	[Brüser et al., 2012], [Scheer et al., 2010], [Lambeth and Kushmerick, 2002], [Mulquiney and Kuchel, 1999]
K_{m5FBP}	$0.002mM$	[Gizak et al., 2008], [Rakus et al., 2005]

Table 7.22: PFKase-FBPase

HKase+PFKase: $GLU + 2ATP \longrightarrow FBP + 2ADP$ For cells not involved in gluconeogenesis, the HKase and PFKase reactions can be considered irreversible and the conversion of GLU into FBP expressed in a modified 2^{nd} order rate law of the form given by the equation in table 7.23 [Horn, 2009], [Wolf et al., 2000], [Brumen and Heinrich, 1984].

$$v_i = k_{invest}[GLU][A_3] \cdot \frac{1}{1 + \left(\frac{[A_3]}{K_i}\right)^n}$$

Parameter	Value	Reference
k_{invest}	$550 \frac{1}{mMmin}$	[Wolf et al., 2000]
K_i	$1mM$	[Wolf et al., 2000], [Brumen and Heinrich, 1984]
n	4	[Wolf et al., 2000], [Brumen and Heinrich, 1984]

Table 7.23: HKase+PFKase kinetics

ALDase+TPIase: $FBP \longleftrightarrow 2GAP$ For the conversion of FBP into glyceraldyde-3-phosphate (GAP), the triosephosphate isomerase (TPIase) reaction is neglected and it is assumed that a lumped aldolase (ALDase) (EC 4.1.2.13) reaction of the form given by the equation in table 7.24 produces 2 molecules of GAP in an ordered uni-bi mechanism [Imperial and Centelles, 2014], [Scheer et al., 2010], [Liebermeister and Klipp, 2006], [Lambeth and Kushmerick, 2002].

$$v_6 = \frac{V_{ALDase} \cdot \frac{[FBP]}{K_{m6FBP}} - V_{ALDase} \cdot \left(\frac{[GAP]}{K_{m6GAP}}\right)^2}{1 + \frac{[FBP]}{K_{m6FBP}} + \frac{2\,[GAP]}{K_{m6GAP}} + \left(\frac{[GAP]}{K_{m6GAP}}\right)^2}$$

Parameter	Value	Reference
V_{ALDase}	$35{,}5 \frac{mM}{min}$	[Esposito et al., 2004], [Mulquiney and Kuchel, 1999], [Kusakabe et al., 1994]
K_{m6FBP}	$0.05mM$	[Esposito et al., 2004], [Lambeth and Kushmerick, 2002], [Kusakabe et al., 1994]
K_{m6GAP}	$1.17mM$	[Rozova et al., 2010], [Lambeth and Kushmerick, 2002]

Table 7.24: ALDase+TPIase kinetics

GDHase+PGKase+PGMase+ENOase:
$GAP + ADP + NAD \longleftrightarrow PEP + ATP + NADH_2$ The glyceraldehyde dehydrogenase (GDHase), phosphoglycerate kinase (PGKase), phosphoglycerate mutase (PGMase), and enolase (ENOase) reactions necessary to convert GAP into **pep!** (**pep!**) are lumped into one reversible reaction of the form given by the equation in table 7.25 [Imperial and Centelles, 2014], [Rohwer, 2012], [Chalhoub et al., 2007].

$$v_7 = \frac{V_{-GAPPEPase} \cdot \frac{[GAP][A_2][N_1]}{K_{m7PEPGAP}} - V_{GAPPEPase} \cdot \frac{[PEP][A_3][N_2]}{K_{m7PEPGAP} K_{eqPEPGAP}}}{1 + \frac{[GAP][A_2][N_1]}{K_{m7GAPPEP}} + \frac{[PEP][A_3][N_2]}{K_{m7PEPGAP}}}$$

$$= \frac{V_{GAPPEPase} \cdot (K_{eqPEPGAP}[GAP][A_2][N_1] - [PEP][A_3][N_2])}{K_{m7PEPGAP} K_{eqPEPGAP} + \frac{K_{m7PEPGAP} K_{eqPEPGAP}[GAP][A_2][N_1]}{K_{m7GAPPEP}} + K_{eqPEPGAP}[PEP][A_3][N_3]}$$

Parameter	Value	Reference
$V_{GAPPEPase}$	$102\frac{mM^*}{min}$	[Chalhoub et al., 2007], [Mulquiney and Kuchel, 1999]
$K_{m7GAPPEP}$	$2.5 \cdot 10^{-6} mM^{3*}$	[Szabó et al., 2008a], [Szabó et al., 2008b], [Mulquiney and Kuchel, 1999]
$K_{m7PEPGAP}$	$4 \cdot 10^{-5} mM^{3*}$	[Szabó et al., 2008a], [Szabó et al., 2008b], [Chalhoub et al., 2007], [Mulquiney and Kuchel, 1999]
$K_{eqPEPGAP}$	4166^*	[Chalhoub et al., 2007], [Lehninger et al., 2005]

* based on GDHase and PGKase reactions

Table 7.25: GDHase+PGKase+PGMase+ENOase kinetics

PKase-(PCase+PCKase): $PEP \xleftrightarrow[ADP \curvearrowright ATP]{2ADP \curvearrowright 2ATP} PYR$ The reversible conversion of **pep!** into **pyr!** (**pyr!**) (by pyruvate kinase (PKase)) of the rapid equilibrium bi-bi form given by the equation in table 7.26 assumes a lumped reaction for the pyruvate carboxylase (PCase) and phosphoenolpyruvate carboxykinase (PEP-CKase) reactions [Chalhoub et al., 2007], [Liebermeister and Klipp, 2006], [Lambeth and Kushmerick, 2002].

$$v_8 = \frac{V_{PKase} \cdot \frac{[PEP][A_2]}{K_{m8PEP} K_{m8A_2}} - V_{PCase+PCKase} \cdot \frac{[PYR]}{K_{m8PYR}} \left(\frac{[A_3]}{K_{m8A_3}}\right)^2}{1 + \frac{[PEP]}{K_{m8PEP}} + \frac{[A_2]}{K_{m8A_2}} + \frac{[PEP][A_2]}{K_{m8PEP} K_{m8A_2}} + \left(1 + \frac{[PYR]}{K_{m8PYR}}\right)\left(1 + \frac{[A_3]}{K_{m8A_2}} + \left(\frac{[A_3]}{K_{m8A_2}}\right)^2\right)}$$

Parameter	Value	Reference
V_{PKase}	$67{,}5\frac{mM}{min}$	[Chalhoub et al., 2007]
$V_{PCase+PCKase}$	$13{,}39\frac{mM}{min}$	[Chalhoub et al., 2007]
K_{m8PEP}	$0.1mM$	[Oria-Hernández et al., 2005], [Lambeth and Kushmerick, 2002], [Hynne et al., 2001]
K_{m8A_2}	$0.3mM$	[Dombrauckas et al., 2005], [Lambeth and Kushmerick, 2002], [Chassagnole et al., 2002], [Hynne et al., 2001]
K_{m8PYR}	$0.22mM$	[Carbone and Robinson, 2003], [Jitrapakdee et al., 1999]
K_{m8A_3}	$0.22mM$	[Lambeth and Kushmerick, 2002], [Hynne et al., 2001], [Jitrapakdee et al., 1999]

Table 7.26: PKase-(PCase+PCKase) kinetics

LDHase: $PYR{+}NADH_2 \longleftrightarrow LAC{+}NAD$ The **pyr!** conversion into LAC by LDHase is assumed to follow a complex ternary complex mechanism, which can be simplified and a described by reversible Michaelis-Menten kinetics by the equation in table 7.27 [Chalhoub et al., 2007], [Lambeth and Kushmerick, 2002], [Mulquiney and Kuchel, 1999].

$$v_9 = \frac{V_{LDHase} \cdot \frac{[PYR][N_2]}{K_{m9PYR}K_{m9N_2}K_{eqLDH}} - V_{LDHase} \cdot \frac{[LAC][N_1]}{K_{m9LAC}K_{m9N_1}}}{1 + \frac{[PYR][N_2]}{K_{m9PYR}K_{m9N_2}} + \frac{[LAC][N_1]}{K_{m9LAC}K_{m9N_1}}}$$

Parameter	Value	Reference
V_{LDHase}	$210\frac{mM}{min}$	[Mulquiney and Kuchel, 1999], [Chalhoub et al., 2007]
K_{m9PYR}	$0.3mM$	[Lambeth and Kushmerick, 2002], [Mulquiney and Kuchel, 1999], [Pettit et al., 1981]
K_{m9N_2}	$0.002mM$	[Lambeth and Kushmerick, 2002], [Mulquiney and Kuchel, 1999]
K_{m9LAC}	$1mM$	[Chalhoub et al., 2007], [Mulquiney and Kuchel, 1999], [Nakae and Stoward, 1997]
K_{m9N_1}	$0.2mM$	[Flores and Ellington, 2005], [Lambeth and Kushmerick, 2002], [Mulquiney and Kuchel, 1999]
K_{eqLDH}	$1.1 \cdot 10^{-4}$	[Williamson et al., 1967], table 7.10 ($2.5 \cdot 10^{-4}$)

Table 7.27: LDHase kinetics

ALTase: $PYR + NADH_2 \longleftrightarrow ALA + NAD$ The **pyr!** conversion into ALA by **altase!** (**altase!**) is assumed to follow a ping-pong bi-bi mechanism, which is described by the equation in table 7.28 [Scheer et al., 2010], [Chalhoub et al., 2007]. The Km-value for ALA in cytosolic **altase!** is typically in the magnitude of $3mM$, but $10 - 20mM$ or above have also been measured for humans and other mammals, which would correspond with the squared denominator of the kinetic equation [Mu et al., 2012], [Scheer et al., 2010], [Sánchez-Muros et al., 1998], [Gubern et al., 1990]. No Km-values for the redox coenzymes could be found, as their presence the **altase!** reaction is only included to balance the LDHase reaction and accommodate for the PEP-CKase reaction inside the mitochondrion and they do not actually participate in the reaction, as was depicted in figure 2.6 [Scheer et al., 2010], [Horn, 2009], [Chalhoub et al., 2007].

$$v_{10} = \frac{V_{ALTase} \cdot \frac{[PYR][N_2]}{K_{m10PYRALA}} - V_{ALTase} \cdot \frac{[ALA][N_1]}{K_{m10PYRALA}}}{1 + \frac{[PYR][N_2]}{K_{m10PYRALA}} + \frac{[ALA][N_1]}{K_{m10ALAPYR}}}$$

Parameter	Value	Reference
V_{ALTase}	$300\frac{mM}{min}$	[Chalhoub et al., 2007], [Sánchez-Muros et al., 1998]
$K_{m10PYRALA}$	$0.006mM^2*$	[Chalhoub et al., 2007], [Scheer et al., 2010], [Mu et al., 2012], [Ward et al., 2000]
$K_{m10ALAPYR}$	$1{,}5mM^2*$	[Chalhoub et al., 2007], [Ward et al., 2000], [Sánchez-Muros et al., 1998]

* assumed by the product of a $K_m = 3mM$ and the respective redox coenzyme concentration of table 7.10

Table 7.28: ALTase kinetics

ATPase: $ATP \longrightarrow ADP$ The adenosine triphosphatase (ATPase) reaction (Na-K ATPase) is assumed to represent the overall ATP consumption of the system, as described by the form of the equation of table 7.29 [Tian et al., 2013], [Chalhoub et al., 2007], [Lambeth and Kushmerick, 2002], [Hynne et al., 2001], [Wolf et al., 2000], [Mulquiney and Kuchel, 1999], Brumen and Heinrich [1984].

$$v_{13} = k_x[A_3]$$

Parameter	Value	Reference
k_{rest}	$0.28\frac{1}{min}$	[Lambeth and Kushmerick, 2002]*, [Schuster et al., 1988], [Termonia and Ross, 1981]
k_{med}	$3.2\frac{1}{min}$	[Tian et al., 2013], [Cloutier et al., 2009], [Lambeth and Kushmerick, 2002]*, [Hynne et al., 2001]
k_{max}	$28\frac{1}{min}$	[Lambeth and Kushmerick, 2002]*, [Wolf et al., 2000]

* in relation to table 7.10

Table 7.29: ATPase kinetics

PDCase: $PYR \longrightarrow ACA$ The conversion of **pyr!** into acetyl coenzyme A (ACA) by a pyruvate dehydrogenase complex (PDCase) is assumed to follow Michaelis-Menten kinetics [Chassagnole et al., 2002], [Hynne et al., 2001].

$$v_{14} = \frac{V_{PDCase} \cdot \frac{[PYR]}{K_{m14PYR}}}{1 + \frac{[PYR]}{K_{m14PYR}}}$$

Parameter	Value	Reference
V_{PDCase}	$35\frac{mM}{min}$	[Hynne et al., 2001]
K_{m14PYR}	$0.3mM$	[Chalhoub et al., 2007], [Hynne et al., 2001], [Chassagnole et al., 2002]

Table 7.30: PDCase kinetics

7.3.3 Correction Factor for Insulin

The contribution of the time dependent, dimensionless scaling factor α ($0 \leq \alpha \geq 1$) to an equation corresponds to the effect insulin has on that process. In the case of the GLUT4 transporter this implies maximum efficiency at $\alpha = 1$ and no glucose transport at all, when insulin is absent ($\alpha = 0$). The insulin dependence is assumed to follow the equation in table 7.31 [Pielmeier, 2010], [Arleth et al., 2000].

$$\alpha = \frac{\left(\frac{Q(t) - Q_0}{\sqrt[d]{(Q(t)-Q_0)^d + {Q_k}^d}} - \frac{Q(0) - Q_0}{\sqrt[d]{(Q(0)-Q_0)^d + {Q_k}^d}} \right)}{\left(1 - \frac{Q(0) - Q_0}{\sqrt[d]{(Q(0)-Q_0)^d + {Q_k}^d}} \right)}$$

Parameter	Value	Reference
Q(t) (steady state)	$18\frac{mIU}{l} = 125.01 \cdot 10^{-6} mM$	[Pielmeier, 2010]
Q_0	$4.9\frac{mIU}{l} = 34.03 \cdot 10^{-6} mM$	[Pielmeier, 2010]
d	1.77	[Pielmeier, 2010]
Q_k	$31.7\frac{mIU}{l} = 220.16 \cdot 10^{-6} mM$	[Pielmeier, 2010]
Q(0) (normal insulin level)	$55 \cdot 10^{-6} mM$	[Meyer et al., 1998], [Consoli et al., 1990b]

Table 7.31: Insulin correction kinetics and parameters

Given the values of table 7.31 and assuming a constant insulin level, α is equal to 0.3. For the programmed version of the model α is independent of the insulin level and kept

constant in thee steps between (0.3, 0.6, 1), as it is imagined to be a potential interface for other models that describe and consider this insulin dependent relation and require further work in that particular direction.

Chapter 8

Model of the Cori Cycle

This chapter presents the developed mathematical model of the Cori cycle.

8.1 General Concept of the Model

The model operates on two layers, cellular level and organ level. The cellular level is described by the production and interaction of metabolites in the intracellular metabolism, that the equations describing the reaction network of the cellular carbohydrate metabolism. The organ level is described by the exchange of metabolites between organs and their accumulation in the blood. This level is described by a compartment model and the flow of masses between several compartments, representing the bloodstream and organs, respectively. This division emerged as the biochemical reactions provide parameters for the processes at organ level in the form of secretion and uptake rates for glucose, lactate and alanine, as well as their accumulation in the blood, which are of interest for the scope of application to evaluate the metabolic state the modeled organism is in. At organ level there are less parameters, which are in vivo comparatively easy to measure, to tweak the model and potentially improve its predictive value for the aimed application as a decision support system.
Each figure of section 8.2 represents one cell of a respective organ and its metabolism in terms of glycolysis and gluconeogenesis. Each of those cells will release and absorb certain metabolites at a certain rate, determined by the equations that describe the intracellular conversion from one metabolite (substrate) to another (product). For the listed cell types to represent an entire organ, their metabolism has to be scaled to organ level, using the cell quantities and volumes derived in chapter 7. To simplify the calculations, it was already implied that the respective organs consist of only one type of cell - the type which has a metabolism described by the presented differential equations (cellular level). Therefore an organ e.g. the liver can be assumed to be represented by one cell that has the volume of the respective organ e.g. $1.73l$, as listed in table 7.4. The released metabolite e.g. GLUx (extracellular glucose) has a blood concentration that is determined by the releasing rate and volume of the organ it originated from, and the blood perfusion of

that organ, which has been derived in chapter 7 for all considered organs. At this point it is feasible to convert the metabolite concentration to a mass related dimension, e.g. mg/dl. The metabolite flow in and out of an organ can again be described by an ODE and for multiple organs by a set of, in this case, linear ODE, which can be solved by using the standard ansatz for a solution of an ODE of that kind: $y = A \cdot e^{\lambda x}$, which has been discussed in chapter 4 in a slightly different context [Merziger, 2004]. Those equations do not possess any unknowns, as they are directly derived from the metabolic reactions inside the cell and the other mentioned other boundary conditions such as organ volume and perfusion. These linear ODE describe the flux between the compartments blood-glucose, -lactate, and -alanine and the organs, respectively, which is illustrated by figure 8.7. Of interest for the application, because easy to measure and used trend and risk evaluation are the metabolite concentrations in the blood. The out-flux of a metabolite is therefore summed in in its respective blood compartment. However, the combined amount of e.g. lactate produced by all considered organs amounts to roughly 2/3 of the total amount produced by the organism, as pointed out in table 6.1 of chapter 6. The remaining 1/3 is assumed to be a constant production by the fatty acid metabolism, which has not been considered for this model at all. At this point is is unclear whether or not this constant flux can be expressed by manipulating existing parameters of other organs and the matter will be further discussed in chapter 10.

8.2 Cellular Level

8.2.1 Skeletal Muscles Metabolic Model

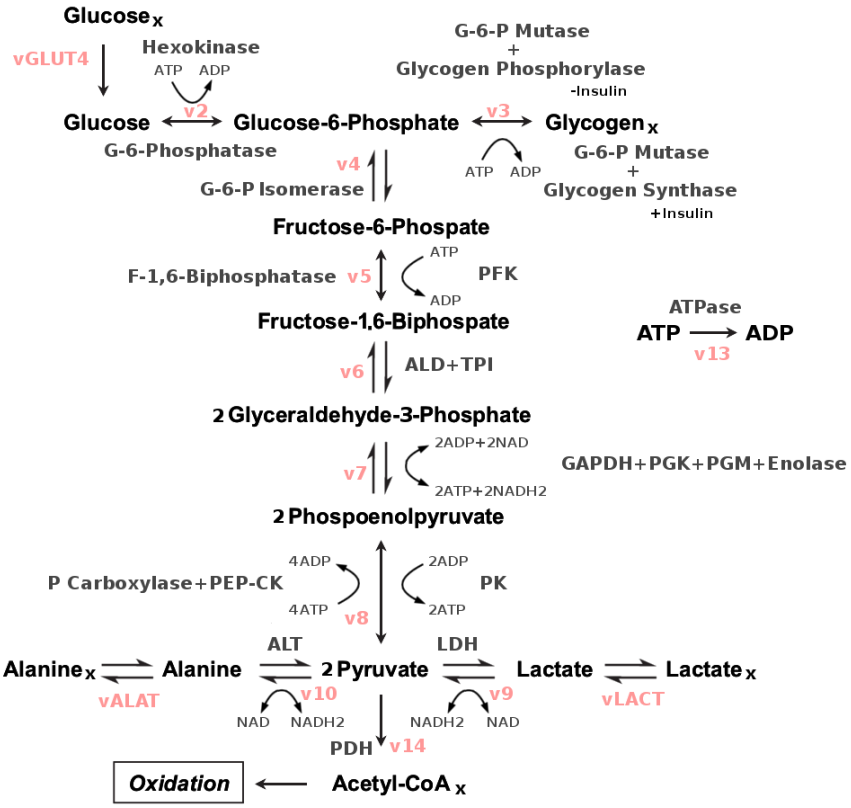

Figure 8.1: The figure shows the structural model for the muscular carbohydrate metabolism that also accounts for 70% of the alanine production [Mizock, 2001].

$$[\dot{\mathrm{GLU}}] = \mathrm{v}_{\mathrm{GLUT4}} - \mathrm{v}_2 \tag{8.1a}$$
$$[\dot{\mathrm{G6P}}] = \mathrm{v}_2 + \mathrm{v}_3 - \mathrm{v}_4 \tag{8.1b}$$
$$[\dot{\mathrm{F6P}}] = \mathrm{v}_4 - \mathrm{v}_5 \tag{8.1c}$$
$$[\dot{\mathrm{FBP}}] = \mathrm{v}_5 - \mathrm{v}_6 \tag{8.1d}$$
$$[\dot{\mathrm{GAP}}] = \mathrm{v}_6 - 2\mathrm{v}_7 \tag{8.1e}$$
$$[\dot{\mathrm{PEP}}] = 2\mathrm{v}_7 - 2\mathrm{v}_8 \tag{8.1f}$$
$$[\dot{\mathrm{PYR}}] = 2\mathrm{v}_8 - \mathrm{v}_9 - \mathrm{v}_{10} - \mathrm{v}_{14} \tag{8.1g}$$
$$[\dot{\mathrm{LAC}}] = \mathrm{v}_9 - \mathrm{v}_{\mathrm{LACT}} \tag{8.1h}$$
$$[\dot{\mathrm{ALA}}] = \mathrm{v}_{10} - \mathrm{v}_{\mathrm{ALAT}} \tag{8.1i}$$
$$[\dot{\mathrm{A}_3}] = -\mathrm{v}_2 - \mathrm{v}_3 - \mathrm{v}_5 + 2\mathrm{v}_7 + 2\mathrm{v}_8 - \mathrm{v}_{13} \tag{8.1j}$$
$$[\dot{\mathrm{N}_2}] = 2\mathrm{v}_7 - \mathrm{v}_9 \tag{8.1k}$$

8.2.2 Liver Metabolic Model

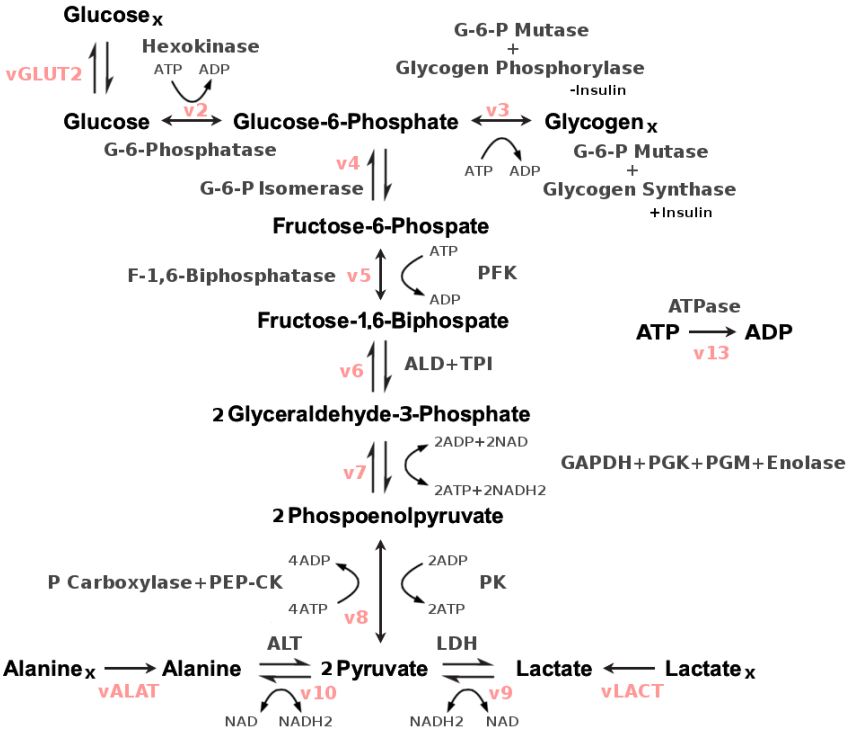

Figure 8.2: The figure shows the structural model for the hepatic carbohydrate metabolism. Differences in comparison to the muscle model are the reversible glucose transport and unidirectional lactate transport, as well as the uptake of alanine.

$$[\dot{\mathrm{GLU}}] = -\mathrm{v}_{\mathrm{GLUT2}} + \mathrm{v}_2 \tag{8.2a}$$
$$[\dot{\mathrm{G6P}}] = -\mathrm{v}_2 - \mathrm{v}_3 + \mathrm{v}_4 \tag{8.2b}$$
$$[\dot{\mathrm{F6P}}] = -\mathrm{v}_4 + \mathrm{v}_5 \tag{8.2c}$$
$$[\dot{\mathrm{FBP}}] = -\mathrm{v}_5 + 2\mathrm{v}_6 \tag{8.2d}$$
$$[\dot{\mathrm{GAP}}] = -2\mathrm{v}_6 + 2\mathrm{v}_7 \tag{8.2e}$$
$$[\dot{\mathrm{PEP}}] = -2\mathrm{v}_7 + 2\mathrm{v}_8 \tag{8.2f}$$
$$[\dot{\mathrm{PYR}}] = -2\mathrm{v}_8 + \mathrm{v}_9 + \mathrm{v}_{10} \tag{8.2g}$$
$$[\dot{\mathrm{LAC}}] = -\mathrm{v}_9 + \mathrm{v}_{\mathrm{LACT}} \tag{8.2h}$$
$$[\dot{\mathrm{ALA}}] = -\mathrm{v}_{10} + \mathrm{v}_{\mathrm{ALAT}} \tag{8.2i}$$
$$[\dot{\mathrm{A}_3}] = -\mathrm{v}_2 - \mathrm{v}_3 - \mathrm{v}_5 + 2\mathrm{v}_7 + 2\mathrm{v}_8 - \mathrm{v}_{13} \tag{8.2j}$$
$$[\dot{\mathrm{N}_2}] = -2\mathrm{v}_7 + \mathrm{v}_9 + \mathrm{v}_{10} \tag{8.2k}$$

8.2.3 Kidney Metabolic Model

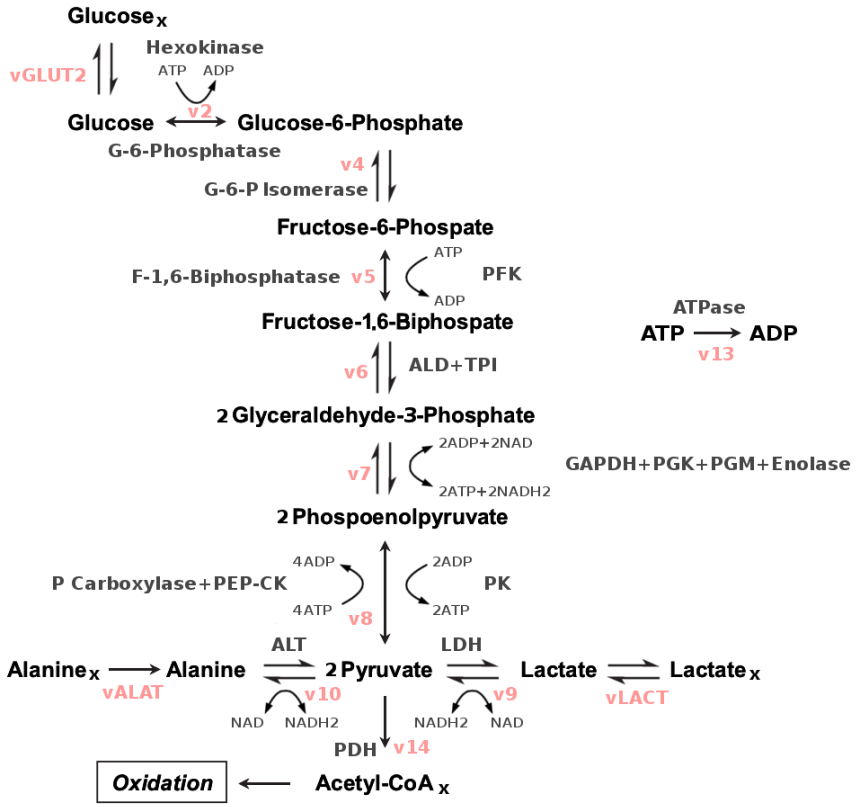

Figure 8.3: The figure shows the structural model for the renal carbohydrate metabolism. The kidney model largely corresponds to the liver model, except for the glycogen conversion, which is not included for the kidneys, and the added possibility to convert **pyr!** into ACA (only renal cortex, not medulla) [Löffler et al., 2007]. Moreover, the bidirectional lactate transporter is used.

$$[\dot{\mathrm{GLU}}] = -\mathrm{v}_{\mathrm{GLUT2}} + \mathrm{v}_2 \tag{8.3a}$$
$$[\dot{\mathrm{G6P}}] = -\mathrm{v}_2 + \mathrm{v}_4 \tag{8.3b}$$
$$[\dot{\mathrm{F6P}}] = -\mathrm{v}_4 + \mathrm{v}_5 \tag{8.3c}$$
$$[\dot{\mathrm{FBP}}] = -\mathrm{v}_5 + 2\mathrm{v}_6 \tag{8.3d}$$
$$[\dot{\mathrm{GAP}}] = -2\mathrm{v}_6 + 2\mathrm{v}_7 \tag{8.3e}$$
$$[\dot{\mathrm{PEP}}] = -2\mathrm{v}_7 + 2\mathrm{v}_8 \tag{8.3f}$$
$$[\dot{\mathrm{PYR}}] = -2\mathrm{v}_8 + \mathrm{v}_9 + \mathrm{v}_{10} - \mathrm{v}_{14} \tag{8.3g}$$
$$[\dot{\mathrm{LAC}}] = -\mathrm{v}_9 + \mathrm{v}_{\mathrm{LACT}} \tag{8.3h}$$
$$[\dot{\mathrm{ALA}}] = -\mathrm{v}_{10} + \mathrm{v}_{\mathrm{ALAT}} \tag{8.3i}$$
$$[\dot{\mathrm{A}}_3] = -\mathrm{v}_2 - \mathrm{v}_5 + 2\mathrm{v}_7 + 2\mathrm{v}_8 - \mathrm{v}_{13} \tag{8.3j}$$
$$[\dot{\mathrm{N}}_2] = -2\mathrm{v}_7 + \mathrm{v}_9 + \mathrm{v}_{10} \tag{8.3k}$$

8.2.4 Blood Cells Metabolic Model

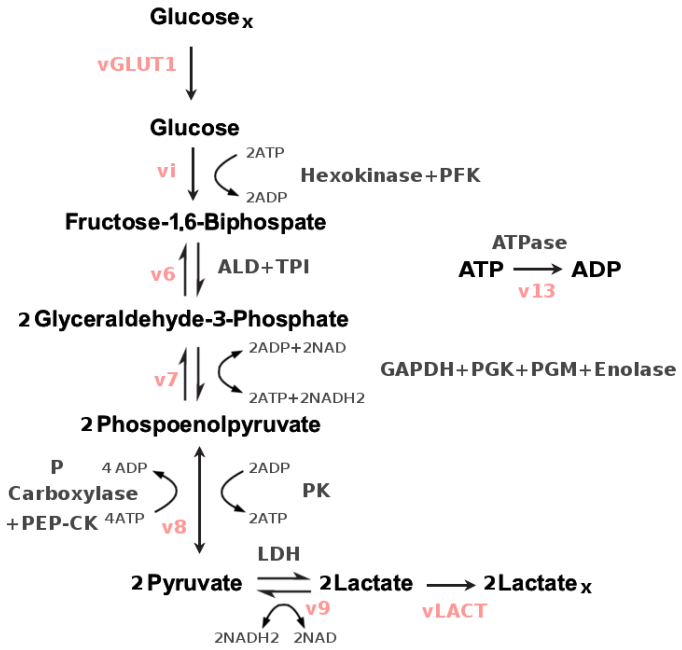

Figure 8.4: The figure shows the structural model for glycolysis in the red blood cell. Contrary to the previous organs presented in figures 8.1a, 8.2, 8.3, the conversion of glucose into FBP and t **pep!** into **pyr!** is assumed irreversible. The reactions have therefore been replaced by v_i and v_p, respectively

$$[\dot{\mathrm{GLU}}] = v_{GLUT1} - v_i \tag{8.4a}$$
$$[\dot{\mathrm{FBP}}] = v_i - 2v_6 \tag{8.4b}$$
$$[\dot{\mathrm{GAP}}] = 2v_6 - 2v_7 \tag{8.4c}$$
$$[\dot{\mathrm{PEP}}] = 2v_7 - 2v_8 \tag{8.4d}$$
$$[\dot{\mathrm{PYR}}] = 2v_8 - 2v_9 \tag{8.4e}$$
$$[\dot{\mathrm{LAC}}] = v_9 - 2v_{LACT} \tag{8.4f}$$
$$[\dot{\mathrm{A}}_3] = -2v_i + 2v_7 + 2v_p - v_{13} \tag{8.4g}$$
$$[\dot{\mathrm{N}}_2] = 2v_7 - 2v_9 \tag{8.4h}$$

8.2.5 Brain Metabolic Model

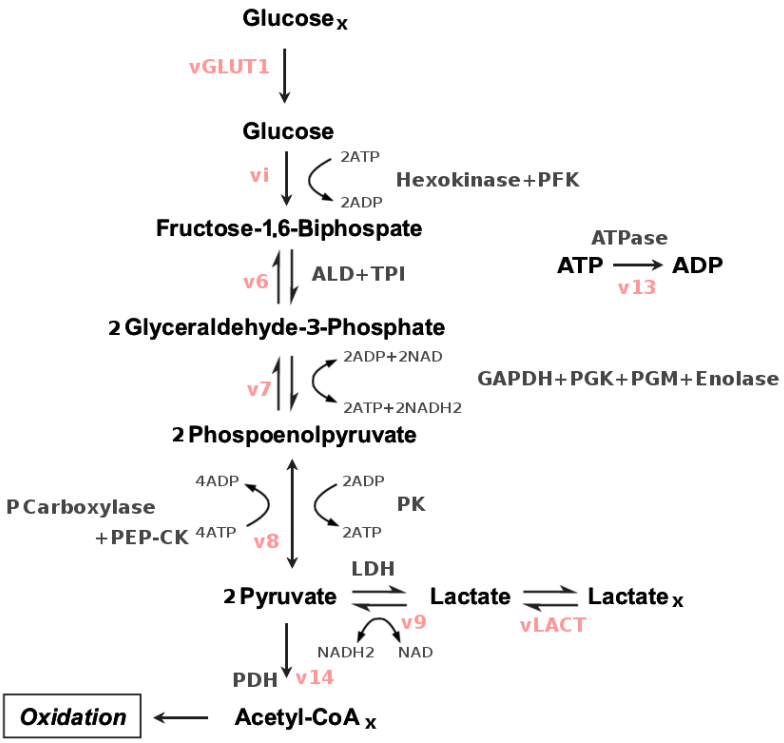

Figure 8.5: The figure shows the structural model for glycolysis in the neurons, as presented in figure 8.4, and additionally accounts for the cerebral lactate uptake.

$$[\dot{\mathrm{GLU}}] = \mathrm{v}_{\mathrm{GLUT1}} - \mathrm{v}_{\mathrm{i}} \tag{8.5a}$$
$$[\dot{\mathrm{FBP}}] = \mathrm{v}_{\mathrm{i}} - 2\mathrm{v}_{6} \tag{8.5b}$$
$$[\dot{\mathrm{GAP}}] = 2\mathrm{v}_{6} - 2\mathrm{v}_{7} \tag{8.5c}$$
$$[\dot{\mathrm{PEP}}] = 2\mathrm{v}_{7} - 2\mathrm{v}_{8} \tag{8.5d}$$
$$[\dot{\mathrm{PYR}}] = 2\mathrm{v}_{8} - 2\mathrm{v}_{9} - 2\mathrm{v}_{14} \tag{8.5e}$$
$$[\dot{\mathrm{LAC}}] = \mathrm{v}_{9} - 2\mathrm{v}_{\mathrm{LACT}} \tag{8.5f}$$
$$[\dot{\mathrm{A}_3}] = -2\mathrm{v}_{\mathrm{i}} + 2\mathrm{v}_{7} + 2\mathrm{v}_{\mathrm{p}} - \mathrm{v}_{13} \tag{8.5g}$$
$$[\dot{\mathrm{N}_2}] = 2\mathrm{v}_{7} - \mathrm{v}_{9} \tag{8.5h}$$

8.2.6 Operating Principle of the Model Equations

Each of the reaction chains depends by and large on the concentration gradients of the respective metabolites. Assuming a sinusoid input to one of the reversible equations that describe a reaction or transport, e.g. a reversible GLUT1 results in a self limiting subsystem. A reversible GLUT1 is not used in the model but was elected to serve example and demonstration purposes. It was implicitly presented in table 7.11 and was implemented in a test VI as the basis for all reaction subVI to come. It is given by equation 8.6.

$$\mathrm{vGLUT}_1 = \frac{\mathrm{VGLUT1}([\mathrm{GLU_x}] - [\mathrm{GLU}])}{\mathrm{KmGLUT1} + [\mathrm{GLU_x}] + [\mathrm{GLU}]} \tag{8.6}$$

A sine ($amplitude = 5mM$, $phase = 0deg$, $cycle = 1.4$) is assumed as changing input to equation (GLU_x). Starting from 0, each time the positive half period is input over time, the result of the equation relates to GLU, each negative half period relates back to the input GLU_x, representing forward and reverse reaction or GLU_x transport into and GLU transport out of the cell. Determined by the parameters and the sine input, GLU from the cell is transported into the blood, which appears as a reduction in GLU from its starting condition, given in table 7.10 of chapter 7. The negative half period of the sine inverts the sign of the reaction constant, which leads to a reverse reaction and the change in output is related to a change in input. In this example the GLU_x concentration increases (reduced output), while the GLU concentration decreases further, as depicted in figure 8.6.

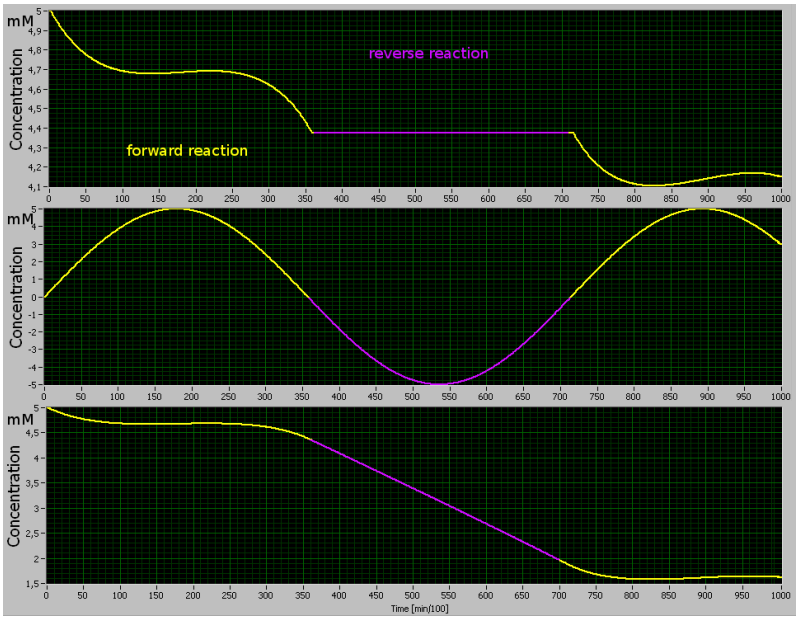

Figure 8.6: The figure shows the output of equation 8.6 with respect to the intracellular glucose concentration (GLU) over 10 minutes. The upper most graph shows the output with the reverse reaction (GLU_x production) set to 0 (= unidirectional), the bottom graph shows the output including the reverse reaction with respect to GLU. The GLU reduction corresponds to a GLU_x production of the same amount, starting from 0 ($\sin(0) = 0$). The graph in the middle displays the sine input with the positive half period marked yellow and the negative marked purple

The differential equations presented in chapter 7.3 have been realized by making the output of one kinetic equation the input to another for them to exactly match match the structural models of chapter 8. It is therefore imperative to determine the sign of the input and relate the change in output, especially since the output of one equation serves as the input for the next. This example further illustrates the necessity to block any output in the substrate direction (by setting the rate change to 0), for any negative input, to prevent obscured data. Unidirectional reactions/transporter have therefore to be modeled slightly differently from reversible reaction, requiring further logical limitations, not the least of which is stopping the reaction, when the substrate is depleted. The details will be presented in chapter 9.

8.3 Organ Level

The reactions of the different cells in muscle, liver, kidney, blood cells, and brain have to be scaled up to organ level to make use of them for evaluating the metabolism of the whole organism. This means the rates at which the respective metabolite is released from the cell is multiplied by the volume of the respective organ, established in chapter 7. A schematic overview of the organ interactions derived from chapter 6 is given in figure 8.7.

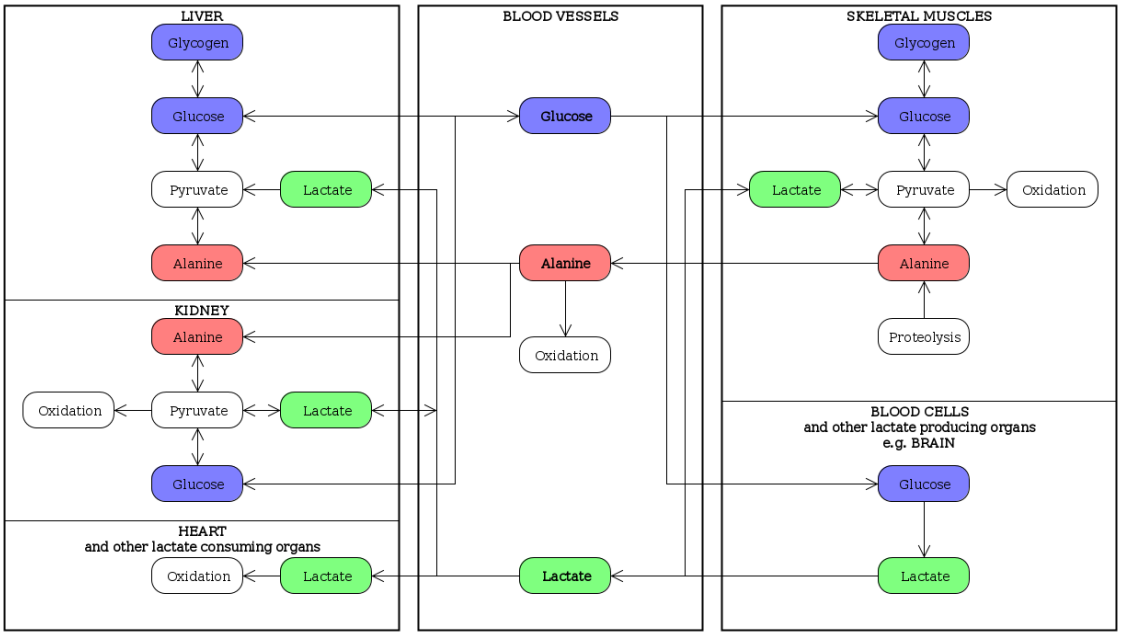

Figure 8.7: The figure shows the structural model at organ level, incorporating the structural model on the molecular level.

This can be simplified to a compartment model with the three compartments for glucose (**G**), lactate(**L**), and alanine (**A**) to represent their respective concentration in the blood, as depicted in figure 8.8. The blood is where they most likely will be measured as parameters with potentially predictive properties on the phase and development of critical illness, as outlined in chapters 1 and 3. The concentration of those metabolites is therefore considered the primary output of the modeled system.

The way they have been modeled on the cellular level all of the organs themselves are compartments. However on organ level that becomes less relevant, as their interaction with each other and thus the blood stream, or blood plasma to be precise, becomes more prominent and important for the scope of application.
The compartmental model exhibits a quite modular structure and is therefore further discussed with only one single compartment as an exemplary and representative in mind. One compartment, as well as all of them can be mathematically described by balance equations that comprise the in- and outflow of the compartment, as depicted in figure 8.9.

These balance equations are linear ODE and become a system of linear ODE when all organs shall be described. The generic compartment **M** shall therefore illustrate the general way to a mathematical solution for the system on organ level. Contrary to

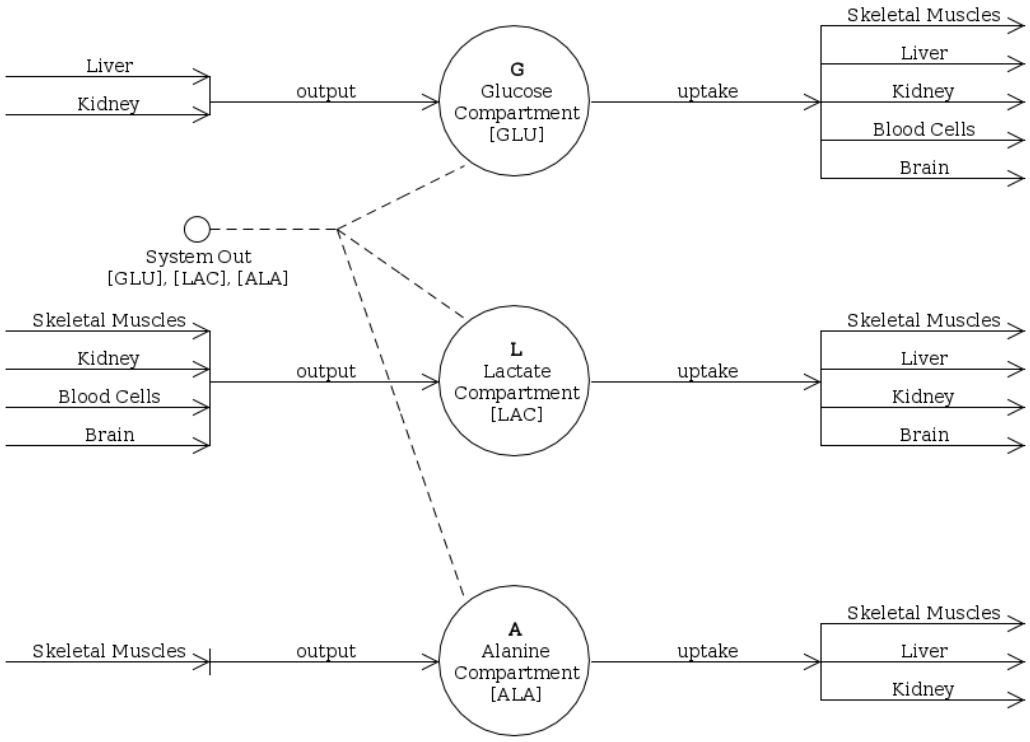

Figure 8.8: The figure shows the developed compartmental model at organ level with skeletal muscles, liver, kidney, blood cells, and brain as the main focus of involved organs. Each of them is assigned a role as either releasing a certain metabolite into the blood stream (output), absorbing it (uptake) or both. This list could almost at will be completed with other organs and potentially improve the model. All compartments are connected by the skeletal muscles.

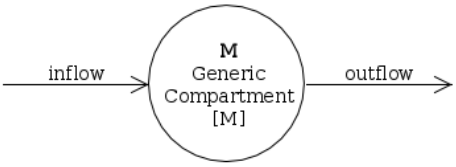

Figure 8.9: The figure shows a generalized simple compartment model **M** with the metabolite concentration [M].

the cellular level, where molecular conversions were described in dependency of molecule concentrations (mmol/l), it is more feasible to rely on mass related balance equations for the organ level. The reason is that molecule concentrations tend to change over the course of a chemical reaction and masses before and after the reaction do not. An example of changing molecule count during glycolysis is the conversion of glucose-1,6-biphosphate into two molecules of glyceraldehyde-3-phosphate. This problem can be addressed by including extra factors/exponents in the Michaelis-Menten equations, as seen in the respective equation of table 7.24.

For **M** is assumed that a particular mass of a particular metabolite M is dissolved in the volume of the compartment, which is $V_0 = 5l = 50dl =$ constant for the whole blood

volume of the human body, as outlined in chapter 7. The mass inflow of **M** equals the organ output of the metabolite M and can therefore be described by the product of organ perfusion p and metabolite amount c of M in that blood, which yields a rate a. The perfusion rate is organ specific and has been established in chapter 7. On the other hand, the organ uptake equals the mass outflow of **M** and is the product of organ perfusion rate p and time dependent metabolite concentration [M] divided by the compartment volume V_0, as seen in equations 8.7a [Blomhøj et al., 2014].

$$[\mathrm{M}]_{\mathrm{inflow}} = \mathrm{p}\frac{dl}{min} \cdot \mathrm{c}\frac{mg}{dl} \cdot \Delta \mathrm{t}min = \mathrm{a}\frac{mg}{min} \cdot \Delta \mathrm{t}min \tag{8.7a}$$

$$[\mathrm{M}]_{\mathrm{outflow}} = \mathrm{p}\frac{dl}{min} \cdot \frac{[\mathrm{M}]}{\mathrm{V}_0}\frac{mg}{dl} \cdot \Delta \mathrm{t}min \tag{8.7b}$$

The difference equation describes the difference between in- and outflow of the compartment over a time step Δt and yields the linear ODE for the total differential of $\Delta \mathrm{t} \to 0$, as seen in equations 8.8a [Blomhøj et al., 2014].

$$\frac{[\mathrm{M}](\mathrm{t}+\Delta \mathrm{t})-[\mathrm{M}]}{\Delta \mathrm{t}} = \mathrm{a}\frac{mg}{min} - \frac{\mathrm{p}[\mathrm{M}]}{\mathrm{V}_0}\frac{mg}{min} \tag{8.8a}$$

$$= \mathrm{a}\frac{mg}{min} - \mathrm{b}[\mathrm{M}]\frac{mg}{min} \tag{8.8b}$$

With b being the quotient of perfusion and blood volume, the rate a being known from the scaled cell output to organ level known from chapter 6, and the established blood volume of $5l$ all parameters of this linear ODE are determined and the equation can be solved by separation of variables and the ansatz $\mathrm{y} = \mathrm{A} \cdot e^{\lambda x}$, which yields the general solution given in equation 8.9.

$$[\mathrm{M}] = \mathrm{d}mg + \mathrm{C}mg \cdot e^{-bt} \tag{8.9}$$

Which can be completely solved for a particular solution by applying an initial condition e.g. the normal BGL of $\mathrm{M}_0 = 90mg/ml$ from table 7.10 to determine the parameter C. Basically, at this point the bottom-up and top-down approach of modeling could meet and complement each other by using independent experimental data for both, model validation and parameters determination. It also becomes apparent that this model basically possesses three hierarchical layers. The first being a single differential equation, describing one reaction based on changing input, the second being the system of differential equations that describe the cellular metabolism by how they are connected to one another, and the third being the interactions of the organs, as described by the compartment model.

Chapter 9

Computer Model of the Cori Cycle

This chapter presents the programed model and documents the program structure, development and features. After a brief introduction to the software used for programming, the user interface is presented and major code fragments are discussed to illustrate the working principle of the program in general and the processing of the calculations in particular.

9.1 Software

The model was implemented using the data stream oriented programming platform and development environment of LabVIEW (National Instruments). Although LabVIEW is not a cryptic programming language like C or Java, but a graphical programming concept, its source code is written in *G* and translated to machine code prior to execution, making it a compiled language. Instead of text, icons are used and variables are represented as wires, with the wire color indicating the data type. The information flow is organized from left to right and visualized as current in an electric circuit to build applications in the block diagram. Those information are output to the front panel, which contains controls and indicators that manipulate the data stream and show the results to the user [Greiner, 2012]. Front panel and block diagram of a LabVIEW program (VI) are presented next to each other in figure 9.1 as an example.

9.2 State Machine

A state machine is a technique or a design pattern in software architecture for to represent the dynamic behavior of a system [Eriksson et al., 2003], [Arlow and Neustadt, 2002]. State machines are used to describe the event history of a single responsive object over its life time and the rules of how it can change between the instances of a finite number of states. A state describes the situation where an object meets a specified condition, is engaged in some activity or waits for an event. An event is the trigger for an object to respond

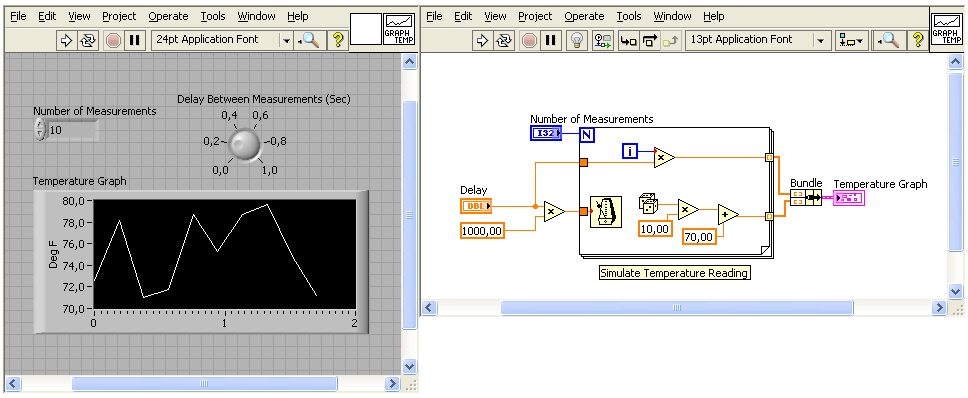

Figure 9.1: The figure shows the front panel (left) and block diagram (right) of the LabVIEW demo VI Graph Temperature.vi

to, e.g. a predefined time is over or a specific condition has been met. The transition describes the change from one state to another as the response to a prior event [Eriksson et al., 2003], [Arlow and Neustadt, 2002].
A state machine was designed to handle user interface, calculations and model output as different states, to divide the individual tasks of the program into smaller, more manageable parts. The design is illustrated by figure 9.2. Starting point is the waiting for input state, which presents the user with the graphical interface and input options.

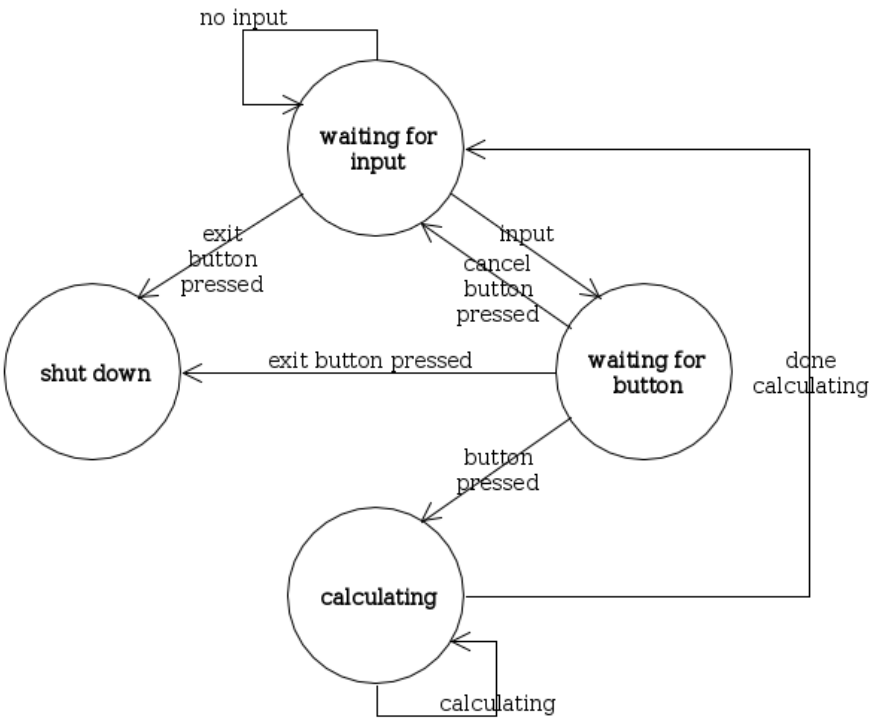

Figure 9.2: The figure shows the state diagram to describe the state machine created for the model, by defining the number of states and the transitions between them.

9.2.1 User Interface

The user interface was constructed in an attempt to capture and address the basic ideas of system usability and user friendliness, which comprise among others [Nielsen, 1994]:

- natural and simple system-user interaction
- low memory load on the user side combined with meaningful and consistent designations
- feedback on user input, as well as comprehensive error messages
- opportunity to abort and exit system functionalities
- system documentation

Figure 9.3 presents the developed user interface for the state machine.

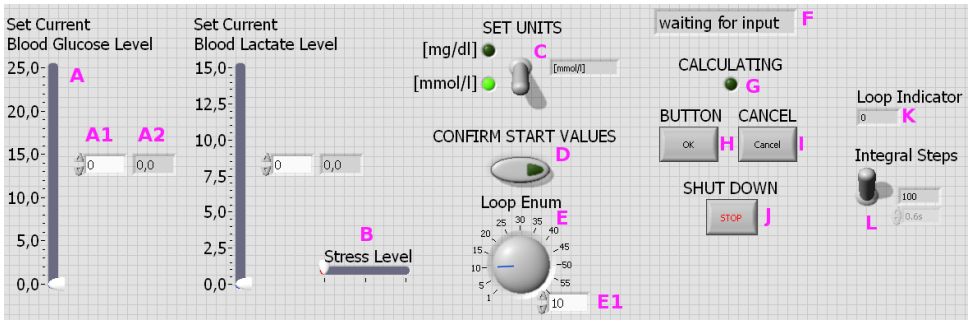

Figure 9.3: The figure shows the user interface generated by the front panel.

On the left hand side there are two vertical pointer slides named Set Current Blood Glucose Level (A) and Set Current Blood Lactate Level, respectively. These two controls are used to define the starting condition (initial value) for the calculations. Both have a set range of accepted input values, as indicated by the scale. The range can easily be modified in the front panel if necessary, however for the current version of the program and its development status it was elected to limit the input values as indicated by the respective scales. This also helps to exclude errors caused by non-realistic input e.g. negative values. Apart from the different scales, both vertical pointer slides are identical and their description is therefore focused to the glucose related and is also valid for the other one. Next to the slide there is a numeric control (A1) that reads the value set by the Pointer Slide Control and can be used to type in the initial value by using the keyboard. Right next to that there is a numeric indicator, which displays the current value and locks for confirmed input values, providing feedback. Additionally to the initial glucose and lactate values, some internal values, required for the calculations can be varied in three stages by using the horizontal pointer slide Stress Level. This control is set to the left most position, which corresponds to the minimal rate constant for ATPase $k_{rest} = 0.28\frac{1}{min}$ and an insulin correction factor $\alpha = 0.3$ that were introduced in chapter 7.3. The next two steps change alpha to $\alpha = 0.6$ and $\alpha = 1$, respectively and iterate through the remaining values of $k_{med} = 3.2\frac{1}{min}$ and

$k_{med} = 28\frac{1}{min}$. This option was included to switch the simulation from normal to two different states of increased metabolism to mimic a stress situation based on the available data. Further parameters could be included. An important part is the selection of the dimension for the input values of glucose and lactate, to give them meaning and relation to the output. Although any input value directly related to the output is internally converted to mg/dl by the program, the user is given the option to select the equally valid unit of $mmol/l$ $(= mM)$ as input dimension. This is achieved by the vertical toggle switch SET UNITS (C) that is connected to two light-emitting diode (LED) flashing up according to the position of the switch and indicate the selected dimension for the initial values. The input has to be confirmed by pressing the push button CONFIRM START VALUES (D) that will flash up as well for confirmation that the desired input has been made and a new state can be initialized. The dial Loop Enum determines the simulation time in minutes and is also limited by it input according to the scale. The simulation time can also be entered using the keyboard and the numeric control that indicates the selected simulation time (E1), identical to e.g. the glucose input (A1). To display to the user, what is expected of him the string indicator (F) displays the state of the program. For the state calculating the LED CALCULATING (G) will flash up to indicate the computing process to the use and turn off again once all calculations are done.
By pressing the CONFIRM START VALUES button all user input is locked and the state waiting for input is left to enter the state waiting for button. In case e.g. there has not yet been an input on the simulation time, the user can return to the state waiting for input by pressing the CANCEL Button (I) and modify the inputs again. Pressing the OK Button (H) after (re)confirming the initial values will cause the program to switch to the state calculating and include the user input to the respective equations. To support feedback of the calculation process besides the LED, the numeric indicator Loop Indicator (K) will display the elapsed loop iterations.
The simulation time can be modified by a factor hundred using the vertical toggle switch integral steps (L). This switch essentially multiplies the simulation time by 100 and scales the yielded results back to the simulation time that was input by the Loop Enum dial. The result is an increased precision in calculating the various metabolite concentrations (by a factor 100) so that one loop iteration represents $0.6s$, rather then one minute $(= 60s)$. The switch thus effectively increases the step size when integrating of the various ODE in the calculation process from one step to 100 and adjusts the output value. This will be presented in more detail in section 9.3. Implementing this switch attempts to address the error resulting from the numerical integration, which became noticeable and more prominent with rapid rate changes and low concentrations over longer simulation times. It was made optional to weigh the required additional computing performance against the possibly not required detailed calculation and thus save time to more quickly respond to the user input.
Additionally, the interface includes waveform graphs indicating the concentration of the main metabolites (glucose, lactate, and alanine), as changing quantities in the blood stream over time.

9.2.2 Waiting for Input

The states waiting for input, waiting for button, calculating, and shut down were realized by creating state variables of a customized, StrictTypeDef enum, which allocates the different states to a case distinction as the control state. This was done to facilitate the long term maintenance and expansion of the program by making it possible, to update all related constants and variables after a program change, e.g. after adding an extra state.
Waiting for input generates buttons and stores the values generated by the user input to different variables for further use. The block diagram of the waiting for input state is presented in figure 9.4.

The program is continuously running using a while loop and an enum initializes a shift register, which will store the value for the state from the previous loop iteration and thus keep the state until it is changed by user input. By entering the while loop the status of the program is output by the indicator (status) for the enum (A). At the same time the exit condition from the while-loop is set to the state shut down, which ends the program (B). Going further inward the next frame is a Case Structure coordinated by the enum (C). The frame inside the case structure is a *Flat Sequence*, which forces LabVIEW to execute the left frame before the right one. In the left part (D) all functional global variables are set to default to avoid obscured data caused by previous calculations.
Functional global variables are a LabVIEW design pattern to e.g. prevent racing conditions. An example of this pattern is presented in figure 9.11. The while-loop in the right frame of the flat sequence (E) sets the interface buttons that are accessible in the waiting for input state. In the top left corner, the stress level can be adjusted by the slide control. The enum (stress) is typecast on the control Stress Level, before a subVI is accessed, that scales the range of the control to an enum value, as depicted in figure 9.5. The adjacent indicators serve only the purpose to check the functionality of the subVI. This is generally the case with all indicators that are present in the various block diagrams but do not show up on the front panel. The enum integral steps is typecast as well and scales the number of loop iterations, generated by Loop Enum, according to the position of the toggle switch Integral Steps (F). Those values are then written to the functional global variables LoopCalc and IntCalc, respectively. The while-loop can be left by pressing either the CONFIRM START VALUES or SHUT DOWN button, which is represented by a local variable (G). When leaving the loop the user input is saved to local variable of the controls Set Current Blood Glucose/Lactate Level (I). Moreover, the unit of the user input, determined by the position of the toggle switch is stored in the enum unit. When the toggle switch is flipped the scales of the input control for glucose and lactate change value between $mmol/l$ and mg/dl (H). After pressing the CONFIRM START VALUES, the LED of the corresponding unit will remain flashed, even though the switch itself can still be flipped.
Leaving the while-loop will cause the selector to permit the progression to the next state in the case structure (waiting for button), while the buttons that were used are being reset to default (J) and (K).

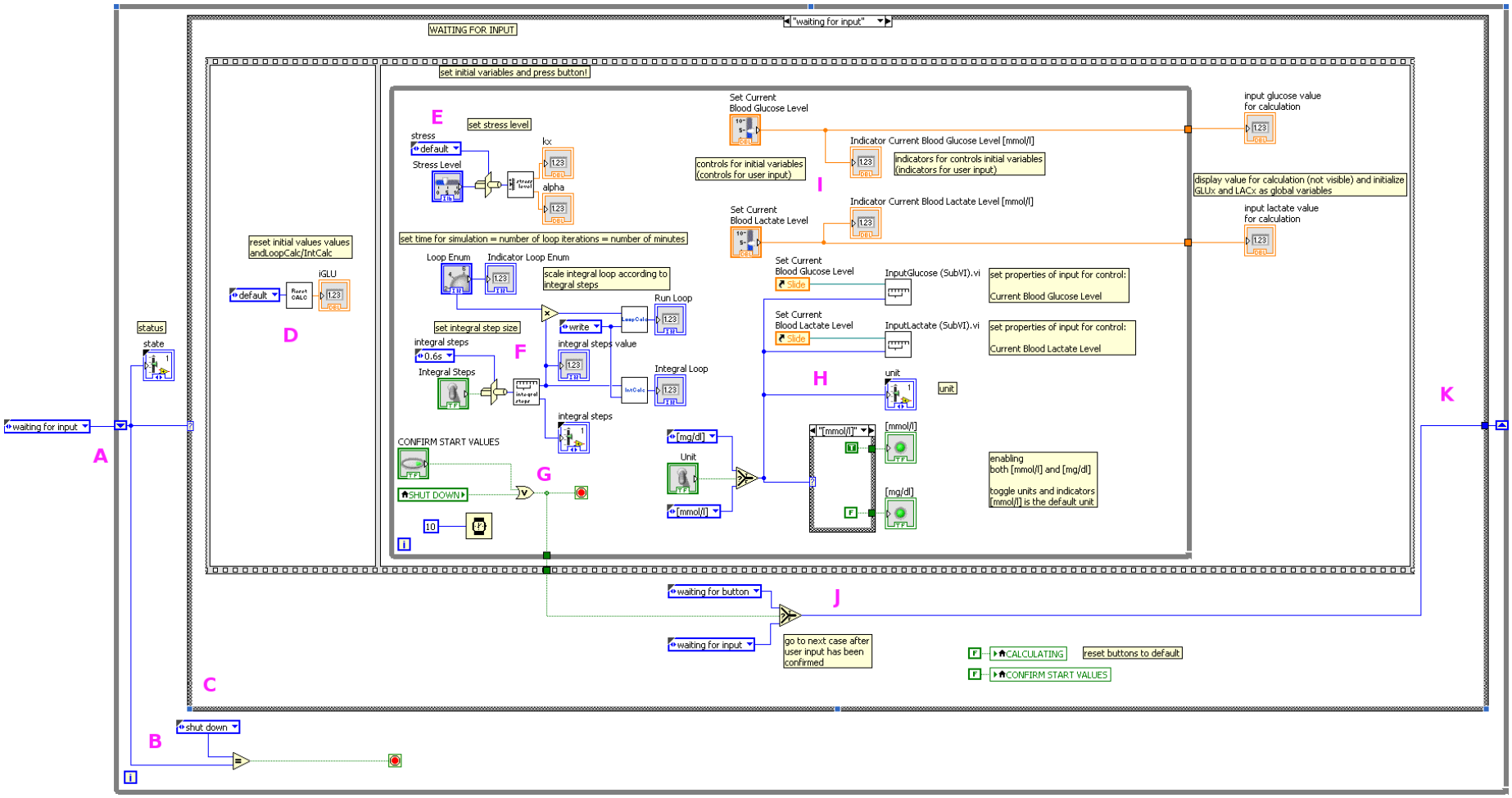

Figure 9.4: The figure shows the waiting for input state and its processes.

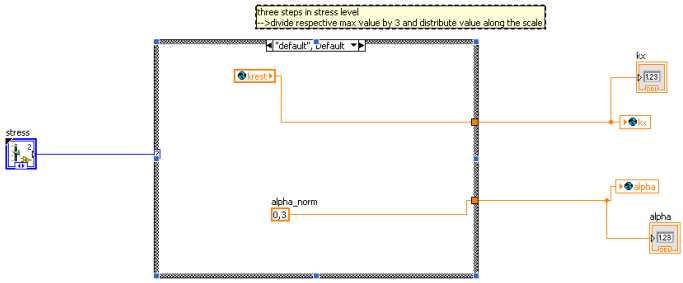

Figure 9.5: The figure shows the subVI StressLevel (SubVI).vi as an example for an enum controlling a case structure to define different values in dependence of certain conditions.

9.2.3 Waiting for Button

Figure 9.6 depicts the next state after successfully leaving the waiting for input state in the forward direction. This state serves as a transition and is intended for the user to

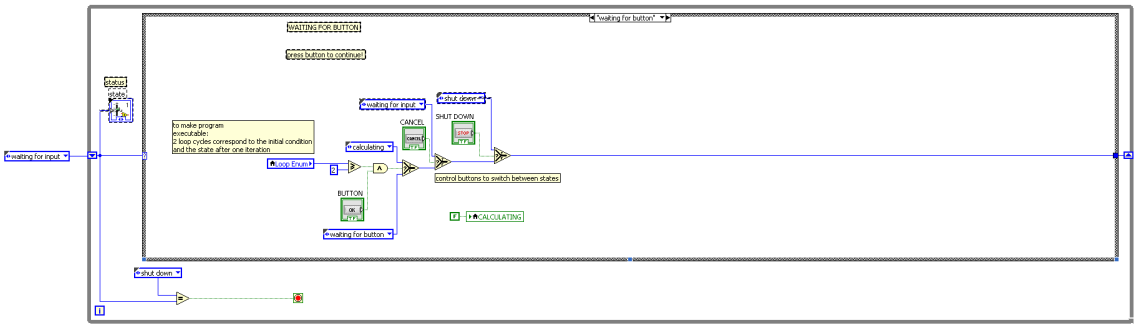

Figure 9.6: The figure shows the state waiting for button.

reflect upon the input and giving the opportunity to change the input by pressing the Cancel button and return to waiting for input. Moreover, the program can be terminated by pressing the STOP button at this point. In case the use wishes to receive the simulation results he may press the OK button. The position of each button determines the next state of the state machine and is selected by evaluating two enums of the state control. The sequence of checking the position of all three button implies a hierarchy with the STOP button on to to overrule all others, as would be expected from an off switch. The first criterion to proceed, however, is the number of calculations, the user wishes performed (Loop Enum). The input there has to be larger than two to receive a simulation over one minute, as the first loop iteration (0) only sets the initial values. This implies that an input of e.g. 11 minutes would technically only simulate over 10 minutes, as one loop iteration is lost for the setup of the initial values. The CALCULATING LED is turned off and in case the OK button was pressed instead of any other, the next state, calculating can be entered. In case the Cancel button is pressed, the user returns to the waiting for input state and in case the STOP button is pressed, the program enters the shut down state.

9.2.4 Shut Down

The shut down state, as depicted in figure 9.7 rests all buttons and LED back to default by writing a false value to their local variables..

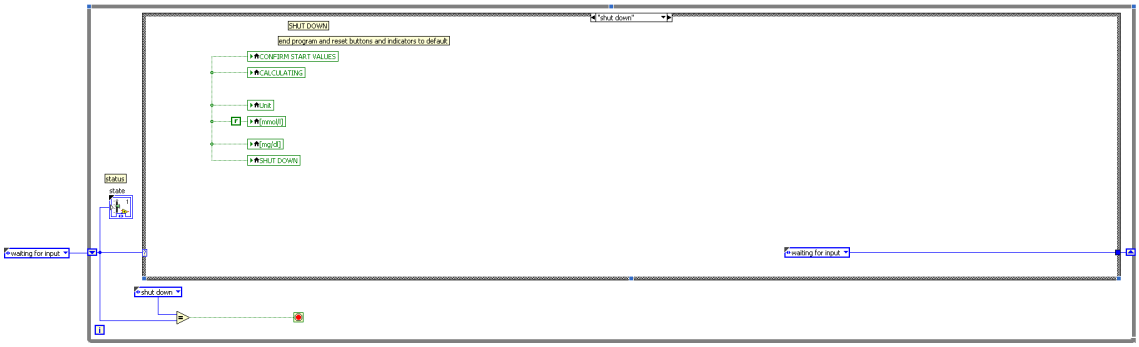

Figure 9.7: The figure shows the state shut down.

9.2.5 Calculating

The program is generally divided into two parts. The state machine design pattern and a producer/consumer design pattern, which is illustrated by figure 9.8. As state machines are a highly effective way of solving sequential problems, they do not excel at parallel processing, which is why the state calculating was implemented using he more suitable producer/consumer pattern to coordinate the multiple interdependent calculations reactions required for the simulation of the Cori cycle. The producer/consumer setup synchronizes multiple parallel operating loops by ensuring that a consumer loop is only executed once the producer loop sends new data. It is otherwise on hold. This enables a coordination of the various calculations from the ODE that is to be expected. This limited data supply is is handled by LabVIEWs queue functions, which operates on a first come, first served basis.

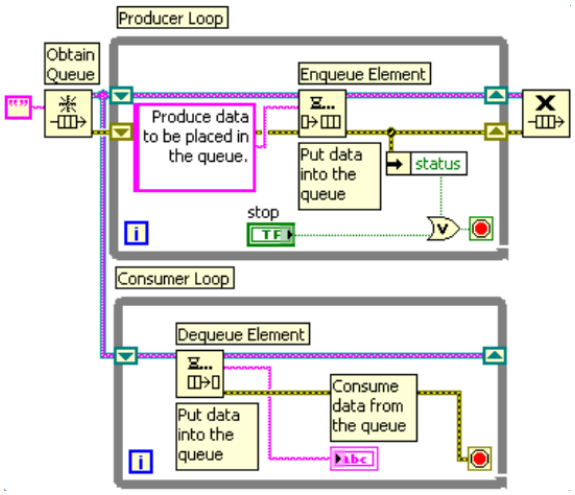

Figure 9.8: The figure shows the producer/consumer design pattern suggested for LabVIEW [Instruments, 2012]

Calculating is the most complex state and contains the VI that solve equations, as well as their organization. It was focused on using the graphical possibilities LabVIEW provides to keep the VI structure as close to the structural models as possible, which is why the case structure of the calculating state mimics the appearance of the compartment model of figure 8.8 with its in- and outflow characteristics, as depicted in figure 9.9.

The user input is called via local variable and independent of the selected unit converted to mg/dl to have a basis for the necessary calculations that follow. The initial alanine concentration is stored in a global variable and converted to mg/dl as well (A). The subVI handling the conversion is depicted in figure 9.10.

For the first loop iteration these values are input into the for-loop as initial values for the calculations and queued by LabVIEWs enqueue function (B). To avoid further wires the values from the while-loop are passed via local variablesto the subVI CL, where they will be input into the differential equations, as described in section 9.3 (C). The output of the equations is handled with functional global variables, as glucose is an input and it was passed on the idea of adding extra wires for the reverse reactions and feedback to keep the VI better structured. Figure 9.11 depicts the block diagram of calc blood as a representative for all functional global variables, which are unique to every organ cell: blood cells (blood), neurons (brain), myocytes (muscle), hepatocytes (liver), and cells of the renal cortex (kidney) (D).

The output values ($mmol/l$) are scaled to organ level by multiplying them with the respective organ volume in liter (E). They are subsequently converted to mg/dl (F) and scaled with the perfusion of the respective organ in dl (G). For organs that consume and produce a particular metabolite the output is split in positive and negative values by a case structure and input into an compound array to be summed (H). This compound array represents the respective metabolite compartment and emphasizes the structure of the for-loop, which is mimicking the the compartment model structure presented in figures 8.8 and 8.9. Consequently the summation of the in- and outflow values (negative inflow represents outflow) represents the difference equation 8.8a for $\Delta t = 1min$, as one loop iteration represents one minute. Therefore the rate change can be read directly by indicators (Ka, Kb, Kc). The change in concentrations requires the point by point integration of the array values.
As the default direction for the chemical reactions in this model is the direction of glycolysis, lactate and alanine are generally viewed as output and glucose generally as input. Therefore the values of lactate and alanine can be directly dequeued and input into their respective compartment (I), (J). The in- and outflow values can be directly red by indicators and and therefore the contribution of each organ to the respective metabolite in the blood, as well as its uptake (K1), (K2). The values input into the main indicators are called by local variables, again to avoid unnecessary wires and matched to the user defined input units by the subVI presented in figure 9.12. The results are displayed on the front panel (M).

When all loop iterations are completed, the calculating state is left for the waiting for input state, where the LED that was activated upon entering the state calculating is turned off indicating the finished calculations to the user (N).

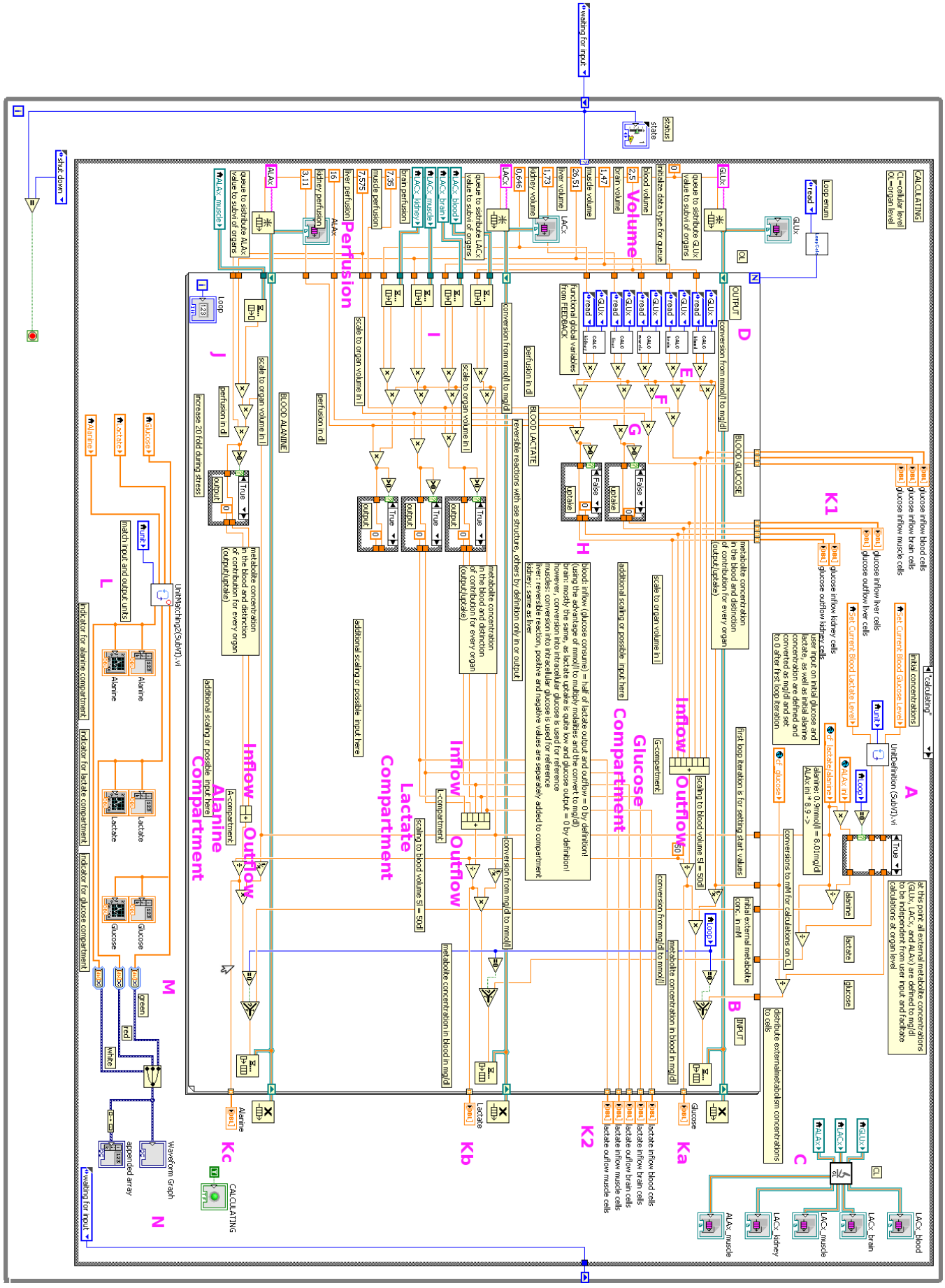

Figure 9.9: The figure shows the waiting for input state and its processes.

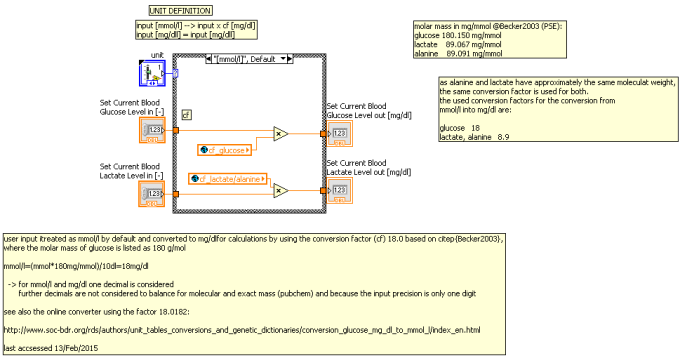

Figure 9.10: The figure shows the subVI, which defines the user input as mg/dl

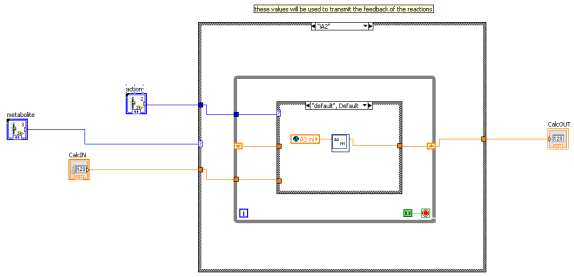

Figure 9.11: The figure shows the subVI *CalcBlood.vi*, which contains the feedback values for the ODE VI presented in section 9.3

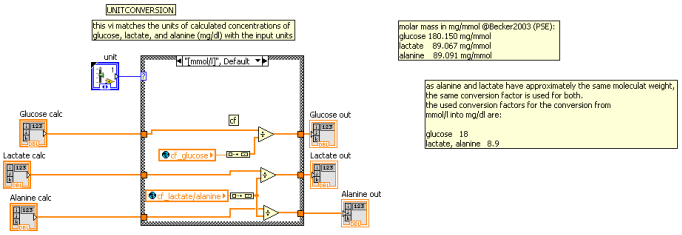

Figure 9.12: The figure shows the subVI, which matches the units of the in- and output by converting them if necessary

9.3 Handling the Model Equations

The differential equations are each handled separately in their respective subVI. Figure 9.13 depicts the organization of the subVI for the cellular level.

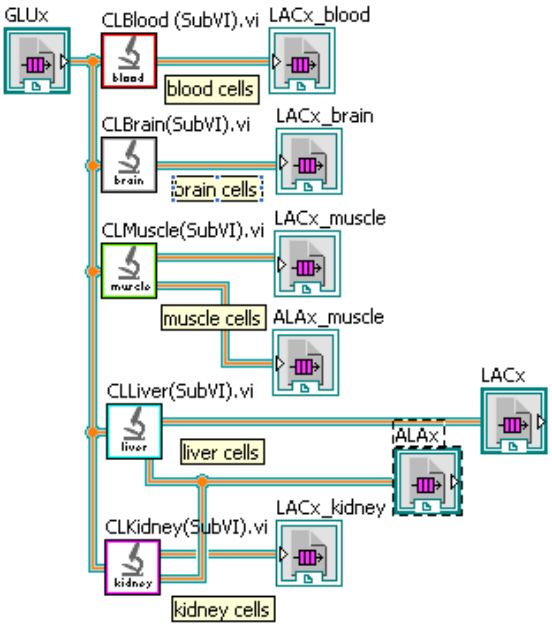

Figure 9.13: The figure shows the subVI *CL (SubVI).vi* from the calculating state

Figures 9.14 to 9.18 depict the subVI structures of the respective cells, which is close to the respective structural models presented in chapter 8. Every subVI in those figures is handling the respective differential equation. The typical LabVIEW characteristic that the wires are the variables becomes very clear by comparing figures to the respective structural.

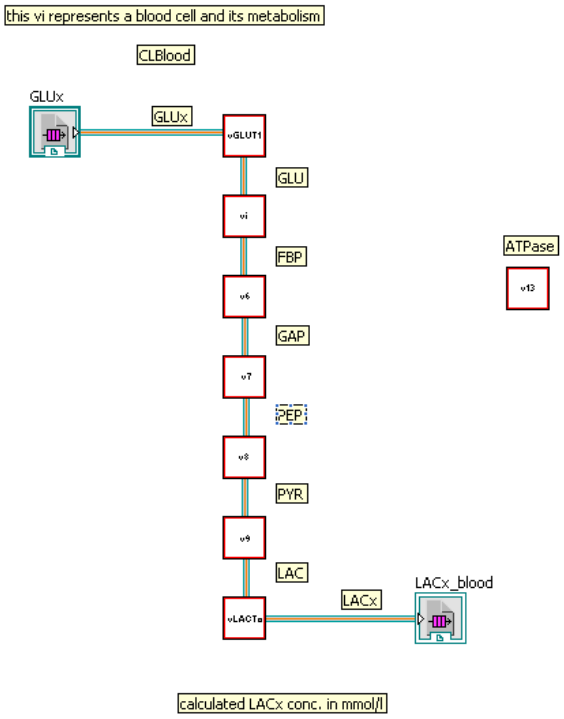

Figure 9.14: The figure shows the subVI for the blood cells

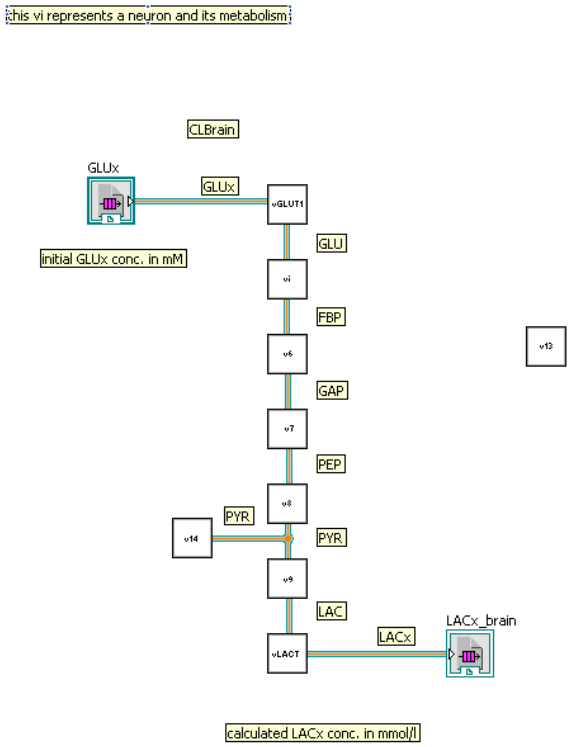

Figure 9.15: The figure shows the subVI for the neurons

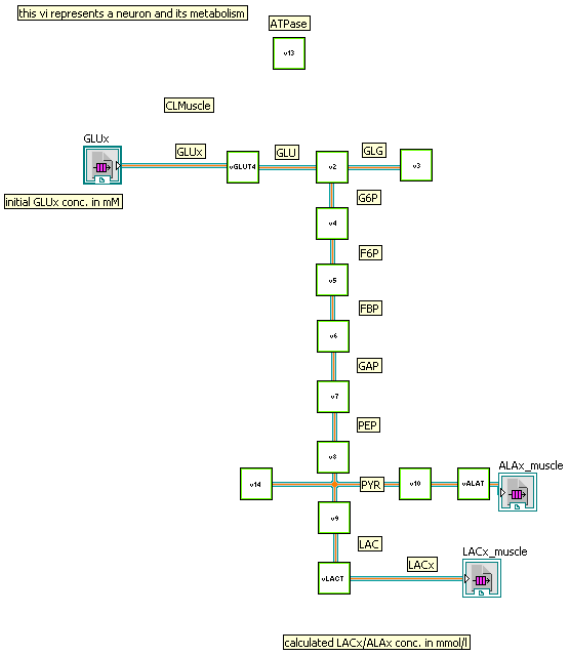

Figure 9.16: The figure shows the subVI for the myocytes

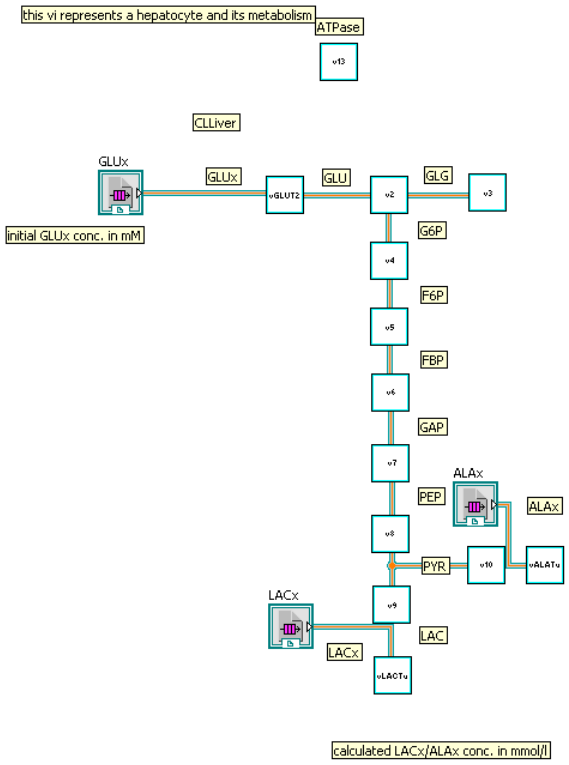

Figure 9.17: The figure shows the subVI for the hepatocytes

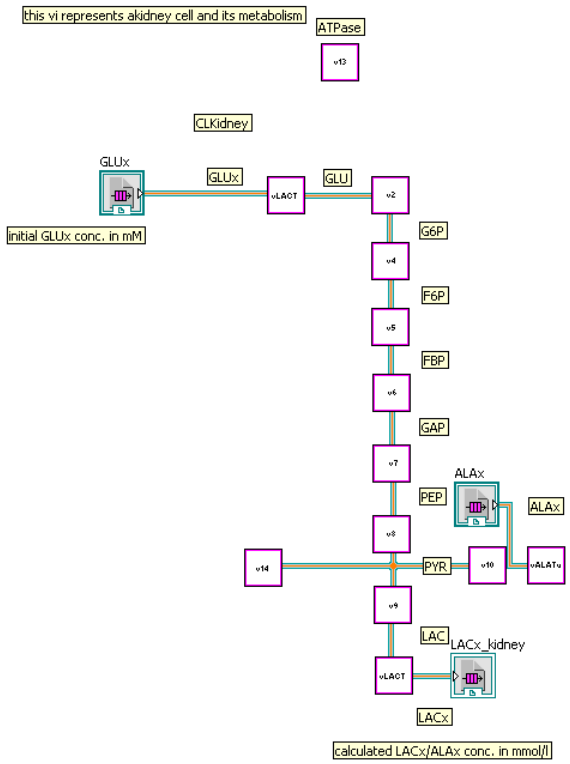

Figure 9.18: The figure shows the subVI for the cells of the renal cortex

The simple diagram of figure 9.19 schematically illustrates how the program handles the differential equations, which directly relates to the forward and backward feedback regulations of reactions that characterize the intra cellular carbohydrate metabolism and have been presented in the structural models of the respective organs in chapter 8 [Mulukutla et al., 2014].

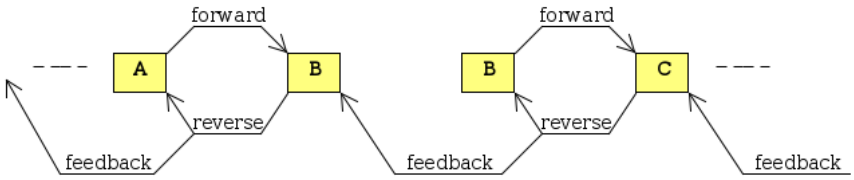

Figure 9.19: The figure shows the conversion of metabolite B from A and further to C in the respective VI. The forward reaction is handled by LabView's queue operations and the reverse reaction is an additive modification to the input inside the loop using a *Shift Register*. The feedback reads and writes values from and to functional global variables that are updated for every loop iteration and initialized with 0.

Figures 9.20, 9.21, and 9.22 depict the irreversible GLUT1, the moderately complex reaction v6, and lumped reaction v7 from chapter 7.3 and illustrate the increasing complexity of the reactions by the increased programming effort.

As the basis for the other VI, the GLUT1 is described as a representative for all reactions and the expansions are mentioned for the rest.
Number of loop iterations and correction factor are handled by the subVI LoopCalc and IntCalc, respectively, as depicted in figures 9.23 and 9.24 (A).

IntCalc determines the integral steps and correction factor by which each value is divided in order to calculate for e.g. 10 minutes, when a step size of $.6s$ is requested by the user, which corresponds to 1000 loop iterations. Usually one loop iteration represents one minute. Therefore 1000 loop iterations divided by 100 that is the step size reduction from $60s$ to $0.6s$, equals 10 minutes. The step size definition is presented in figure 9.25 (A1).

The input to the ODE is called from local and global variables (B) and sent into a formula node (C). The result from the calculation is compared to the sign of the input value for the substrate metabolite that is to be converted into the product metabolite (D). A positive sign means input in the reaction in the direction of glycolysis. A negative sign corresponds to demand and therefore gluconeogenesis direction. At equilibrium the change in rate, which in fact is exactly what is being calculated in the formula node, is equal to 0 and neither forward or reverse reaction occur. In the unidirectional reactions and transport processes any reverse reaction is ignored and therefore set to 0 (D). However, they are calculated separately for reversible reactions, which is the reason for the increased complexity of e.g. v6 in figure 9.21. After the change in rate corresponding to the change in input is calculated it is integrated by the LabVIEWs point by point integration function (E). The output is stored in a shift register for reference in the next loop iteration. On the other hand it is added to the initial value of the product to yield the total concentration of

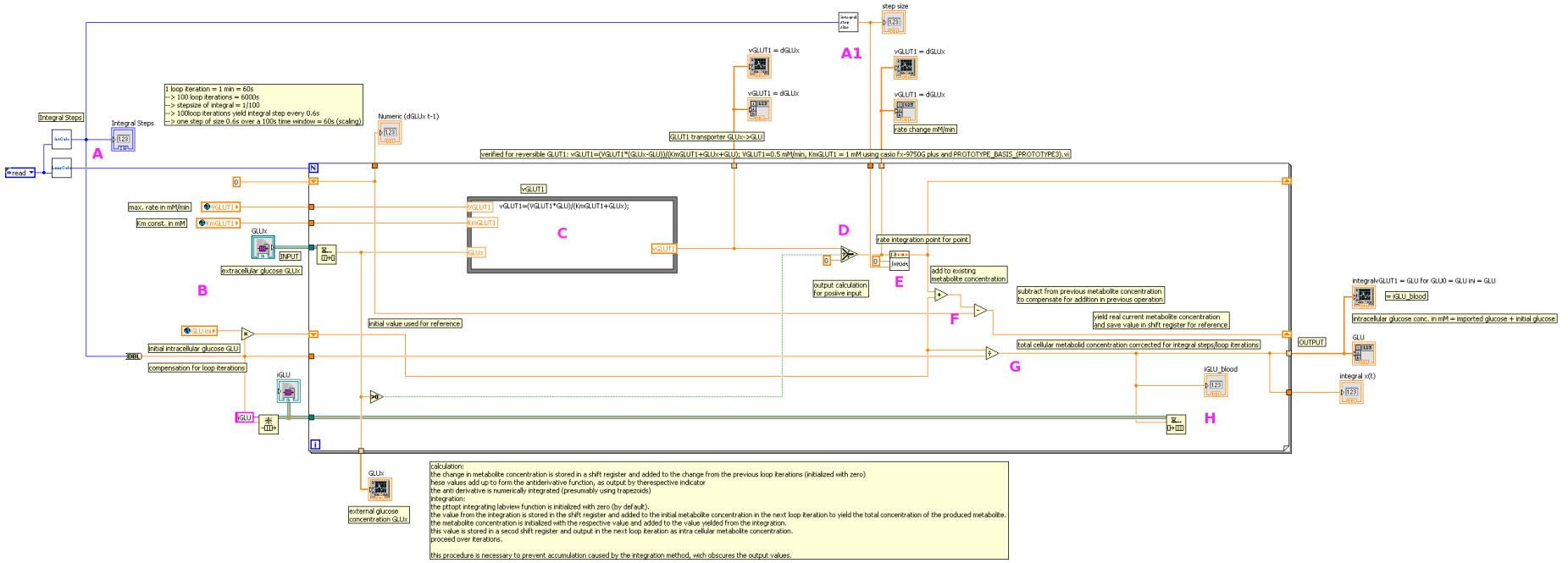

Figure 9.20: The figure shows the block diagram of GLUT1

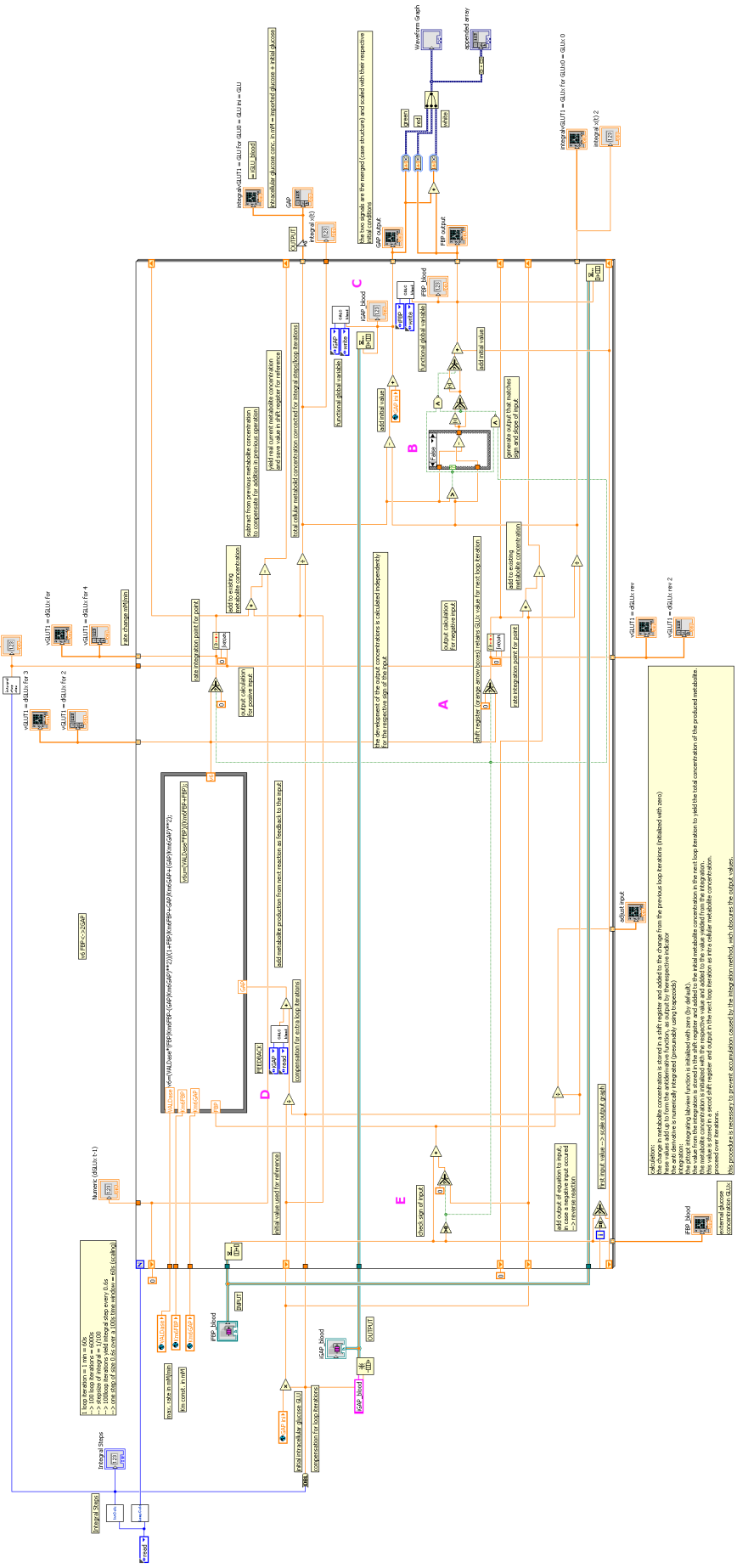

Figure 9.21: The figure shows the block diagram of reaction v6

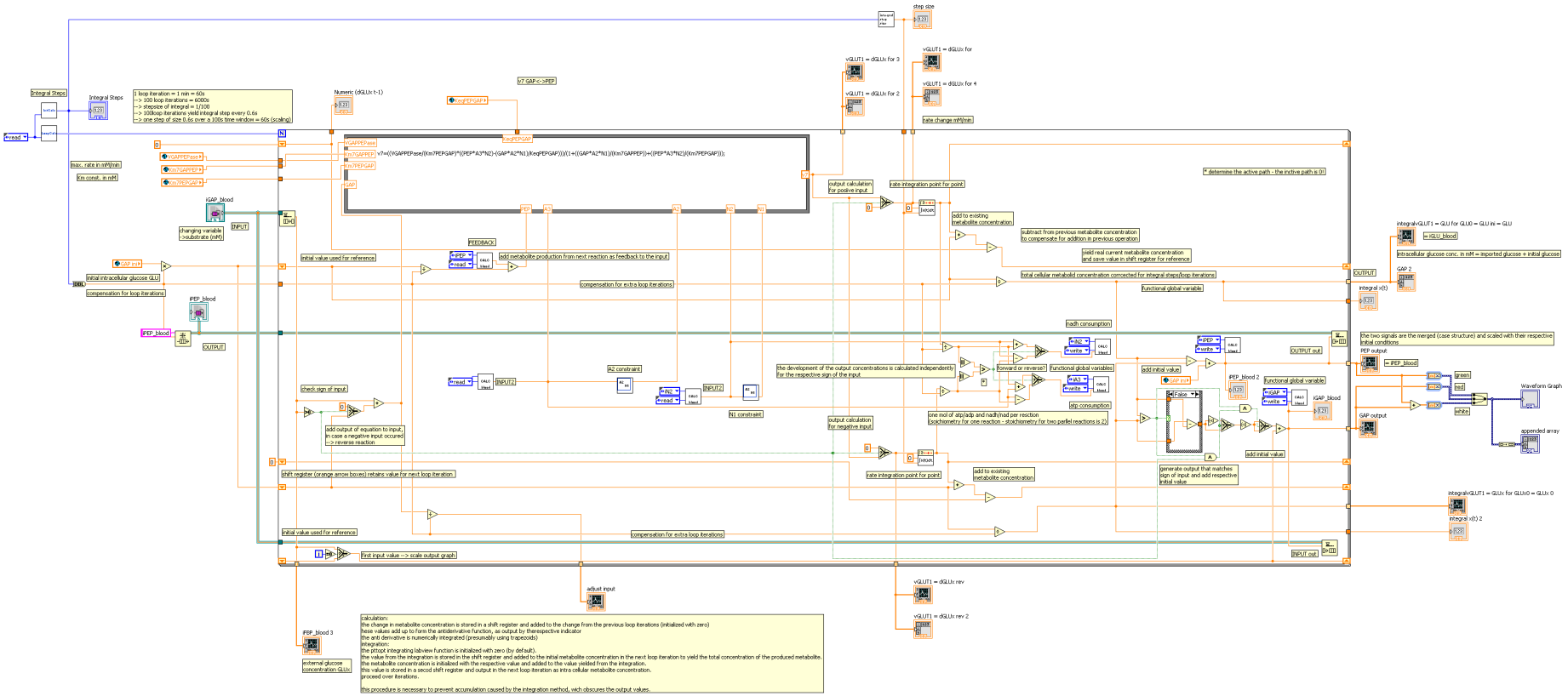

Figure 9.22: The figure shows the block diagram of reaction v6

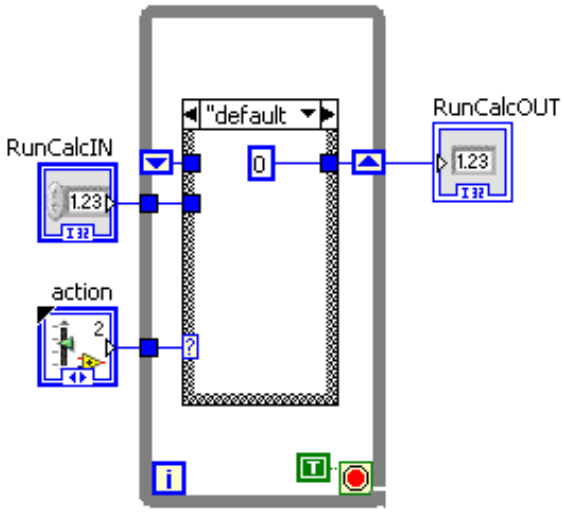

Figure 9.23: The figure shows the subVI LoopCalc (SubVI).vi

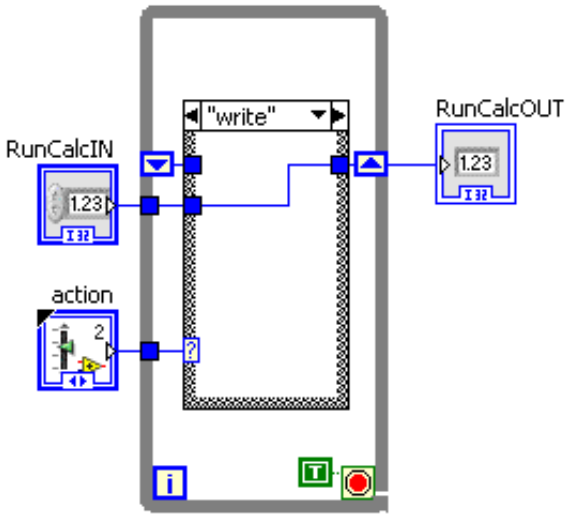

Figure 9.24: The figure shows the subVI IntCalc (SubVI).vi

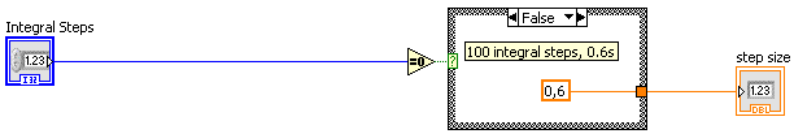

Figure 9.25: The figure shows the VI StepSize.vi

a metabolite inside a cell. To avoid double count from the integration, the concentration value from the previous loop iteration is subtracted (F). In case the small integration steps were chosen, the result is now scaled by dividing with 100 and then enqueued into the uniquely named queue function (H) to serve as input for the following reaction, as depicted in figures 9.14 to 9.18.

In addition to the processes mentioned for figure 9.20, the VI presented in figure 9.21 calculates the reverse reaction (A). This influences the output of the product in glycolysis direction in case substrate is produced upon negative input. Therefore the substrate

output is subtracted from the product output (B) and the substrate output matched by a logic query regarding positive or negative input values (B). Both outputs are then enqueued into the queue function and saved to a functional global variable that will be used to provide an input value for the next adjacent reaction (D) (input from previous reaction). At the same time the value of the substrate input is adjusted to the potentially produced output (E).
Additional modifications of the VI are necessary for reactions that consume/produce ATP or $NADH + H^+$. As presented in figure 9.22, the values for those cosubstrates are being called from functional global variables (A) that directly influence the amount of ADP or NAD^+ by the dependency described in equation 7.4a and implemented in the subVI presented in figure 9.26 (B).

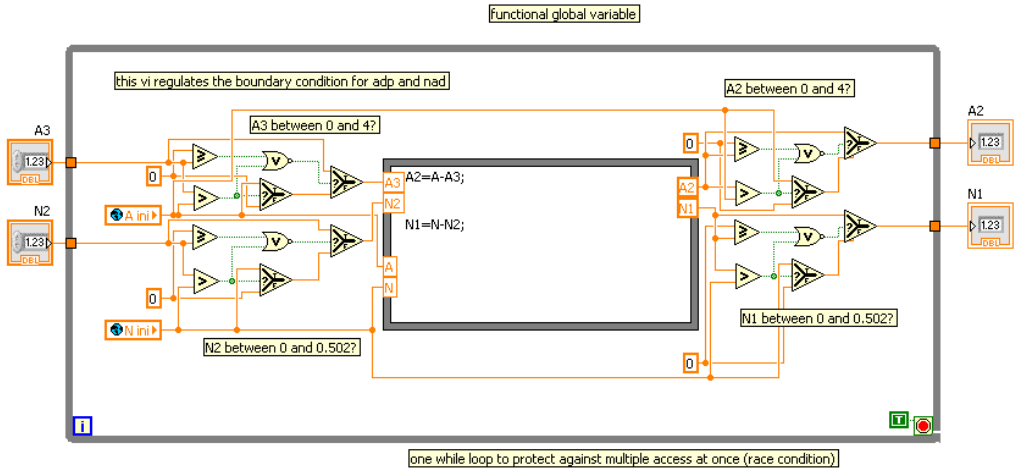

Figure 9.26: The figure shows the A2_N1_dependency(SubVI).vi, which esures the boundary conditions for the total amount of nucleotides and redox coenzymes in the cell

Moreover, the produced/consumed amount of nucleotides and redox coenzymes is determined by the concentration of the produced substrate and it has therefore to be determined which substrate is produced (forward/reverse reaction) to update the respective functional global variable (C).
Special boundary conditions like not consuming glycogen, when there is none available in the cell or producing it when the storage capacities are already reached have been implemented as well in the respective VI and work similar to those shown for the presented representatives GLUT1, v6, and v7.

9.3.1 Output Plots

Example plots for the reaction VI are given in figures 9.27 to 9.46. They present the test data obtained from running equation v6 of table 7.24 in a test VI to verify and test the function for plausible output before encapsulating it in the VI presented in figure 9.21 and thus in the main program. They are shown as a representative example of all reaction VI, as they were built from the same program basis. Each figure depicts a sine input with an amplitude of 5 and a cycle of 1.4 over the duration of 10 min as the top graph. This input is then varied in phase over the group (0, 90, 180, and 270 *deg*)

and offset over the image series (0, 2, 6, -2, and -6 mM). Bottom and middle graph of each figure depict the output of reverse and forward reaction, respectively. The result is a simulation of all possible inputs to the equation e.g positive/negative. The initial concentration of the output metabolite of the reverse reaction is set equal to the input metabolite concentration and the initial concentration of the metabolite synthesized in the forward reaction is constantly fixed to $5mM$. Therefore the effect of the varied offset can be shown in relation to the initial conditions of both metabolites. As a result, situations of complete forward or reverse reactions can be observed in figures 9.35 to 9.38 and 9.43 to 9.46, respectively. A side effect the sine input the constant concentration of the sum of the converted molecules, which can be expressed by adding the two output graphs of the reverse and forward reaction. This has been used to develop the output logic of the reverse reaction, as presented in figure 9.21, and verify the values of both outputs.

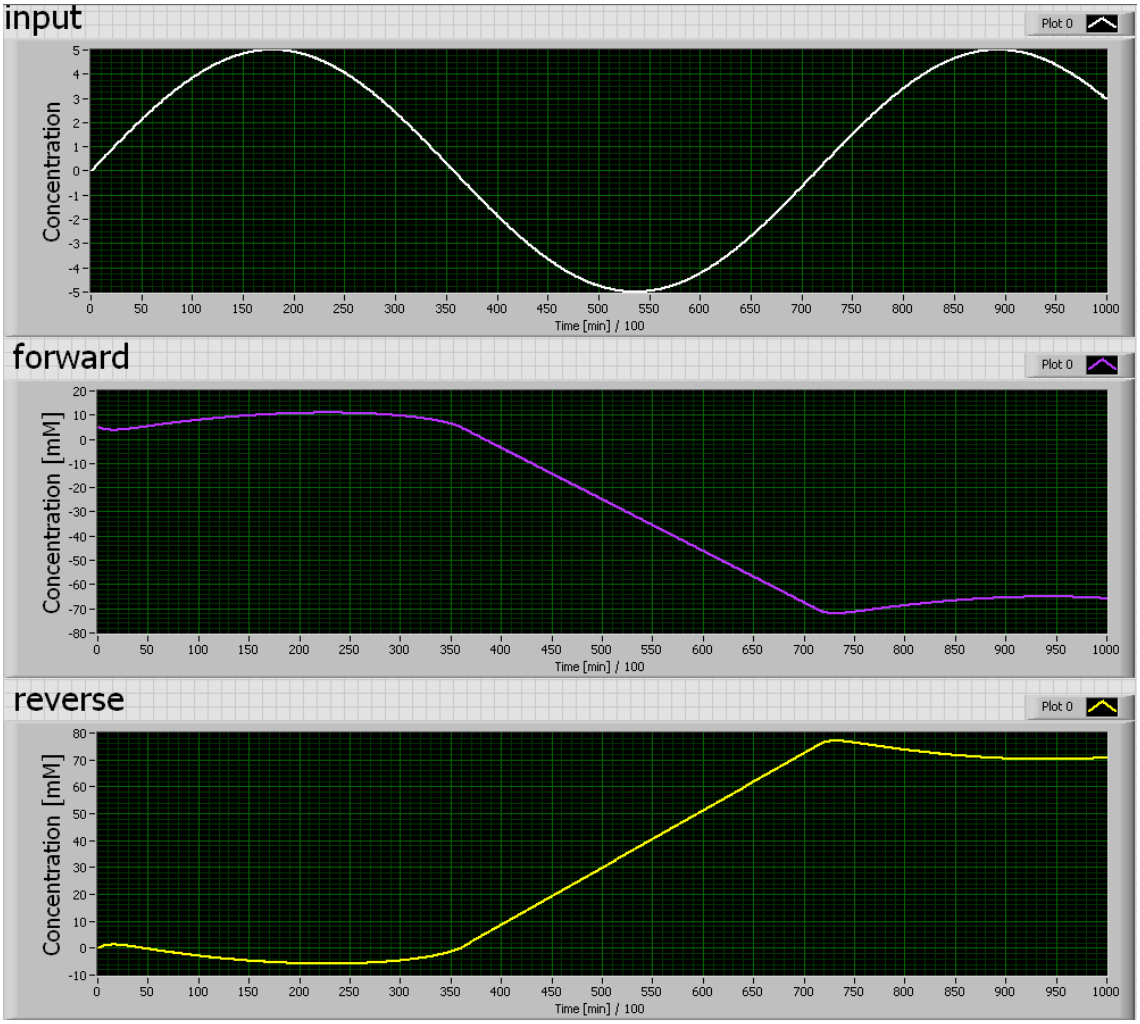

Figure 9.27: The figure shows the output of v6 upon the input sine

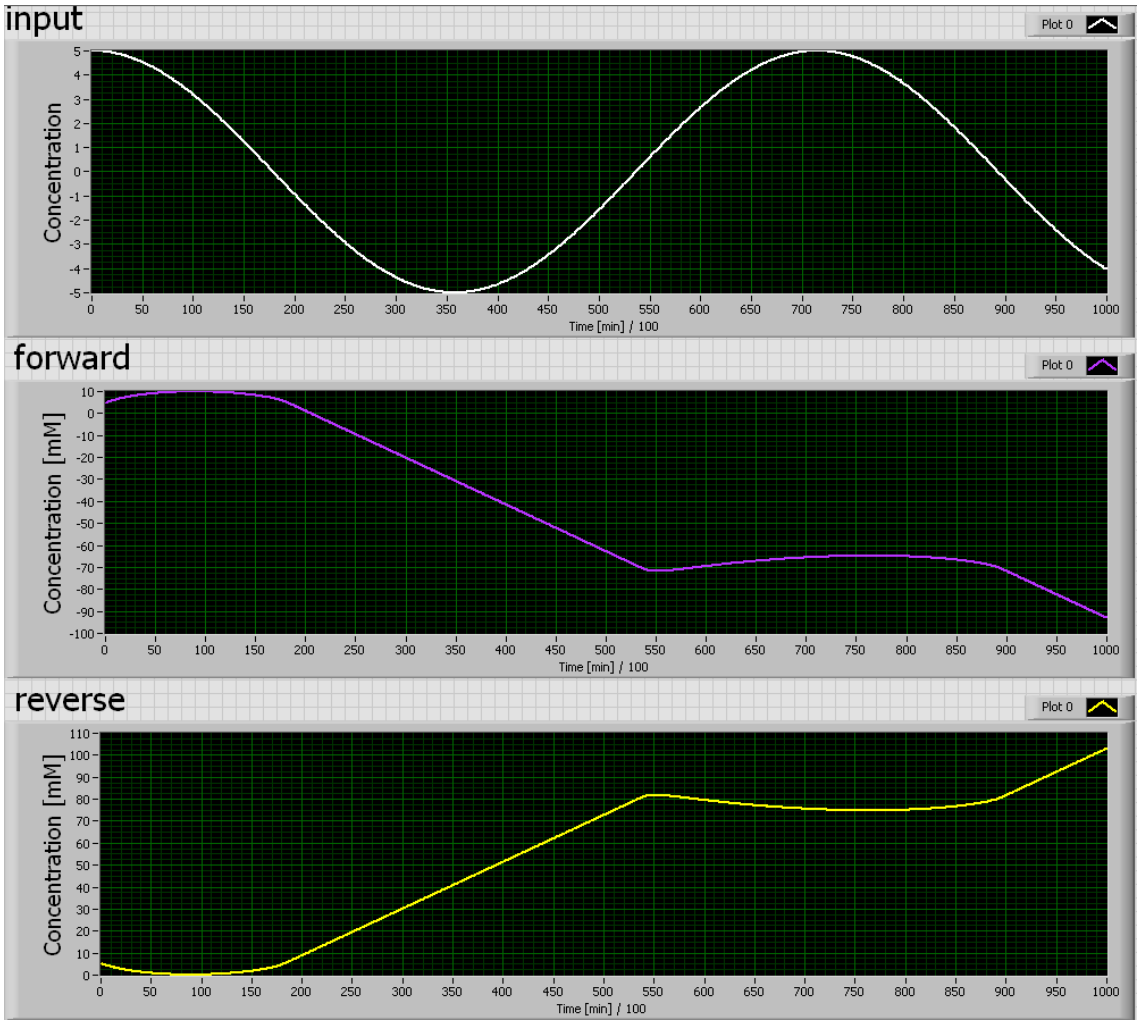

Figure 9.28: The figure shows the output of v6 upon the input sine

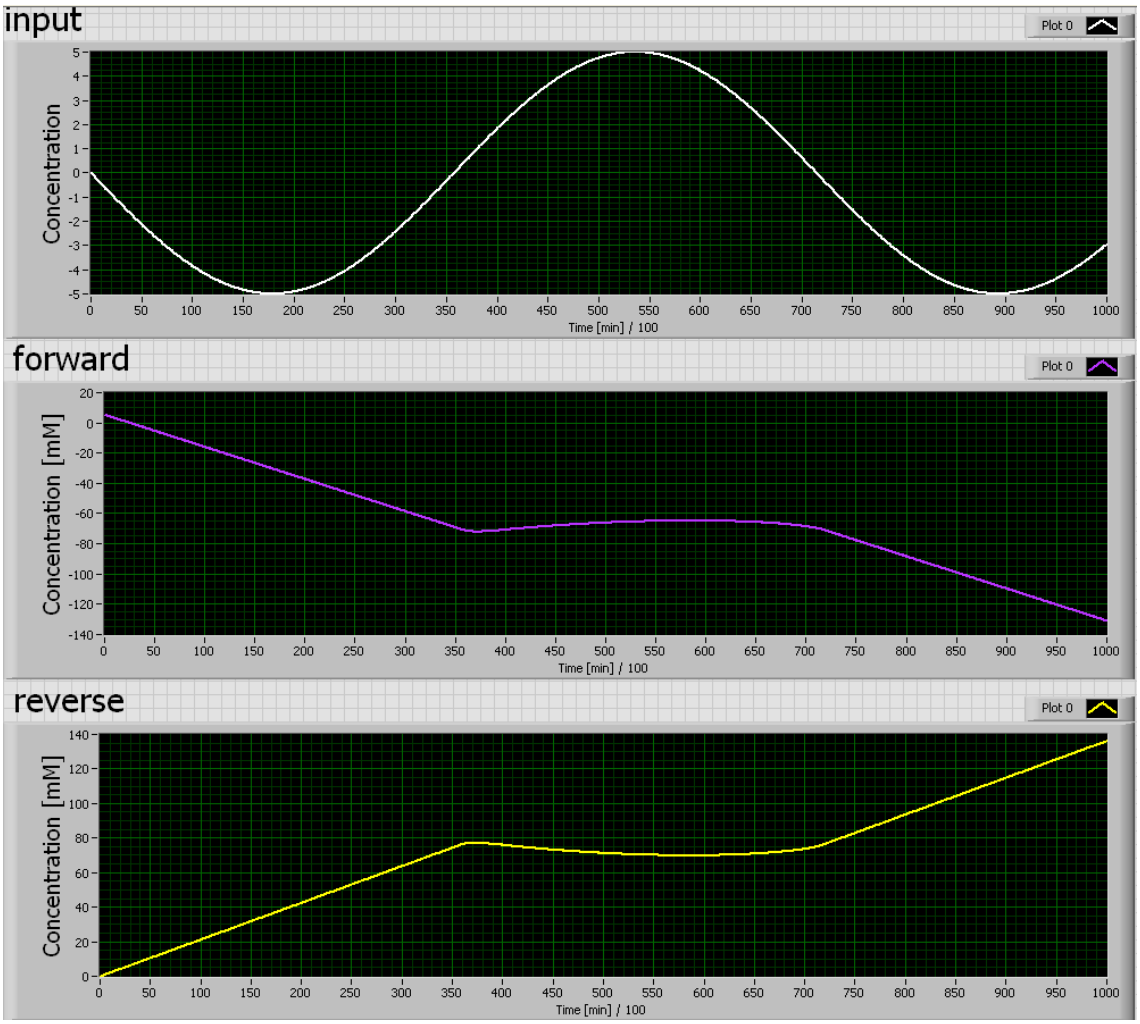

Figure 9.29: The figure shows the output of v6 upon the input sine

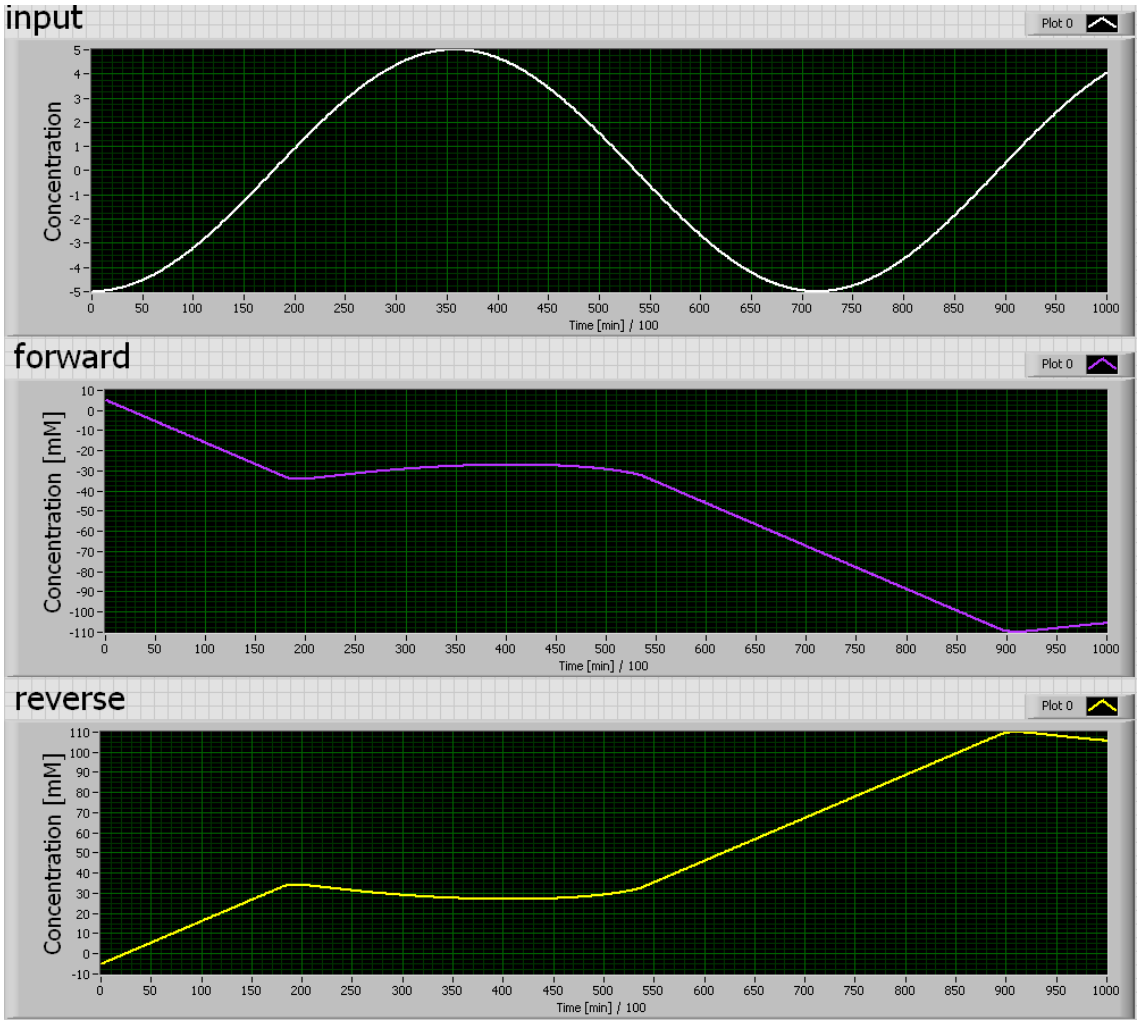

Figure 9.30: The figure shows the output of v6 upon the input sine

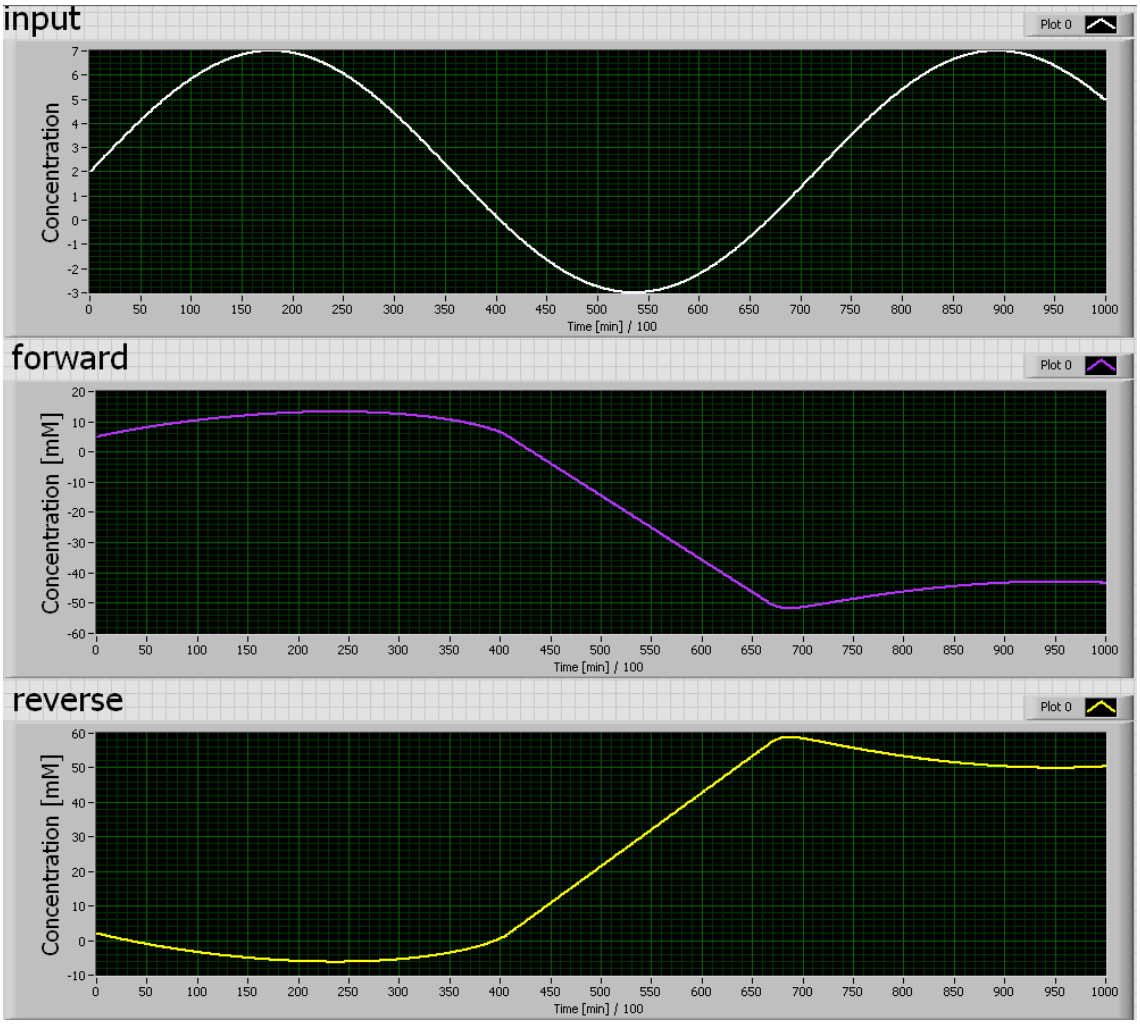

Figure 9.31: The figure shows the output of v6 upon the input sine

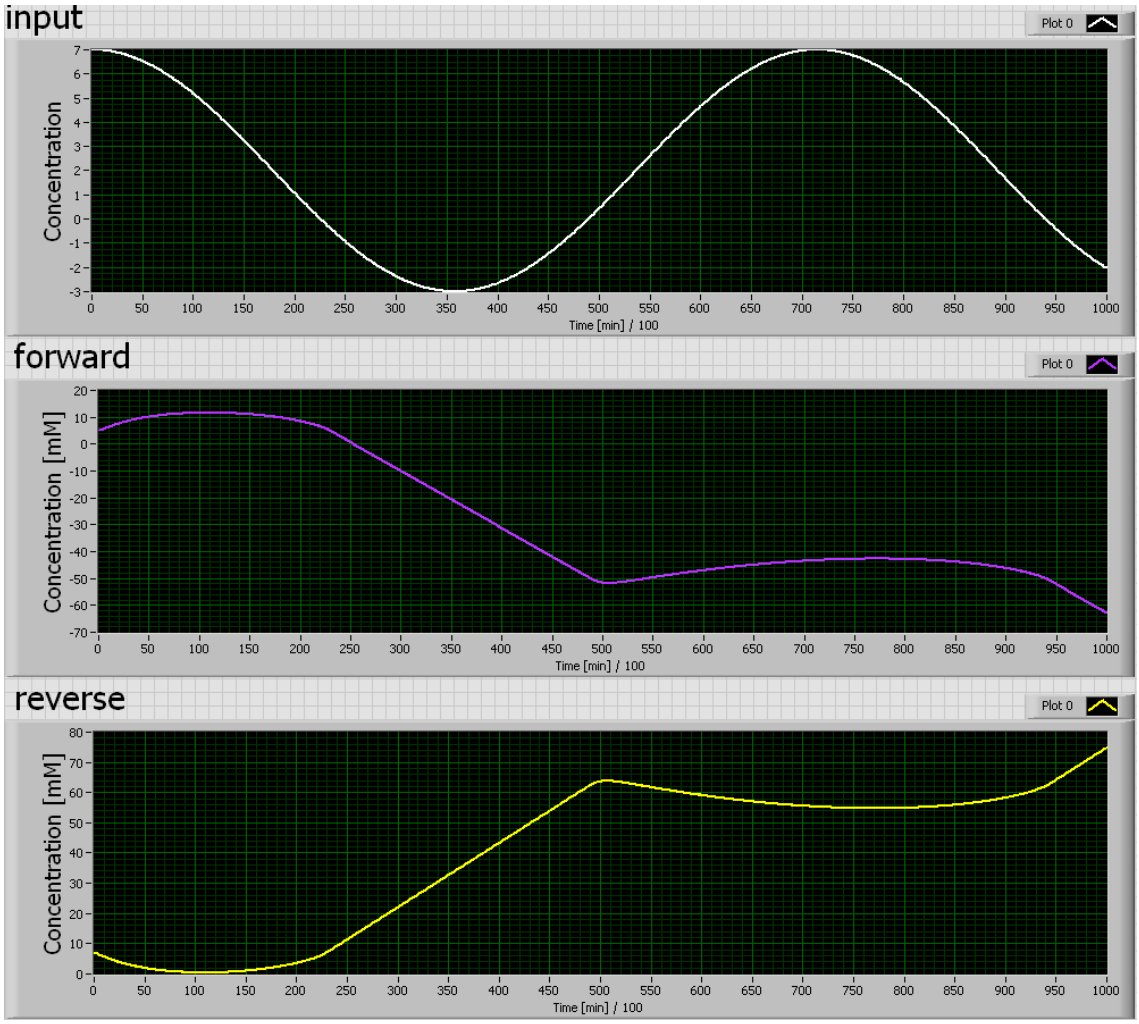

Figure 9.32: The figure shows the output of v6 upon the input sine

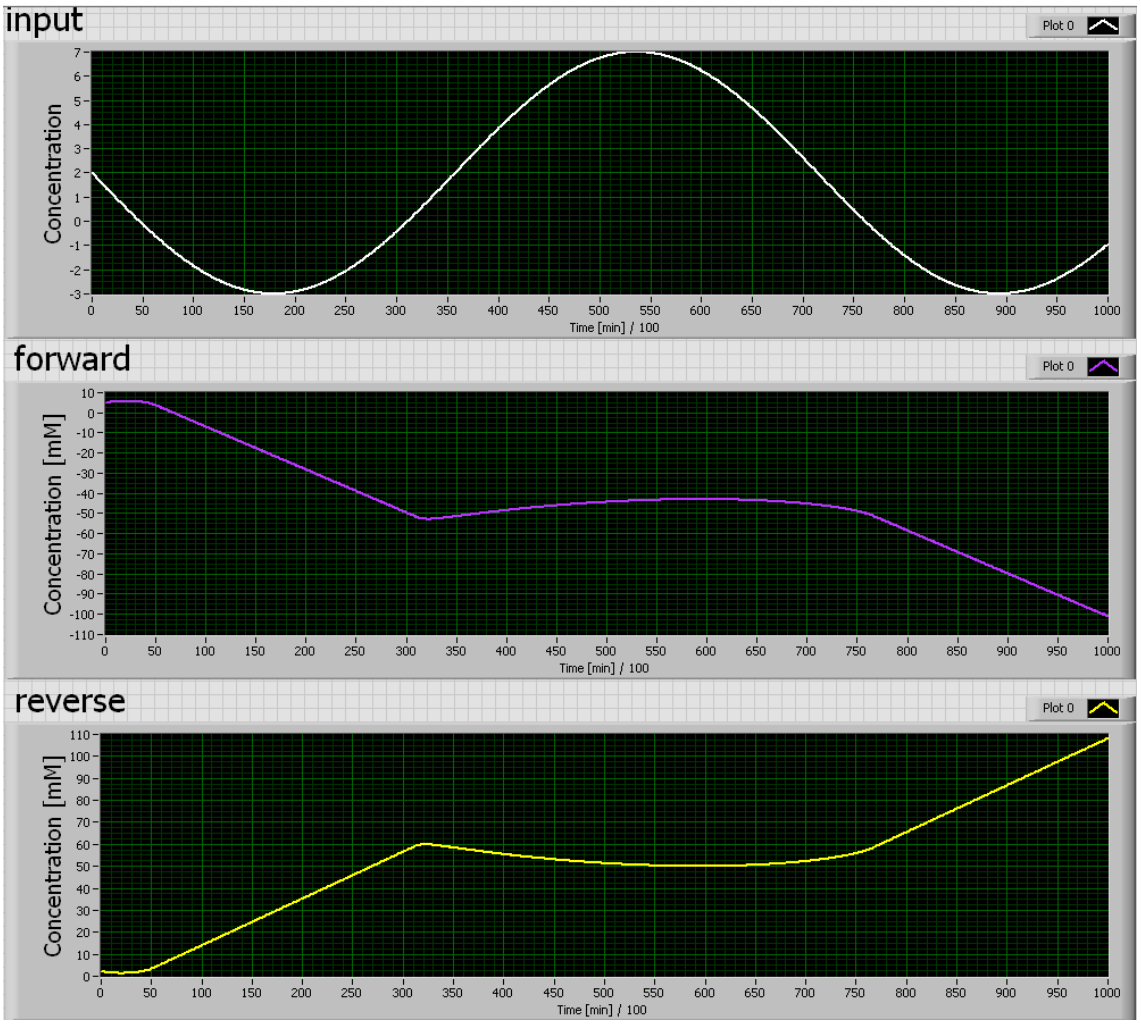

Figure 9.33: The figure shows the output of v6 upon the input sine

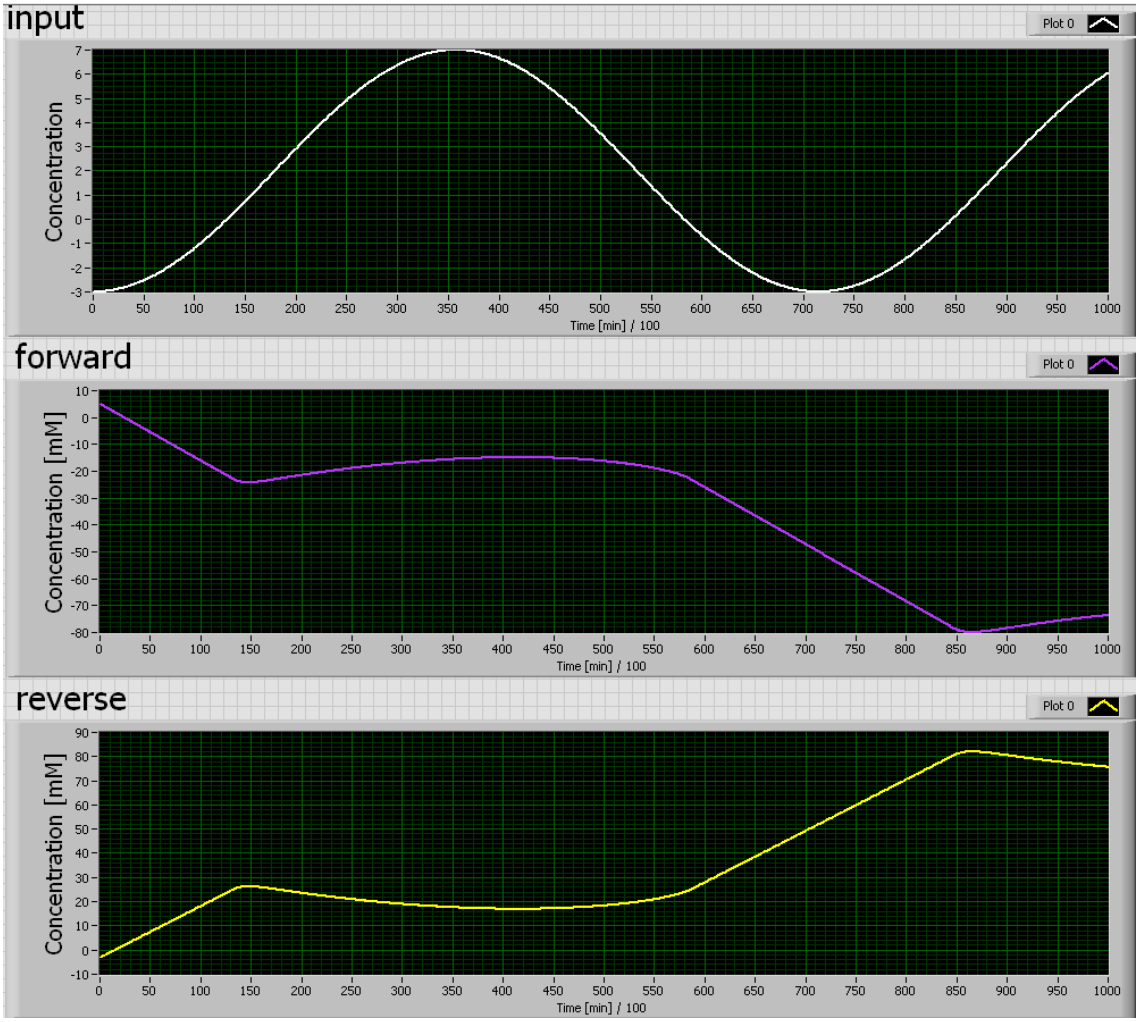

Figure 9.34: The figure shows the output of v6 upon the input sine

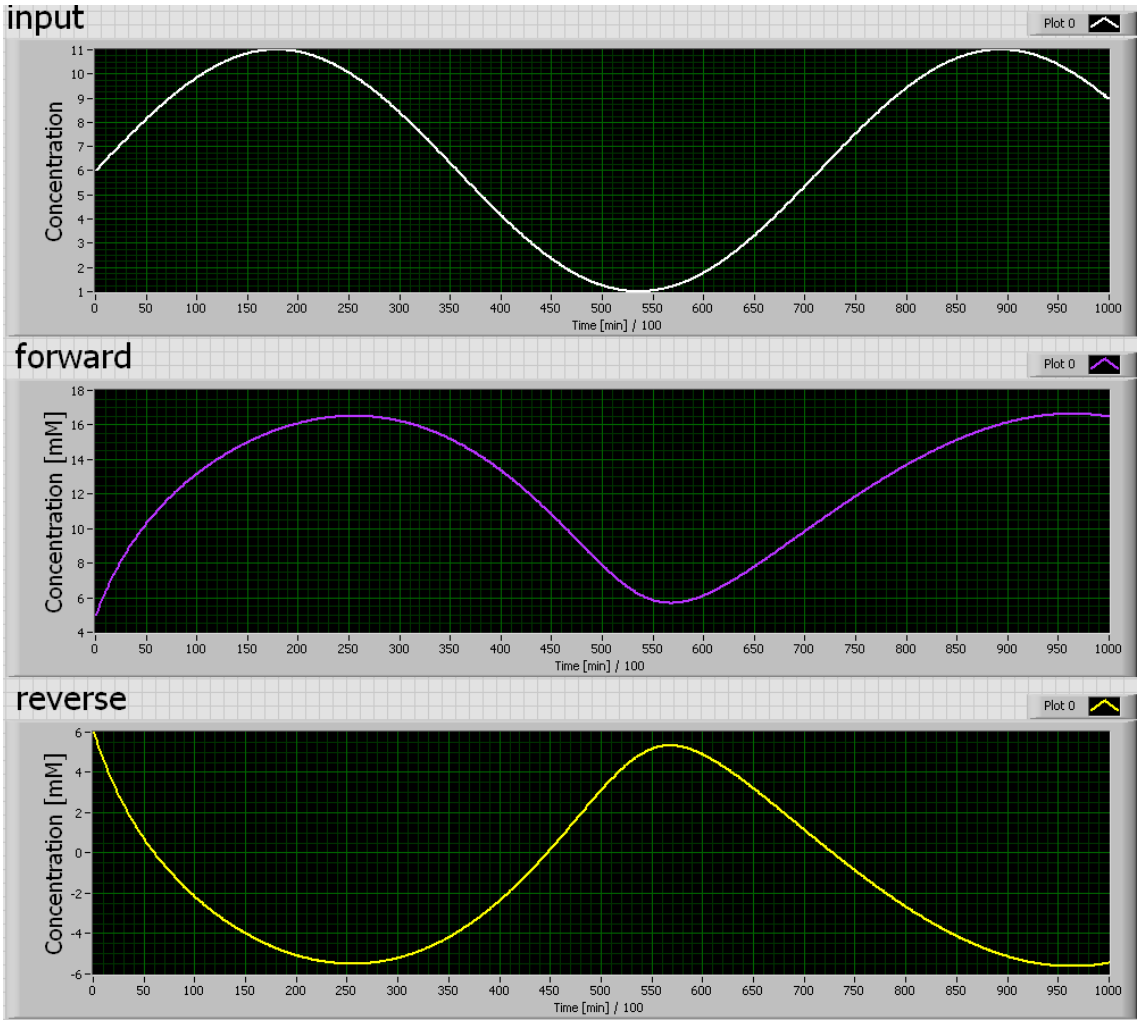

Figure 9.35: The figure shows the output of v6 upon the input sine

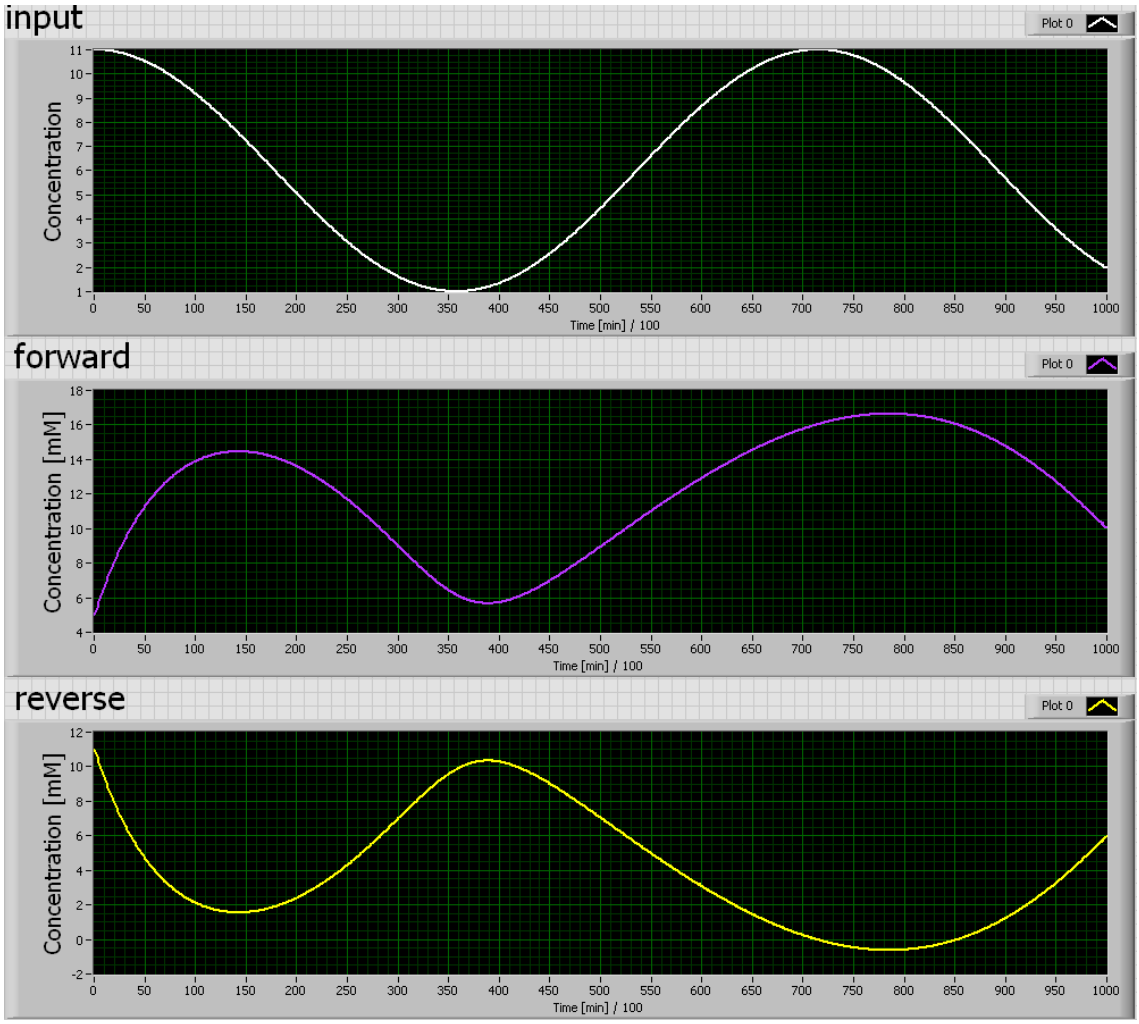

Figure 9.36: The figure shows the output of v6 upon the input sine

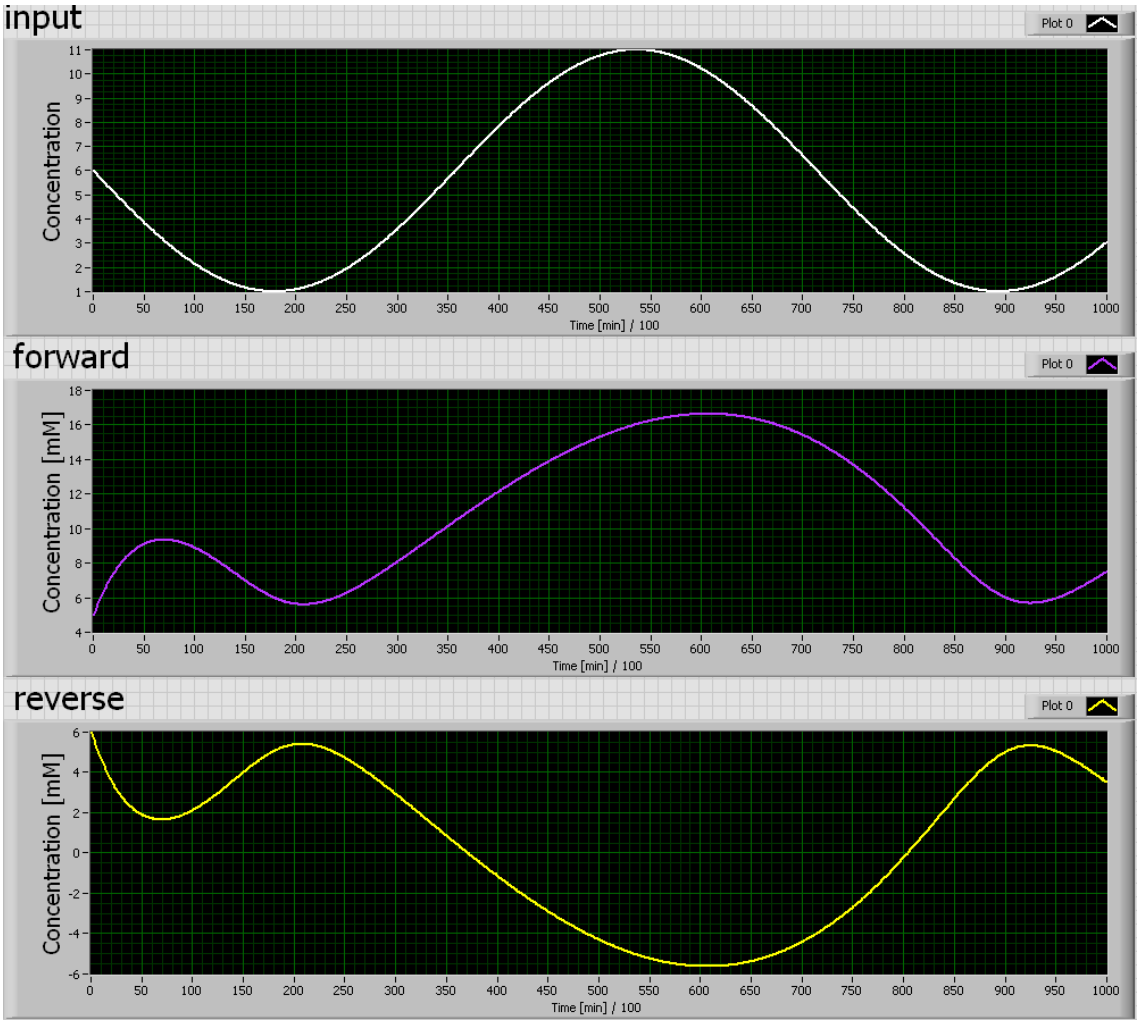

Figure 9.37: The figure shows the output of v6 upon the input sine

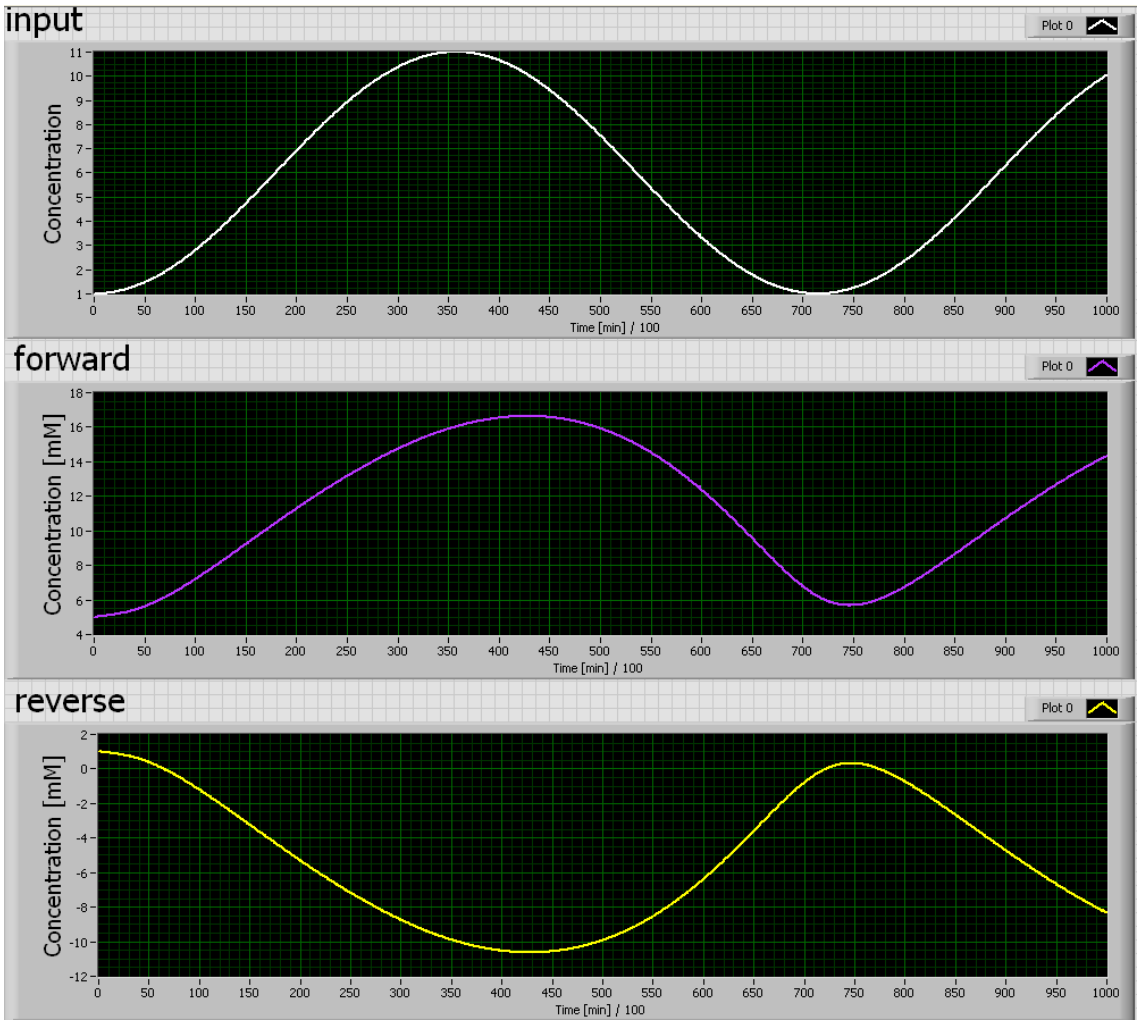

Figure 9.38: The figure shows the output of v6 upon the input sine

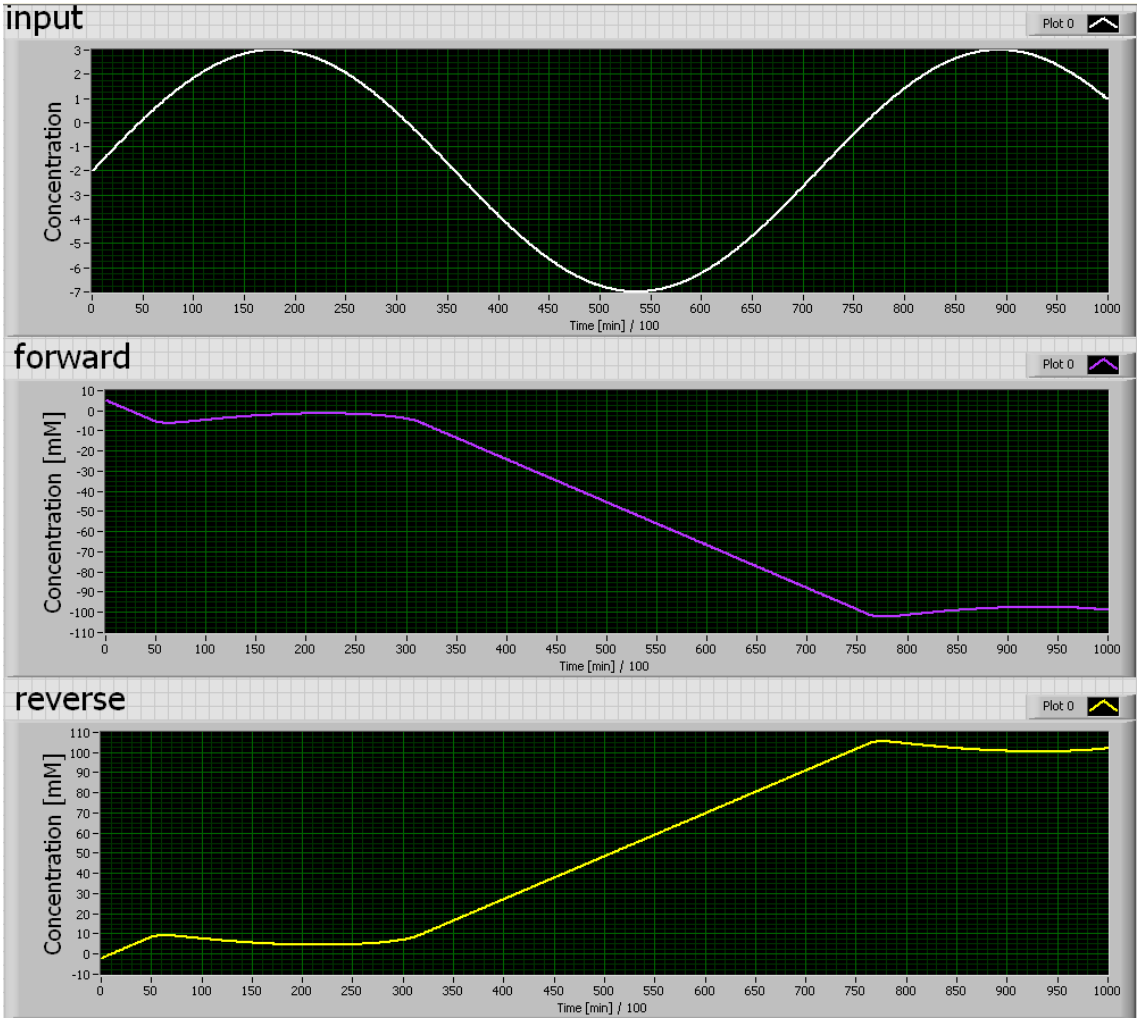

Figure 9.39: The figure shows the output of v6 upon the input sine

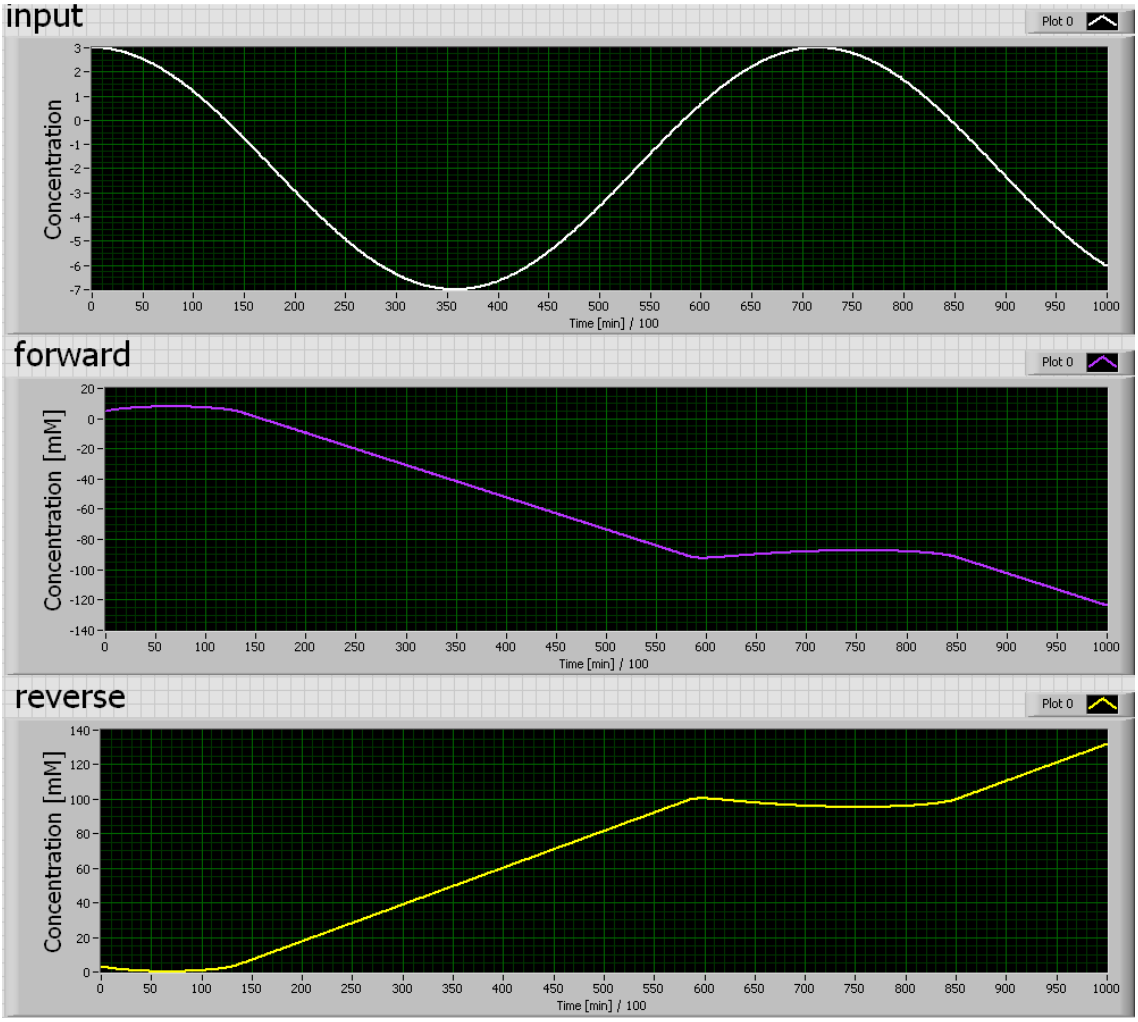

Figure 9.40: The figure shows the output of v6 upon the input sine

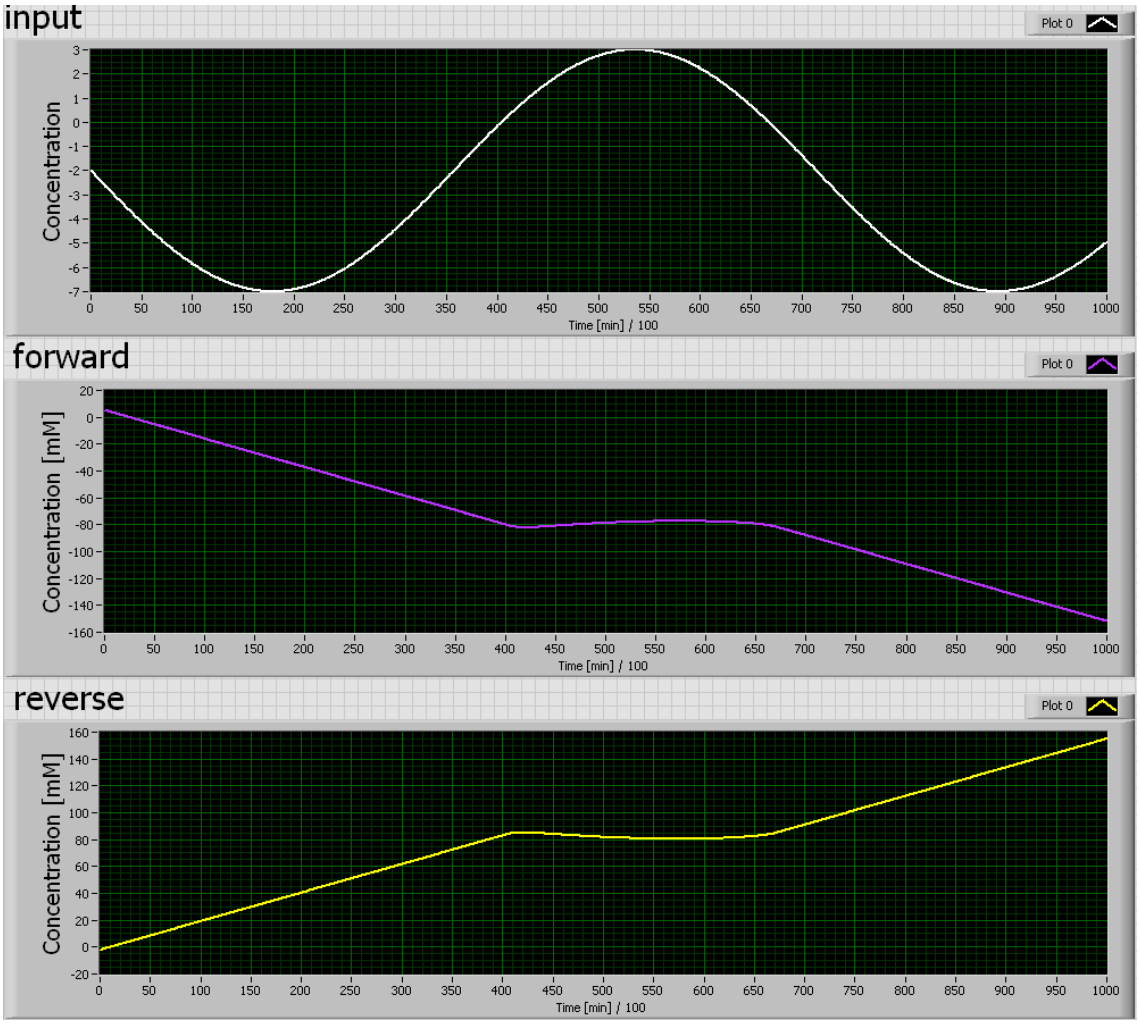

Figure 9.41: The figure shows the output of v6 upon the input sine

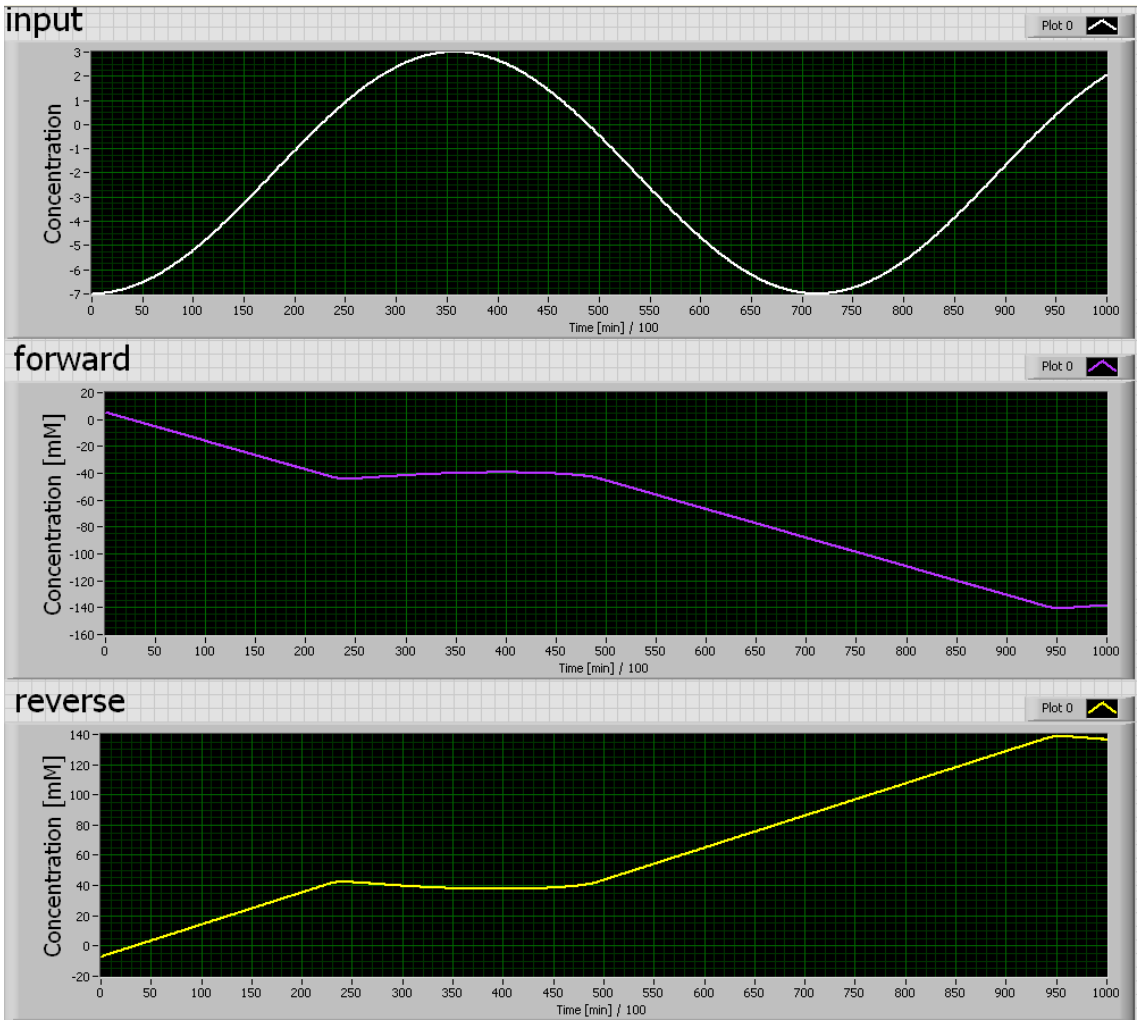

Figure 9.42: The figure shows the output of v6 upon the input sine

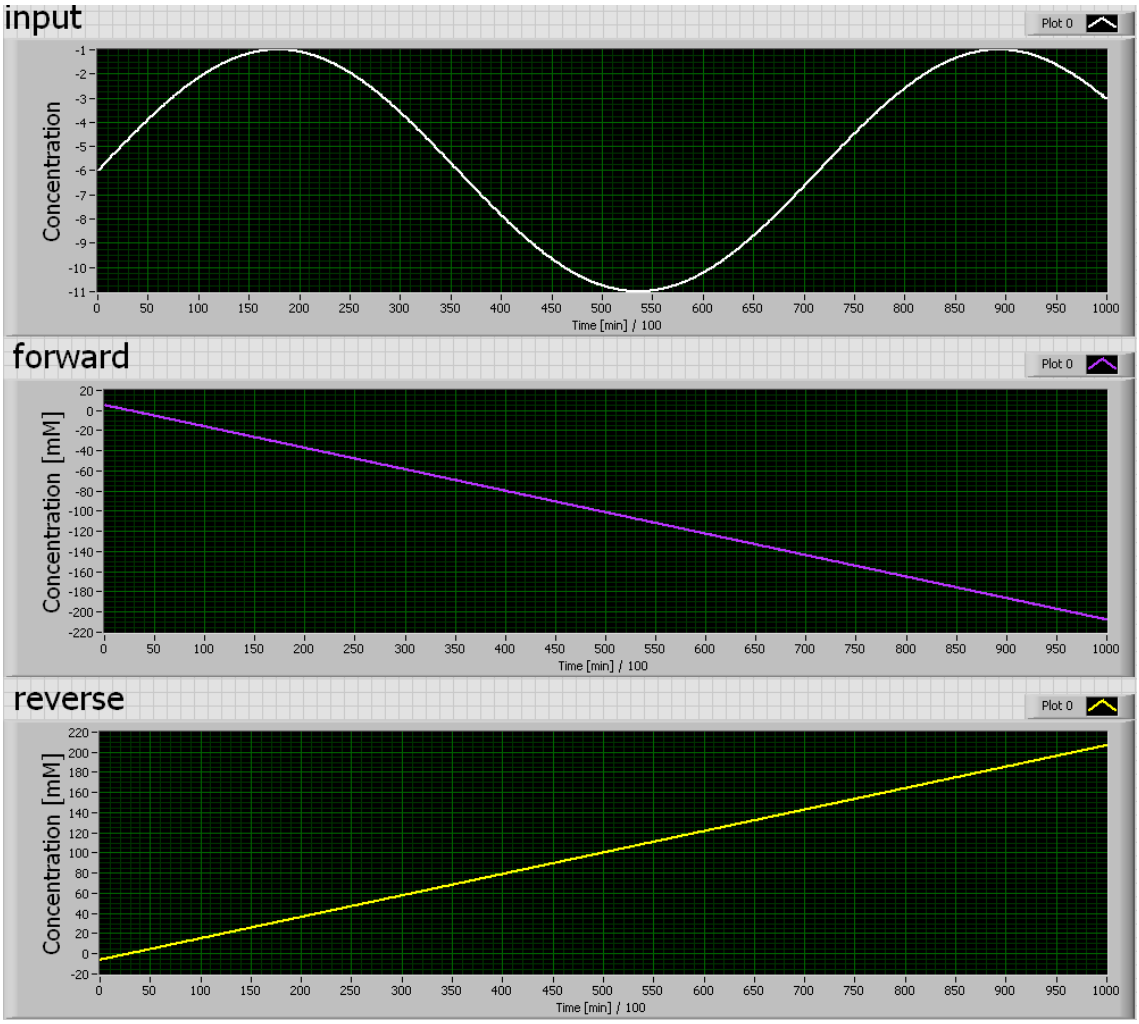

Figure 9.43: The figure shows the output of v6 upon the input sine

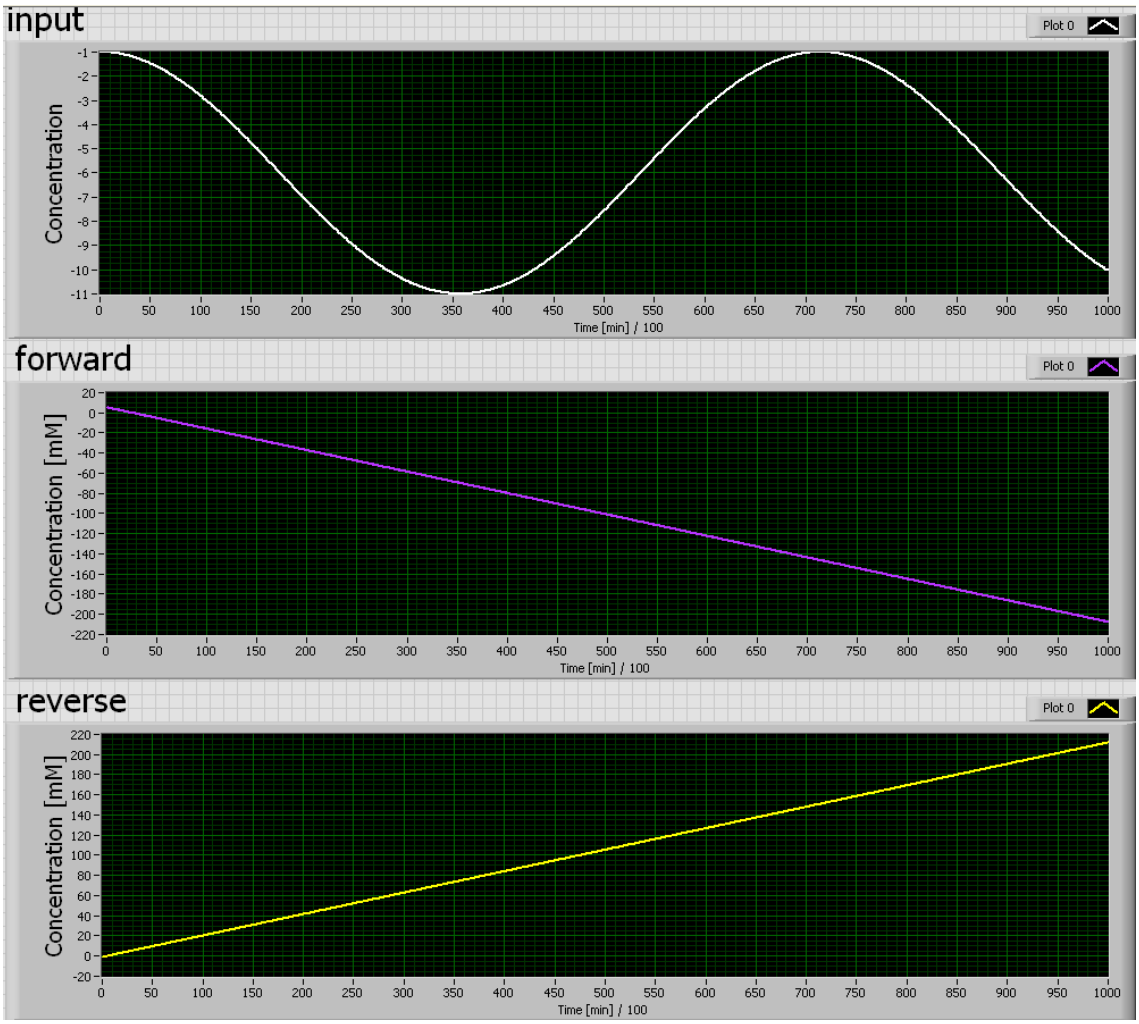

Figure 9.44: The figure shows the output of v6 upon the input sine

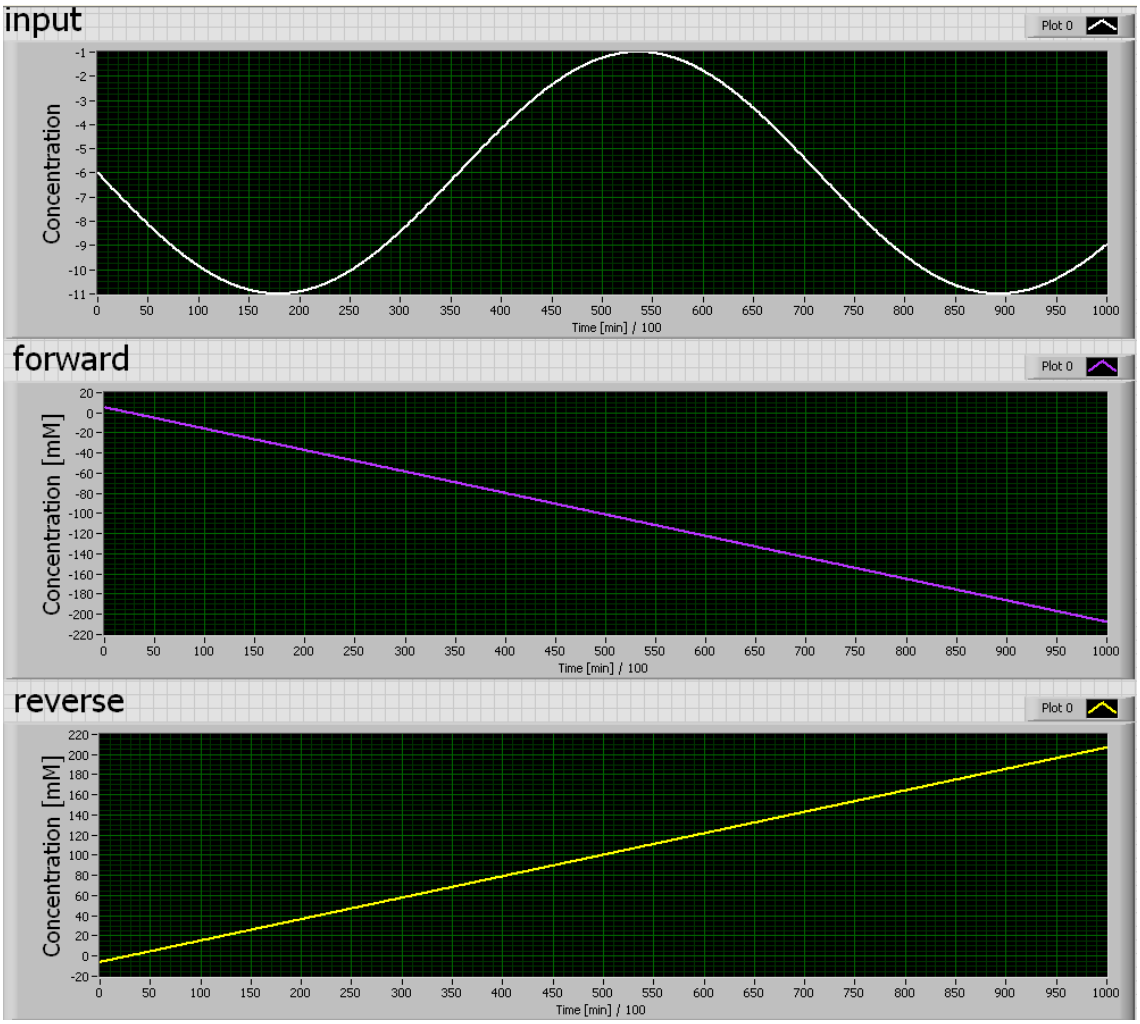

Figure 9.45: The figure shows the output of v6 upon the input sine

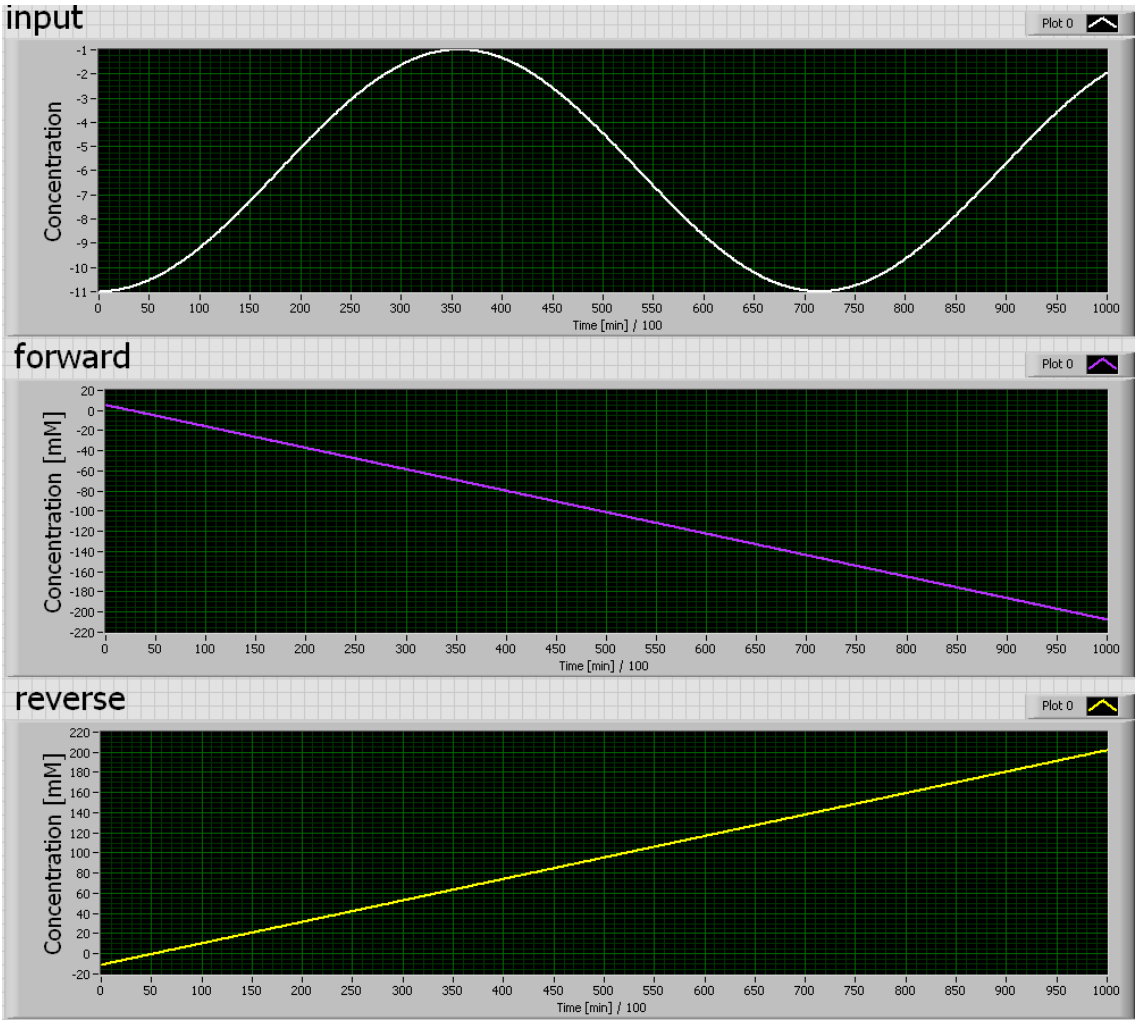

Figure 9.46: The figure shows the output of v6 upon the input sine

Part IV

Synthesis

Chapter 10

Discussion

10.1 Applicability of the Model

This project aimed at developing a computerized model to simulate the Cori cycle in ICU patients suffering from critical illness. The more distant perspective of that development is a decision support system that would support physicians in their prediction for the progression of critical illness in a patient e.g. sepsis. It was recently affirmed that the increased use of decision support systems in clinical environments improves the performance of physicians. However, it remains debatable on whether costs could be reduced and patient outcome improved at the same time [**?**]. However, decision support does not imply to replace the physician but improving the basis upon which situations are being and decisions are being made. Neither is it supposed do induce a kind of dependency of the physician on the system. An advantage for the implementation of the presented model as a decision support system is its intuitive and user friendly interface that might give options but really requires only little input to work. The thus far limited options could easily be expanded upon, as the model is quite modular in its entire structure. A simple modification could be to include more parameters in the Stress Level pointer slide to modify the normal metabolism.

10.2 Validation of the Model

The purpose of this model was fairly specific and therefore limited to begin with, which is reflected e.g. by parameter definitions such as the increased lactate-pyruvate ratio at steady state, which is increased to 16. There is also the muscle mass estimated on the lower boundary of possible values. However, the the general basis of the model was the normal healthy metabolism that was only intended to be tweaked during the validation process. The idea was to use controls to manipulate the flow into and out of the compartment, according to the data from chapter 6 to fit the model observations. Once satisfied the offset values could all be hardwired into the program. Over all, program changes are achieved with relative little effort due to the modular structure throughout the program

ensuring flexibility. The program could also very well be adapted to a similar purpose by keeping the state machine and switching program fragments in the calculation state.

10.3 Strengths and Weaknesses of the Model

The greatest weakness of the model is its incomplete implementation as a computer program. Therefore it is impossible to validate it, even though there has been plenty of suitable data compiled in chapter 6 for validation. The model therefore fails at the ultimate criterion for a model - its predictive value, which is practically inexistent at this point of development. Admittedly the model is fully programmed and computerized, but does run. Moreover, its fair level of complexity, compared to a more simple compartment model with simpler equations and a more direct approach to use e.g. measured data from the level the model is supposed to operate might be problematic. However, even though following LabVIEW recommendations in terms of design pattern and testing code fragments before implementation, the program could not be completed in time before the deadline of this project. Since LabVIEW itself does not issue a clear error code it is assumed that most likely a programming error occurred that prevents the program from properly executing such as not correctly wiring components together or using incorrect LabVIEW functions. The most likely reason is a failed synchronization of the multiple loops in the cellular level.
Apart from that a lot of simplifications were made for the model. Intracellular inhibitory regulation by metabolites other then those already present were ignored. This includes the strong effect of AMP as a sign for acute energy demand. Another example is the feedback effect of FBP on **ldhase!** (**ldhase!**) which were partly ignored for programming convenience, partly considering the aimed application. However these effects can be added easily when deemed necessary. For the application in critically ill it was assumed to be of lesser importance to as accurately as possible describe every conceivable detailed aspect of intracellular the metabolism and favor a more rough approach in this regard.
One could argue, that the available mass of input parameters based on the measurements of various species and isoenzymes with no coherency is not much better than simply guessing those parameters. Especially when, as mentioned in chapter 2, isoenzymes may have quite detrimental properties under only slight varying conditions. However, it has to be said that those parameters listed on databases like BRENDA are more or less the only available data source there is and it is doubtful that measured blood values for metabolite concentrations would actually exhibit less of a spread in their measurement results.
During the modeling process it was noticed that some of the model equations provided by the referenced sources could not be applied for various reasons one being e.g. the incompatibility of unit parameters with the equation. Therefore a great deal of rare was put into the creation of the model equation bey extensively cross-referencing equation multiple articles and own efforts that consider stoichiometry, reaction mechanism, and suitable degree of complexity for the scope of application to provide the best possible basis for the subsequent development steps. A big advantage of the developed model is therefore its deep grounding in reality and solid base of development by relying heavily on measured data and background informations over simplifications. There are a lot of enzyme mechanisms documented and evaluated and the general mathematical description

Michaelis-Menten kinetic is intuitive. By looking at single reaction chains of the very complex structure, that is the human body, let alone a diseased human body, parameters to tweak the model with are fond in abundance and potentially suggest a high degree of accuracy as well as flexibility in its predictions. Moreover, as far as could be told, a model of this complexity has not been attempted to build before. Most metabolic models tend to focus on single cell organisms e.g. yeast or one organ e.g. liver, ultimately making this quite unique.
Theoretically, the model should be able to perform as desired, especially with the option of regulating certain parameters stepwise through a realistic range to resemblance of reality.

Chapter 11

Conclusion

The capabilities and and acceptance of decision support systems grows regardless of implementation problems at the workplace [**?**]. Therefor it is believed that the developed model will reach its full potential once it has been a little further developed. It certainly needs to be validated first to make any claims. The model can deliver relevant data be an effective support in an ICU, as it is user friendly, comprehensible, and easy to operate within its limitations for critically ill patients.

Bibliography

Alexander, S. P., Benson, H. E., Faccenda, E., Pawson, A. J., Sharman, J. L., Spedding, M., Peters, J. A., and Harmar, A. J. (2013). The concise guide to pharmacology 2013/14: enzymes. *British journal of pharmacology*, 170(8):1797–1867.

Ankney, C. D. (1992). Sex differences in relative brain size: The mismeasure of woman, too? *Intelligence*, 16(3):329–336.

Appleton, R. and Kinsella, J. (2012). Intensive care unit-acquired weakness. *Continuing Education in Anaesthesia, Critical Care & Pain*, 12(2):62–66.

Arleth, T., Andreassen, S., Federici, M. O., and Benedetti, M. M. (2000). A model of the endogenous glucose balance incorporating the characteristics of glucose transporters. *Computer methods and programs in biomedicine*, 62(3):219–234.

Arlow, J. and Neustadt, I. (2002). *UML and the Unified Process: Practical Object-oriented Analysis and Design*. Component software series. Addison-Wesley.

Aumüller, G., Engele, J., Kirsch, J., and Mense, S. (2007). *Duale Reihe Anatomie*. Duale Reihe Herausgegeben von Alexander Bob und Konstantin Bob. Thieme.

Bakker, J. and Jansen, T. C. (2007). Don't take vitals, take a lactate. *Intensive care medicine*, 33(11):1863–1865.

Bakker, J., Nijsten, M. W., and Jansen, T. C. (2013). Clinical use of lactate monitoring in critically ill patients. *Ann Intensive Care*, 3(1):12.

Balkovetz, D., Leibach, F., Mahesh, V., and Ganapathy, V. (1988). A proton gradient is the driving force for uphill transport of lactate in human placental brush-border membrane vesicles. *Journal of Biological Chemistry*, 263(27):13823–13830.

Baynes, J. and Dominiczak, M. (2014). *Medical Biochemistry*. Elsevier Health Sciences UK, 4th edition.

Becker, F. (2003). *Formelsammlung: Formeln, Tabellen, Daten ; Mathematik, Physik, Astronomie, Chemie, Biologie, Informatik ; [bis zum Abitur ; mit CD-ROM und Internetportal]*. Duden Schulbuch.

Behrends, J. (2010). *Physiologie: 93 Tabellen*. Duale Reihe. Thieme.

Bellomo, R. (2002). Bench-to-bedside review: lactate and the kidney. *Critical Care*, 6(4):322.

Berg, J., Tymoczko, J., and Stryer, L. (2002). *Biochemistry, Fifth Edition*. W.H. Freeman.

Billat, L. V. (1996). Use of blood lactate measurements for prediction of exercise performance and for control of training. *Sports medicine*, 22(3):157–175.

Blomhøj, M., Kjeldsen, T., and Ottesen, J. (2014). Compartment models.

Blomstrand, E. and Saltin, B. (1999). Effect of muscle glycogen on glucose, lactate and amino acid metabolism during exercise and recovery in human subjects. *The Journal of physiology*, 514(1):293–302.

Bolton, J. D. (2007). Clinical use of lactate testing in shock states. In *Seminars in Anesthesia, Perioperative Medicine and Pain*, volume 26, pages 35–39. Elsevier.

Boyd, J. H. and Walley, K. R. (2008). Is there a role for sodium bicarbonate in treating lactic acidosis from shock? *Current opinion in critical care*, 14(4):379–383.

Brooks, G. (2002). Lactate shuttles in nature. *Biochemical Society Transactions*, 30(2):258–264.

Brooks, G. A. (2009). Cell–cell and intracellular lactate shuttles. *The Journal of physiology*, 587(23):5591–5600.

Brumen, M. and Heinrich, R. (1984). A metabolic osmotic model of human erythrocytes. *Biosystems*, 17(2):155–169.

Brüser, A., Kirchberger, J., and Schöneberg, T. (2012). Altered allosteric regulation of muscle 6-phosphofructokinase causes tarui disease. *Biochemical and biophysical research communications*, 427(1):133–137.

Canham, P. and Burton, A. C. (1968). Distribution of size and shape in populations of normal human red cells. *Circulation Research*, 22(3):405–422.

Carbone, M. A. and Robinson, B. H. (2003). Expression and characterization of a human pyruvate carboxylase variant by retroviral gene transfer. *Biochemical Journal*, 370(Pt 1):275.

Carson, E. and Cobelli, C. (2013). *Modeling methodology for physiology and medicine*. Newnes.

Cerretelli, P. and Samaja, M. (2003). Acid–base balance at exercise in normoxia and in chronic hypoxia. revisiting the" lactate paradox". *European journal of applied physiology*, 90(5-6):431–448.

Chalhoub, E., Hanson, R. W., and Belovich, J. M. (2007). A computer model of gluconeogenesis and lipid metabolism in the perfused liver. *American Journal of Physiology-Endocrinology And Metabolism*, 293(6):E1676–E1686.

Chapman, R. G., Hennessey, M., Waltersdorph, A. M., Huennekens, F., and Gabrio, B. W. (1962). Erythrocyte metabolism. v. levels of glycolytic enzymes and regulation of glycolysis. *Journal of Clinical Investigation*, 41(6):1249.

Chassagnole, C., Noisommit-Rizzi, N., Schmid, J. W., Mauch, K., and Reuss, M. (2002). Dynamic modeling of the central carbon metabolism of escherichia coli. *Biotechnology and bioengineering*, 79(1):53–73.

Cloutier, M., Bolger, F. B., Lowry, J. P., and Wellstead, P. (2009). An integrative dynamic model of brain energy metabolism using in vivo neurochemical measurements. *Journal of computational neuroscience*, 27(3):391–414.

Cobelli, C. and Carson, E. (2008). *Introduction to modeling in physiology and medicine*. Academic Press.

Consoli, A. and Nurjhan, N. (1990). Contribution of gluconeogenesis to overall glucose output in diabetic and nondiabetic men. *Annals of medicine*, 22(3):191–195.

Consoli, A., Nurjhan, N., Reilly Jr, J., Bier, D., and Gerich, J. (1990a). Contribution of liver and skeletal muscle to alanine and lactate metabolism in humans. *American Journal of Physiology-Endocrinology and Metabolism*, 259(5):E677–E684.

Consoli, A., Nurjhan, N., Reilly Jr, J., Bier, D., and Gerich, J. (1990b). Mechanism of increased gluconeogenesis in noninsulin-dependent diabetes mellitus. role of alterations in systemic, hepatic, and muscle lactate and alanine metabolism. *Journal of Clinical Investigation*, 86(6):2038.

Cori, C. (1981). The glucose-lactic acid cycle and gluconeogenesis. *Current topics in cellular regulation*, 18:377.

Damsbo, P., Vaag, A., Hother-Nielsen, O., and Beck-Nielsen, H. (1991). Reduced glycogen synthase activity in skeletal muscle from obese patients with and without type 2 (non-insulin-dependent) diabetes mellitus. *Diabetologia*, 34(4):239–245.

De Backer, D., Creteur, J., Zhang, H., Norrenberg, M., and Vincent, J.-L. (1997). Lactate production by the lungs in acute lung injury. *American journal of respiratory and critical care medicine*, 156(4):1099–1104.

de Jonghe, B., Lacherade, J.-C., Sharshar, T., and Outin, H. (2009). Intensive care unit-acquired weakness: risk factors and prevention. *Critical care medicine*, 37(10):S309–S315.

Dellinger, R. P., Levy, M. M., Rhodes, A., Annane, D., Gerlach, H., Opal, S. M., Sevransky, J. E., Sprung, C. L., Douglas, I. S., Jaeschke, R., et al. (2013). Surviving sepsis campaign: international guidelines for management of severe sepsis and septic shock, 2012. *Intensive care medicine*, 39(2):165–228.

Despopoulos, A. and Silbernagl, S. (2003). *Color Atlas of Physiology*. Thieme Flexibook, 5th edition.

Deutsch, J. (2003). *Bestimmung der Laktatkonzentration in Plasma und Vollblut. Ein Methodenvergleich der enzymatischen und ionenselektiven Messung mit der GC-MS Referenzmethode*. PhD thesis, Eberhard-Karls-Universität Tübingen.

Devereux, R. B. and Reichek, N. (1977). Echocardiographic determination of left ventricular mass in man. anatomic validation of the method. *Circulation*, 55(4):613–618.

Dienel, G. A. (2014). Lactate shuttling and lactate use as fuel after traumatic brain injury: metabolic considerations. *Journal of Cerebral Blood Flow & Metabolism*, 34(11):1736–1748.

Dombrauckas, J. D., Santarsiero, B. D., and Mesecar, A. D. (2005). Structural basis for tumor pyruvate kinase m2 allosteric regulation and catalysis. *Biochemistry*, 44(27):9417–9429.

Durante, A., Raleigh, X., Gomez, M. E., Campos, G., and Ryder, E. (1995). Isozyme analysis of human normal polymorphonuclear leukocyte phosphofructokinase. *Biochemical and biophysical research communications*, 216(3):898–905.

Elke, G., Wang, M., Weiler, N., Day, A. G., and Heyland, D. K. (2014). Close to recommended caloric and protein intake by enteral nutrition is associated with better clinical outcome of critically ill septic patients: secondary analysis of a large international nutrition database. *Crit Care*, 18:R29.

Eriksson, H., Penker, M., Lyons, B., and Fado, D. (2003). *UML 2 Toolkit*. OMG. Wiley.

Esposito, G., Vitagliano, L., Costanzo, P., Borrelli, L., Barone, R., Pavone, L., Izzo, P., Zagari, A., and Salvatore, F. (2004). Human aldolase a natural mutants: relationship between flexibility of the c-terminal region and enzyme function. *Biochem. J*, 380:51–56.

Evans, E. and Fung, Y.-C. (1972). Improved measurements of the erythrocyte geometry. *Microvascular research*, 4(4):335–347.

Fall, P. J. and Szerlip, H. M. (2005). Lactic acidosis: from sour milk to septic shock. *Journal of intensive care medicine*, 20(5):255–271.

Felig, P., Marliss, E., Pozefsky, T., and Cahill Jr, G. F. (1970). Amino acid metabolism in the regulation of gluconeogenesis in man. *The American journal of clinical nutrition*, 23(7):986–992.

Flores, H. and Ellington, A. D. (2005). A modified consensus approach to mutagenesis inverts the cofactor specificity of bacillus stearothermophilus lactate dehydrogenase. *Protein Engineering Design and Selection*, 18(8):369–377.

Fox, J. E. M., Meredith, D., and Halestrap, A. P. (2000). Characterisation of human monocarboxylate transporter 4 substantiates its role in lactic acid efflux from skeletal muscle. *The Journal of physiology*, 529(2):285–293.

Franceschini, M. A., Thaker, S., Themelis, G., Krishnamoorthy, K. K., Bortfeld, H., Diamond, S. G., Boas, D. A., Arvin, K., and Grant, P. E. (2007). Assessment of infant brain development with frequency-domain near-infrared spectroscopy. *Pediatric research*, 61:546–551.

Garcia-Alvarez, M., Marik, P., and Bellomo, R. (2014a). Sepsis-associated hyperlactatemia. *Critical Care*, 18(5):503.

Garcia-Alvarez, M., Marik, P., and Bellomo, R. (2014b). Stress hyperlactataemia: present understanding and controversy. *The Lancet Diabetes & Endocrinology*, 2(4):339–347.

Gerich, J. E., Meyer, C., Woerle, H. J., and Stumvoll, M. (2001). Renal gluconeogenesis its importance in human glucose homeostasis. *Diabetes care*, 24(2):382–391.

Gilbert, H. (2000). *Basic Concepts in Biochemistry: A Student's Survival Guide*. Basic sciences series. McGraw-Hill Education.

Gizak, A., Maciaszczyk, E., Dzugaj, A., Eschrich, K., and Rakus, D. (2008). Evolutionary conserved n-terminal region of human muscle fructose 1, 6-bisphosphatase regulates its activity and the interaction with aldolase. *Proteins: Structure, Function, and Bioinformatics*, 72(1):209–216.

Gladden, L. B. (2004). Lactate metabolism: a new paradigm for the third millennium. *The Journal of physiology*, 558(1):5–30.

Gladden, L. B. (2008). A lactatic perspective on metabolism. *Medicine and science in sports and exercise*, 40(3):477–485.

Grau, T. and Bonet, A. (2009). Caloric intake and liver dysfunction in critically ill patients. *Current Opinion in Clinical Nutrition & Metabolic Care*, 12(2):175–179.

Greiner, F. (2012). *LabVIEW Ein Grundkurs*. RRZN-Handbuch. Regionales Rechenzentrum für Niedersachsen / Leibniz Universität Hannover und Institut für Experimentelle und Angewandte Physik Christian-Albrechts-Universität zu Kiel, 1 edition.

Griffiths, R. D. and Hall, J. B. (2010). Intensive care unit-acquired weakness. *Critical care medicine*, 38(3):779–787.

Gubern, G., Imperial, S., Busquets, M., and Cortes, A. (1990). Partial characterization of the alanine aminotransferase isoenzymes from human liver. *Biochemical Society transactions*, 18(6):1288–1289.

Gunnerson, K. J., Saul, M., He, S., and Kellum, J. A. (2006). Lactate versus non-lactate metabolic acidosis: a retrospective outcome evaluation of critically ill patients. *Critical Care*, 10(1):R22.

Handy, J. (2006). Lactate—the bad boy of metabolism, or simply misunderstood? *Current Anaesthesia & Critical Care*, 17(1):71–76.

Handy, J. (2007). The origin and interpretation of hyperlactataemia during low oxygen delivery states. *Crit Care*, 11(1):104.

Hardern, R. and Quinn, N. (2003). Emergency management of diabetic ketoacidosis in adults. *Emergency medicine journal: EMJ*, 20(3):210.

Heinemann, A., Wischhusen, F., Püschel, K., and Rogiers, X. (1999). Standard liver volume in the caucasian population. *Liver transplantation and surgery*, 5(5):366–368.

Hick, C. and Hick, A. (2000). *Kurzlehrbuch Physiologie*. Urban & Fischer.

Holmes, R. (2007). *A Cell Biologist's Guide to Modeling and Bioinformatics*. Wiley.

Horn, F. (2009). *Biochemie des Menschen: das Lehrbuch für das Medizinstudium : 1200 Abbildungen*. Thieme.

Huckabee, W. E. (1958). Relationships of pyruvate and lactate during anaerobic metabolism. i. effects of infusion of pyruvate or glucose and of hyperventilation. *Journal of clinical investigation*, 37(2):244.

Hughes, S. D., Quaade, C., Johnson, J. H., Ferber, S., and Newgard, C. (1993). Transfection of att-20ins cells with glut-2 but not glut-1 confers glucose-stimulated insulin secretion. relationship to glucose metabolism. *Journal of Biological Chemistry*, 268(20):15205–15212.

Hunt, T. K., Aslam, R. S., Beckert, S., Wagner, S., Ghani, Q. P., Hussain, M. Z., Roy, S., and Sen, C. K. (2007). Aerobically derived lactate stimulates revascularization and tissue repair via redox mechanisms. *Antioxidants & redox signaling*, 9(8):1115–1124.

Hynne, F., Danø, S., and Sørensen, P. G. (2001). Full-scale model of glycolysis in< i> saccharomyces cerevisiae</i>. *Biophysical chemistry*, 94(1):121–163.

Imperial, S. and Centelles, J. J. (2014). Enzyme kinetic equations of irreversible and reversible reactions in metabolism. *Journal of Biosciences and Medicines*, 2(04):24.

Instruments, N. (2012). Application design patterns: Producer/consumer.

Jackson, A. S. and Pollock, M. L. (1978). Generalized equations for predicting body density of men. *British journal of nutrition*, 40(03):497–504.

Jay, A. (1975). Geometry of the human erythrocyte. i. effect of albumin on cell geometry. *Biophysical journal*, 15(3):205.

Jenssen, T., Nurjhan, N., Consoli, A., and Gerich, J. (1990). Failure of substrate-induced gluconeogenesis to increase overall glucose appearance in normal humans. demonstration of hepatic autoregulation without a change in plasma glucose concentration. *Journal of Clinical Investigation*, 86(2):489.

Jitrapakdee, S., Walker, M. E., and Wallace, J. C. (1999). Functional expression, purification, and characterization of recombinant human pyruvate carboxylase. *Biochemical and biophysical research communications*, 266(2):512–517.

Juel, C. (1997). Lactate-proton cotransport in skeletal muscle. *Physiological Reviews*, 77(2):321–358.

Juel, C. (2004). Laktattransport im skelettmuskel: Trainingsinduzierte anpassung und bedeutung bei körperlicher belastung. *Deutsche Zeitschrift für Sportmedizin*, 55(6):157–160.

Kauffman, K. J., Prakash, P., and Edwards, J. S. (2003). Advances in flux balance analysis. *Current opinion in biotechnology*, 14(5):491–496.

Kavanagh, D. and Goodship, T. (2010). Genetics and complement in atypical hus. *Pediatric nephrology*, 25(12):2431–2442.

Kelmer-Bracht, A. M., Santos, C. P. B., Ishii-Iwamoto, E. L., Broetto-Biazon, A. C., and Bracht, A. (2003). Kinetic properties of the glucose 6-phosphatase of the liver from arthritic rats. *Biochimica et Biophysica Acta (BBA)-Molecular Basis of Disease*, 1638(1):50–56.

Kenner, T. (1989). The measurement of blood density and its meaning. *Basic research in cardiology*, 84(2):111–124.

Klein, S. (1998). *Quantitative morphologische Untersuchungen an Herzen, Nieren und Nebennieren von Wildschweinen verschiedenen Alters und Geschlechts*. PhD thesis, Freie Universität Berlin, Germany.

Kruse, J., Haupt, M., Puri, V., and Carlson, R. (1990). Lactate levels as predictors of the relationship between oxygen delivery and consumption in ards. *CHEST Journal*, 98(4):959–962.

Kusakabe, T., Motoki, K., and Hori, K. (1994). Human aldolase c: characterization of the recombinant enzyme expressed in escherichia coli. *Journal of biochemistry*, 115(6):1172–1177.

Lacherade, J.-C., Jacqueminet, S., and Preiser, J.-C. (2009). An overview of hypoglycemia in the critically ill. *Journal of diabetes science and technology*, 3(6):1242–1249.

Lambeth, M. J. and Kushmerick, M. J. (2002). A computational model for glycogenolysis in skeletal muscle. *Annals of biomedical engineering*, 30(6):808–827.

Lane, A. N., Fan, T. W.-M., and Higashi, R. M. (2009). Metabolic acidosis and the importance of balanced equations. *Metabolomics*, 5(2):163–165.

Lecker, S. H., Solomon, V., Mitch, W. E., and Goldberg, A. L. (1999). Muscle protein breakdown and the critical role of the ubiquitin-proteasome pathway in normal and disease states. *The Journal of nutrition*, 129(1):227S–237S.

Lee, S., Hong, Y., Park, D., Choi, S., Moon, S., Park, J., Kim, J., and Baek, K. (2008). Lactic acidosis not hyperlactatemia as a predictor of inhospital mortality in septic emergency patients. *Emergency Medicine Journal*, 25(10):659–665.

Lehninger, A., Nelson, D., and Cox, M. (2005). *Lehninger Principles of Biochemistry*. W. H. Freeman.

Lenzen, E. (2012). *Der Einfluss intermittierender Hypoxie auf den Laktattransport in den Erythrozyten und Skelettmuskelzellen des Typ-2-Diabetikers*. PhD thesis, Deutsche Sporthochschule Köln.

Levraut, J., Ciebiera, J.-P., Chave, S., Rabary, O., Jambou, P., Carles, M., and Grimaud, D. (1998). Mild hyperlactatemia in stable septic patients is due to impaired lactate clearance rather than overproduction. *American journal of respiratory and critical care medicine*, 157(4):1021–1026.

Levy, B. (2006). Lactate and shock state: the metabolic view. *Current opinion in critical care*, 12(4):315–321.

Levy, B., Bollaert, P.-E., Charpentier, C., Nace, L., Audibert, G., Bauer, P., Nabet, P., and Larcan, A. (1997). Comparison of norepinephrine and dobutamine to epinephrine for hemodynamics, lactate metabolism, and gastric tonometric variables in septic shock: a prospective, randomized study. *Intensive care medicine*, 23(3):282–287.

Levy, B., Gibot, S., Franck, P., Cravoisy, A., and Bollaert, P.-E. (2005). Relation between muscle na+ k+ atpase activity and raised lactate concentrations in septic shock: a prospective study. *The Lancet*, 365(9462):871–875.

Liebermeister, W. and Klipp, E. (2006). Bringing metabolic networks to life: integration of kinetic, metabolic, and proteomic data. *Theoretical Biology and Medical Modelling*, 3(1):42.

Liu, M.-S. and Spitzer, J. J. (1978). Oxidation of palmitate and lactate by beating myocytes isolated from adult dog heart. *Journal of Molecular and Cellular Cardiology*, 10(5):415–426.

Löffler, G., Petrides, P. E., and Heinrich, P. C. (2007). *Biochemie und Pathobiochemie*. Springer-Lehrbuch. Springer London, Limited, 8th edition.

Madison, P. and Madison, A. (2006). *Enzymatic Reaction Mechanisms*. Oxford University Press, USA.

Mansoor, O., Beaufrere, B., Boirie, Y., Ralliere, C., Taillandier, D., Aurousseau, E., Schoeffler, P., Arnal, M., and Attaix, D. (1996). Increased mrna levels for components of the lysosomal, ca2+-activated, and atp-ubiquitin-dependent proteolytic pathways in skeletal muscle from head trauma patients. *Proceedings of the National Academy of Sciences*, 93(7):2714–2718.

Mansoor, O., Breuillé, D., Béchereau, F., Buffière, C., Pouyet, C., Beaufrère, B., Vuichoud, J., Van't-Of, M., and Obled, C. (2007). Effect of an enteral diet supplemented with a specific blend of amino acid on plasma and muscle protein synthesis in icu patients. *Clinical Nutrition*, 26(1):30–40.

Marik, P. E. (2014). Early management of severe sepsis: Concepts and controversies. *CHEST Journal*, 145(6):1407–1418.

Marko, P., Gabrielli, A., Caruso, L. J., Mizock, B. A., and Franklin, C. (2004). Too much lactate or too little liver? *Journal of clinical anesthesia*, 16(5):389–395.

Mendoza-Juez, B., Martínez-González, A., Calvo, G. F., and Pérez-García, V. M. (2012). A mathematical model for the glucose-lactate metabolism of in vitro cancer cells. *Bulletin of mathematical biology*, 74(5):1125–1142.

Merziger, G. (2004). *Formeln und Hilfen zur höheren Mathematik*. Binomi.

Meyer, C., Stumvoll, M., Nadkarni, V., Dostou, J., Mitrakou, A., and Gerich, J. (1998). Abnormal renal and hepatic glucose metabolism in type 2 diabetes mellitus. *Journal of Clinical Investigation*, 102(3):619.

Miller, B. F., Fattor, J. A., Jacobs, K. A., Horning, M. A., Navazio, F., Lindinger, M. I., and Brooks, G. A. (2002). Lactate and glucose interactions during rest and exercise in men: effect of exogenous lactate infusion. *The Journal of physiology*, 544(3):963–975.

Minassian, C., Daniele, N., Bordet, J., Zitoun, C., and Mithieux, G. (1995). Liver glucose-6 phosphatase activity is inhibited by refeeding in rats. *The Journal of nutrition*, 125(11):2727–2732.

Mitch, W. E., Medina, R., Grieber, S., May, R. C., England, B. K., Price, S. R., Bailey, J. L., and Goldberg, A. L. (1994). Metabolic acidosis stimulates muscle protein degradation by activating the adenosine triphosphate-dependent pathway involving ubiquitin and proteasomes. *Journal of Clinical Investigation*, 93(5):2127.

Mitrakou, A. (2011). Kidney: its impact on glucose homeostasis and hormonal regulation. *Diabetes research and clinical practice*, 93:S66–S72.

Mizock, B. A. (2001). Alterations in fuel metabolism in critical illness: hyperglycaemia. *Best Practice & Research Clinical Endocrinology & Metabolism*, 15(4):533–551.

Molnes, J., Teigen, K., Aukrust, I., Bjørkhaug, L., Søvik, O., Flatmark, T., and Njølstad, P. R. (2011). Binding of atp at the active site of human pancreatic glucokinase–nucleotide-induced conformational changes with possible implications for its kinetic cooperativity. *FEBS Journal*, 278(13):2372–2386.

Mortimer, C. and Schilling, G. (1980). *Chemie: das Basiswissen der Chemie in Schwerpunkten ; mit Übungsaufgaben ; anorganische Chemie, organische Chemie, Theorie der chemischen Bindung, physikalische Chemie, Radio-Chemie*. Thieme, 3rd edition.

Mu, X., Qi, L., Qiao, J., Zhang, H., and Ma, H. (2012). Study on alanine aminotransferase kinetics by microchip electrophoresis. *Analytical biochemistry*, 421(2):499–505.

Müller, M., Boeing, H., Bosy-Westphal, A., Löser, C., Przyrembel, H., Selberg, O., Weinmann, A., and Westenhöfer, J. (2007). *Ernährungsmedizinische Praxis: Methoden - Prävention - Behandlung*. Springer Berlin Heidelberg.

Mulquiney, P. and Kuchel, P. (1999). Model of 2, 3-bisphosphoglycerate metabolism in the human erythrocyte based on detailed enzyme kinetic equations1: equations and parameter refinement. *Biochem. J*, 342:581–596.

Mulukutla, B., Yongky, A., Daoutidis, P., Hu, W., and Dzeja, P. (2014). Bistability in glycolysis pathway as a physiological switch in energy metabolism. *PLoS ONE*, 9(6).

Nakae, Y. and Stoward, P. J. (1997). Kinetic parameters of lactate dehydrogenase in liver and gastrocnemius determined by three quantitative histochemical methods. *Journal of Histochemistry & Cytochemistry*, 45(10):1427–1431.

Nathwani, R. A., Pais, S., Reynolds, T. B., and Kaplowitz, N. (2005). Serum alanine aminotransferase in skeletal muscle diseases. *Hepatology*, 41(2):380–382.

Nielsen, J. (1994). *Usability engineering*. Elsevier.

Nurjhan, N., Consoli, A., and Gerich, J. (1992). Increased lipolysis and its consequences on gluconeogenesis in non-insulin-dependent diabetes mellitus. *Journal of Clinical Investigation*, 89(1):169.

Oakes, N. D., Cooney, G. J., Camilleri, S., Chisholm, D. J., and Kraegen, E. W. (1997). Mechanisms of liver and muscle insulin resistance induced by chronic high-fat feeding. *Diabetes*, 46(11):1768–1774.

Oliva, P. B. (1970). Lactic acidosis. *The American journal of medicine*, 48(2):209–225.

Oria-Hernández, J., Cabrera, N., Pérez-Montfort, R., and Ramírez-Silva, L. (2005). Pyruvate kinase revisited the activating effect of k+. *Journal of Biological Chemistry*, 280(45):37924–37929.

Pettit, S. M., Nealon, D. A., and Henderson, A. R. (1981). Purification of lactate dehydrogenase isoenzyme-5 from human liver. *Clinical chemistry*, 27(1):88–93.

Pielmeier, U. (2010). *Decision support for blood glucose control in critically ill patients: development and clinical pilot testing of the Glucosafe system*. PhD thesis, Videnbasen for Aalborg UniversitetVBN, Aalborg UniversitetAalborg University, Det Sundhedsvidenskabelige FakultetThe Faculty of Medicine, Institut for Medicin og SundhedsteknologiDepartment of Health Science and Technology.

Pretty, C. G., Chase, J. G., Le Compte, A., Shaw, G. M., and Signal, M. (2010). Hypoglycemia detection in critical care using continuous glucose monitors: an in silico proof of concept analysis. *Journal of diabetes science and technology*, 4(1):15–24.

Proshin, A. P. and Solodyannikov, Y. V. (2013). Mathematical modeling of lactate metabolism with applications to sports. *Automation and Remote Control*, 74(6):1004–1019.

Quistorff, B., Secher, N. H., and Van Lieshout, J. J. (2008). Lactate fuels the human brain during exercise. *The FASEB Journal*, 22(10):3443–3449.

Rakus, D., Maciaszczyk, E., Wawrzycka, D., Ułaszewski, S., Eschrich, K., and Dzugaj, A. (2005). The origin of the high sensitivity of muscle fructose 1, 6-bisphosphatase towards amp. *FEBS letters*, 579(25):5577–5581.

Rehm, H. and Hammar, F. (2005). *Biochemie light*. Deutsch.

Richter, E. A. and Hargreaves, M. (2013). Exercise, glut4, and skeletal muscle glucose uptake. *Physiological reviews*, 93(3):993–1017.

Robergs, R. A., Ghiasvand, F., and Parker, D. (2004). Biochemistry of exercise-induced metabolic acidosis. *American Journal of Physiology-Regulatory, Integrative and Comparative Physiology*, 287(3):R502–R516.

Rohwer, J. (2012). Kinetic modelling of plant metabolic pathways. *Journal of experimental botany*, 63(6):2275.

Rozova, O., Khmelenina, V., Mustakhimov, I., Reshetnikov, A., and Trotsenko, Y. (2010). Characterization of recombinant fructose-1, 6-bisphosphate aldolase from methylococcus capsulatus bath. *Biochemistry (Moscow)*, 75(7):892–898.

Rutten, E. P., Engelen, M. P., Schols, A. M., and Deutz, N. E. (2005). Skeletal muscle glutamate metabolism in health and disease: state of the art. *Current Opinion in Clinical Nutrition & Metabolic Care*, 8(1):41–51.

Sánchez-Muros, M. J., García-Rejón, L., García-Salguero, L., Lupiáñez, J. A., et al. (1998). Long-term nutritional effects on the primary liver and kidney metabolism in rainbow trout. adaptive response to starvation and a high-protein, carbohydrate-free diet on glutamate dehydrogenase and alanine aminotransferase kinetics. *The international journal of biochemistry & cell biology*, 30(1):55–63.

Saxena, M. K. and Hodgson, C. L. (2012). Intensive care unit acquired weakness. *Anaesthesia & Intensive Care Medicine*, 13(4):145–147.

Schallau, K. and Junker, B. H. (2010). Simulating plant metabolic pathways with enzyme-kinetic models. *Plant physiology*, 152(4):1763–1771.

Scheer, M., Grote, A., Chang, A., Schomburg, I., Munaretto, C., Rother, M., Söhngen, C., Stelzer, M., Thiele, J., and Schomburg, D. (2010). Brenda, the enzyme information system in 2011. *Nucleic acids research*, page gkq1089.

Schuster, R., Holzhütter, H.-G., and Jacobasch, G. (1988). Interrelations between glycolysis and the hexose monophosphate shunt in erythrocytes as studied on the basis of a mathematical model. *Biosystems*, 22(1):19–36.

Scopes, R. K. (1973). Studies with a reconstituted muscle glycolytic system. the rate and extent of creatine phosphorylation by anaerobic glycolysis. *Biochem. J*, 134:197–208.

Singer, P., Berger, M. M., Van den Berghe, G., Biolo, G., Calder, P., Forbes, A., Griffiths, R., Kreyman, G., Leverve, X., and Pichard, C. (2009). Espen guidelines on parenteral nutrition: intensive care. *Clinical nutrition*, 28(4):387–400.

Smith, C., Marks, A., Lieberman, M., and Marks, D. (2005). *Marks' Basic Medical Biochemistry: A Clinical Approach*. Marks' Basic Medical Biochemistry: A Clinical Approach. Lippincott Williams & Wilkins, 2nd edition.

Stacpoole, P. W., Wright, E. C., Baumgartner, T. G., Bersin, R. M., Buchalter, S., Curry, S. H., Duncan, C., Harman, E. M., Henderson, G. N., Jenkinson, S., et al. (1994). Natural history and course of acquired lactic acidosis in adults. *The American journal of medicine*, 97(1):47–54.

Stein, J. and Schröder, O. (2006). Prüfung der leberdurchblutung und des portosystemischen shuntvolumens. *Funktionsdiagnostik in der Gastroenterologie*, pages 191–196.

Steuer, R. and Junker, B. H. (2009). Computational models of metabolism: stability and regulation in metabolic networks. *Advances in chemical physics*, 142:105.

Stumvoll, M., Meyer, C., Mitrakou, A., Nadkarni, V., and Gerich, J. (1997). Renal glucose production and utilization: new aspects in humans. *Diabetologia*, 40(7):749–757.

Stumvoll, M., Perriello, G., Meyer, C., and Gerich, J. (1999). Role of glutamine in human carbohydrate metabolism in kidney and other tissues. *Kidney international*, 55(3):778–792.

Szabó, J., Varga, A., Flachner, B., Konarev, P. V., Svergun, D. I., Závodszky, P., and Vas, M. (2008a). Communication between the nucleotide site and the main molecular hinge of 3-phosphoglycerate kinase†. *Biochemistry*, 47(26):6735–6744.

Szabó, J., Varga, A., Flachner, B., Konarev, P. V., Svergun, D. I., Závodszky, P., and Vas, M. (2008b). Role of side-chains in the operation of the main molecular hinge of 3-phosphoglycerate kinase. *FEBS letters*, 582(9):1335–1340.

Tappy, L. (2008). Basics in clinical nutrition: Carbohydrate metabolism. *European e-Journal of Clinical Nutrition and Metabolism*, 3(5):e192–e195.

Termonia, Y. and Ross, J. (1981). Oscillations and control features in glycolysis: numerical analysis of a comprehensive model. *proceedings of the national academy of sciences*, 78(5):2952–2956.

Teusink, B., Passarge, J., Reijenga, C. A., Esgalhado, E., van der Weijden, C. C., Schepper, M., Walsh, M. C., Bakker, B. M., van Dam, K., Westerhoff, H. V., et al. (2000). Can yeast glycolysis be understood in terms of in vitro kinetics of the constituent enzymes? testing biochemistry. *European Journal of Biochemistry*, 267(17):5313–5329.

Tian, L.-P., Shi, Z.-K., and Wu, F.-X. (2013). Complexity analysis and parameter estimation of dynamic metabolic systems. *Computational and mathematical methods in medicine*, 2013.

Trabold, O., Wagner, S., Wicke, C., Scheuenstuhl, H., Hussain, M. Z., Rosen, N., Seremetiev, A., Becker, H. D., and Hunt, T. K. (2003). Lactate and oxygen constitute a fundamental regulatory mechanism in wound healing. *Wound repair and regeneration*, 11(6):504–509.

Uldry, M. and Thorens, B. (2004). The slc2 family of facilitated hexose and polyol transporters. *Pflügers Archiv*, 447(5):480–489.

Van Beneden, R. J. and Powers, D. A. (1989). Structural and functional differentiation of two clinally distributed glucosephosphate isomerase allelic isozymes from the teleost fundulus heteroclitus. *Molecular biology and evolution*, 6(2):155–170.

Van Cromphaut, S. (2009). Hyperglycaemia as part of the stress response: the underlying mechanisms. *Best Practice & Research Clinical Anaesthesiology*, 23(4):375–386.

van Hall, G. (2010). Lactate kinetics in human tissues at rest and during exercise. *Acta physiologica*, 199(4):499–508.

van Hall, G., Strømstad, M., Rasmussen, P., Jans, Ø., Zaar, M., Gam, C., Quistorff, B., Secher, N. H., and Nielsen, H. B. (2009). Blood lactate is an important energy source for the human brain. *Journal of Cerebral Blood Flow & Metabolism*, 29(6):1121–1129.

Vassella, F., Mumenthaler, M., Rossi, E., Moser, H., and Wiesmann, U. (1967). Die kongenitale muskeldystrophie. *Deutsche Zeitschrift für Nervenheilkunde*, 190(4):349–374.

Vincent, J.-L. (1995). Lactate levels in critically ill patients. *Acta Anaesthesiologica Scandinavica*, 39(s107):261–266.

Vivian, E. M. (2014). Sodium-glucose co-transporter 2 (sglt2) inhibitors: a growing class of antidiabetic agents. *Drugs in context*, 3.

von Grumbckow, L., Elsner, P., Hellsten, Y., Quistorff, B., and Juel, C. (1999). Kinetics of lactate and pyruvate transport in cultured rat myotubes. *Biochimica et Biophysica Acta (BBA)-Biomembranes*, 1417(2):267–275.

Wahl, P., Yue, Z., Zinner, C., Bloch, W., and Mester, J. (2011). A mathematical model for lactate transport to red blood cells. *The Journal of Physiological Sciences*, 61(2):93–102.

Wang, Y., Bolton, E., Dracheva, S., Karapetyan, K., Shoemaker, B. A., Suzek, T. O., Wang, J., Xiao, J., Zhang, J., and Bryant, S. H. (2010). An overview of the pubchem bioassay resource. *Nucleic acids research*, 38(suppl 1):D255–D266.

Ward, D. E., Kengen, S. W., van der Oost, J., and de Vos, W. M. (2000). Purification and characterization of the alanine aminotransferase from the hyperthermophilic archaeon pyrococcus furiosus and its role in alanine production. *Journal of bacteriology*, 182(9):2559–2566.

Weiler, E. and Nover, L. (2008). *Allgemeine und molekulare Botanik*. Thieme.

Welsch, U. and Sobotta, J. (2003). *Lehrbuch Histologie: Zytologie, Histologie, mikroskopische Anatomie ; Mit 811 Abbildungen und 21 Tabellen]*. Elsevier, Urban & Fischer.

Westermark, P. O. and Lansner, A. (2003). A model of phosphofructokinase and glycolytic oscillations in the pancreatic β-cell. *Biophysical journal*, 85(1):126–139.

Wexler, L., Bergel, D. H., Gabe, I. T., Makin, G. S., and Mills, C. J. (1968). Velocity of blood flow in normal human venae cavae. *Circulation Research*, 23(3):349–359.

Wilhelms, S. B., Huss, F. R., Granath, G., and Sjöberg, F. (2010). Assessment of incidence of severe sepsis in sweden using different ways of abstracting international classification of diseases codes: difficulties with methods and interpretation of results. *Critical care medicine*, 38(6):1442–1449.

Williamson, D., Lund, P., and Krebs, H. (1967). The redox state of free nicotinamide-adenine dinucleotide in the cytoplasm and mitochondria of rat liver. *Biochem. j*, 103:514–527.

Wischmeyer, P. E. (2013). The evolution of nutrition in critical care: how much, how soon? *Critical Care*, 17(1):1–8.

Wolf, J., Passarge, J., Somsen, O. J., Snoep, J. L., Heinrich, R., and Westerhoff, H. V. (2000). Transduction of intracellular and intercellular dynamics in yeast glycolytic oscillations. *Biophysical journal*, 78(3):1145–1153.

Wolfe, R. (1999). Sepsis as a modulator of adaptation to low and high carbohydrate and low and high fat intakes. *European journal of clinical nutrition*, 53:S136–42.

Xu, L. Z., Harrison, R. W., Weber, I. T., and Pilkis, S. J. (1995). Human β-cell glucokinase dual role of ser-151 in catalysis and hexose affinity. *Journal of Biological Chemistry*, 270(17):9939–9946.

Yamada, K., Hara, N., Shibata, T., Osago, H., and Tsuchiya, M. (2006). The simultaneous measurement of nicotinamide adenine dinucleotide and related compounds by liquid chromatography/electrospray ionization tandem mass spectrometry. *Analytical biochemistry*, 352(2):282–285.

Yang, H., Yang, T., Baur, J. A., Perez, E., Matsui, T., Carmona, J. J., Lamming, D. W., Souza-Pinto, N. C., Bohr, V. A., Rosenzweig, A., et al. (2007). Nutrient-sensitive mitochondrial nad+ levels dictate cell survival. *Cell*, 130(6):1095–1107.

Zhang, T. C., Janik, J. J., and Grill, W. M. (2014). Modeling effects of spinal cord stimulation on wide-dynamic range dorsal horn neurons: influence of stimulation frequency and gabaergic inhibition. *Journal of neurophysiology*, 112(3):552–567.